How do we see exciton dynamics in antenna networks with 2D spectroscopy?

Master Thesis

For the Topmaster Nanoscience Programme
Cohort 2018-2021

by

Teun Zijp (they/them)

Supervisor/First Examiner:

prof. dr. T.L.C. (Thomas) Jansen (he/him)

Second Examiner:

prof. dr. R.W.A. (Remco) Havenith (he/him)

Abstract

Introduction   The capture of light by molecular antennas and the subsequent energy transfer are processes widely spread in nature and artificial light harvesting (LH) systems. This makes photosynthesis a fundamentally interesting topic to study. Normal plants are actually not so efficient when it comes to capturing light, but green sulphur bacteria and purple nonsulphur bacteria have developed light harvesting antenna's that make them super efficient with capturing light.

Upto now, the connectivity within the natural light harvesting networks in bacteria is typically studied with two dimensional electronic spectroscopy (2DES), which actually has a very low signal to noise ratio. Jennifer P. Ogilvie recently invented fluorescence detected two dimensional electronic spectroscopy (FD-2DES), which has a significantly higher signal to noise ratio. It must be noted that the results of both 2DES and FD-2DES images are hard to interpret, but since FD-2DES is a new technique, there is still a lot to learn and discover.

Aim.   Since the FD-2DES technique is new, I developed a theoretical model to predict FD-2DES spectra. The theoretical model is meant to be a toy model, so that we can play with various variables, beyond what can be measured with the FD-2DES spectroscopy technique. Finally, the toy model is exploited to predict a wide scale of spectra, which ideally would mimic the light harvesting systems from those which are used in low light conditions, to the light harvesting systems which are used under high light conditions.

Conclusion.   The model predicts that there is a negative correlation between the cross peak intensity and the concentration of LH1. It also predicts that the upper and lower diagonal peaks should be as intense, irrespective of LH1 concentration. This is something that could be measured.

Discussion.   The purple non-sulphur bacteria are known to be able to adjust their light harvesting antenna, from optimal under low light conditions (a dense network with loads of LH2), to optimal for high light conditions (a thin network with more LH1). This is also what I tried to model. However, while transitioning from low light to high light conditions, LH2 changes itself too. This is something which wasn't taken into account in the current model.

Keywords:

Contents

Chapter 1

General Introduction

1.1 Introduction

Photosynthesis in normal plants, like grass, actually isn't that efficient, it only has an energy efficiency of 3∼6%[1]. For grass, this is not a problem, because there is plenty of light anyways.

Not all organisms have the luxury of growing up in a sun-rich environment. For example, green sulphur bacteria live on bottom of the sea. They don't live of light from the sun (which only penetrates 100∼200 meter into the ocean), but from the glow of hydrothermal vents. Because the light of these hydrothermal vents is so dim, it pays off to create a very efficient light harvesting system for low light intensity conditions[2]. The antenna networks of these green sulphur bacteria is so efficient, that they can survive with 1% of full moonlight intensity light[3].

Since the discovery of the antenna networks in green sulphur bacteria, scientists found the light harvesting antenna systems in purple non-sulphur bacteria too (e.g. Rhodoblastus acidophilus[4, 5], R. sphaeroides[6] and Rhodospirillum photometricum[7]). Although this may sound like convergent evolution, the photo systems in purple and green bacteria actually have a common ancestor[8].

Scientists are excited to study how these light harvesting systems work exactly, and ideally want to compare the exciton dynamics in many different species. However, there is one problem: these bacteria are used to low light conditions, and they die very fast under normal daylight, not to mention the lasers the scientists intent to use for their experiments.

Fortunately, Jennifer Ogilvie has recently discovered a new technique which has a high signal to noise ratio at relatively low laser light intensities: fluorescence detected two dimensional electronic spectroscopy (FD-2DES)[9].

In this master thesis, I describe the development of tools capable of simulating the exciton dynamics on light harvesting (LH) antenna networks in these kind of systems.

The light harvesting complexes are used to capture light for photosynthesis. Several colaborating light harvesting complexes together form an antenna network, see Figure 1.1.
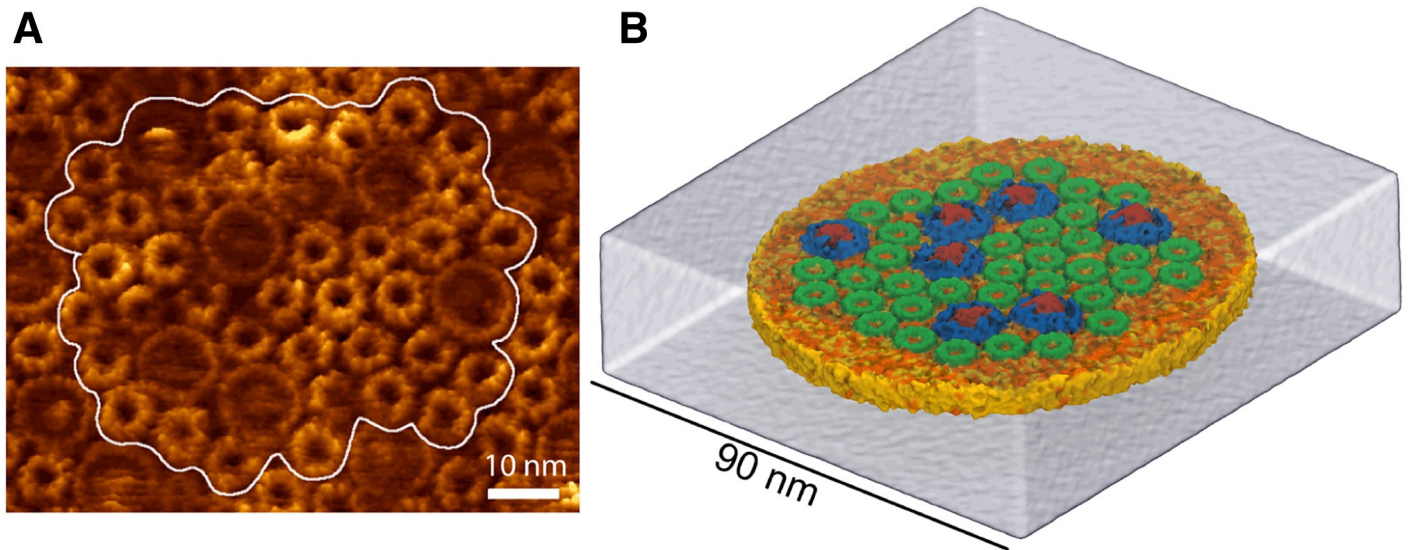
Figure 1.1: (A) AFM topograph of the native Rhodospirillum photometricum photosynthetic membrane. (B) and (C) are schematic representations, with LH1 in blue (with red reaction center) and LH2 in green. Note that LH1 typically has 7 neighbors and LH2 typically has 6 neighbors. Reprinted with permission from Ref. [7].

1.1.1 The LH1/LH2 system

The structural model of the LH2 complex is shown in Figure 1.2. Inside this complex, we find molecules that absorb light near 800 nm (B800) and molecules that absorb near 850 nm (B850).
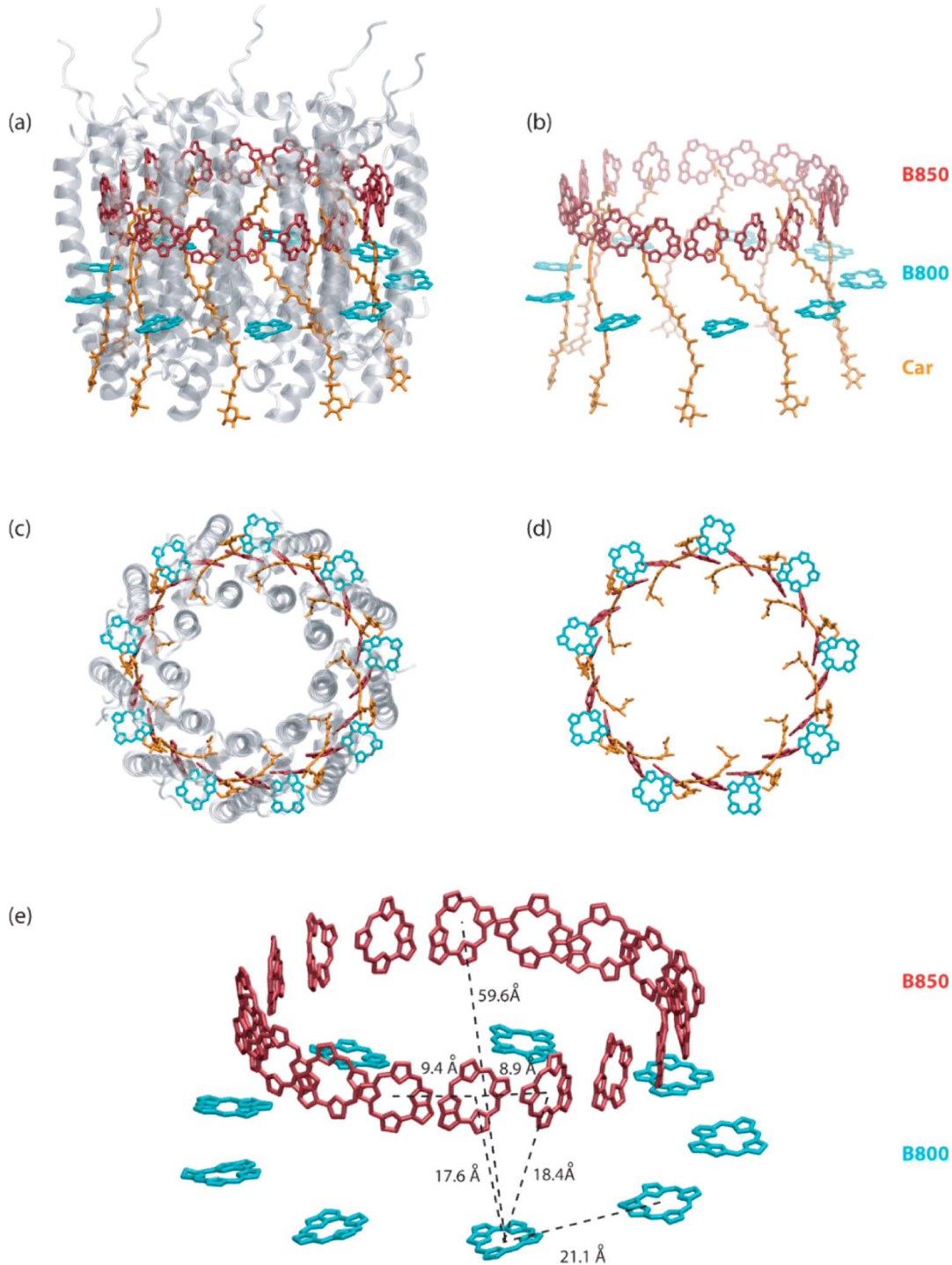
Figure 1.2: Structural model of the LH2 complex. An exciton on one of the 9 B800 molecules is localized, but it can be transferred to one of the 18 B850 molecules. An exciton on the B850 molecules is delocalized over all 18 B850 molecules [10]. Reprinted with permission from Ref. [11].

An excited state has many degrees of freedom in an antenna network. The key-processes are high-lighted in Figure 1.3, however, there is a lot of discussion about the rates[10, 7, 11], and therefore I will use different rates than those indicated in this Figure. Also note that this Figure has the wrong number of B850 molecules.

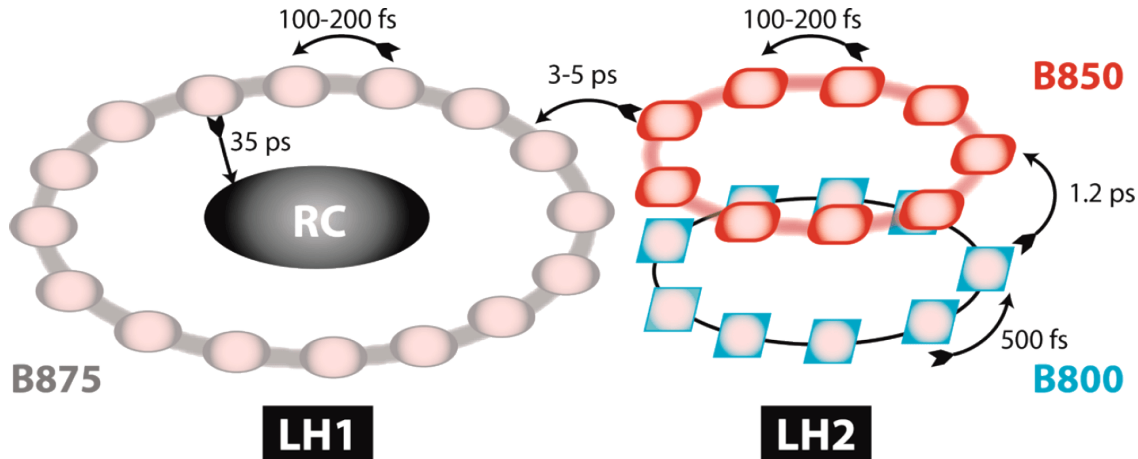**Figure 1.3:** Energy transfer-lifetimes (inverse of the rates). Note that this Figure has multiple issues: there should be 18 B850 molecules instead of 9 (recall Figure 1.2 on the preceding page). Excitons on B800 can be seen as localized, and excitons on on B850 and B875 can be viewed as delocalized[10]. The rate constant between LH1 and LH2 will be pulled from Ref. [7]. Figure reprinted from Ref. [11] with permission from Ref. [12].

1.2 Double sided Feynman diagrams

In this master thesis, we will explore different processes that occur in light harvesting (LH) antenna networks. In Chapter 3, these processes are described by double sided Feynman diagrams[1]. For learning more about these Feynman diagrams, I refer to the textbooks of Boyd[13], Hamm and Zanni[14]. For those who ware not familiar with double sided Feynman diagrams, these are introduced briefly here.

In the language of double sided Feynman diagrams, we describe the system by states. We follow both the bra ($\langle b|$) and the ket ($|a\rangle$). If the bra and the ket are in the same state ($|a\rangle\langle b|$ with a = b), then the system is in a state in which the electron density is stationary. If $a \neq b$ then the system is in a state in which the electron density oscillates. These oscillating states can either absorb or emit an electromagnetic wave, or the state may lose it's vibration due to dephasing. Depending on the number of interactions, we can use different spectroscopic techniques, see next section (section 1.3).

The first state is always a stationary state. For convenience, I will take the first state to be the ground-state, which, in short-hand-notation is indicated by |00|. From there on, the idea is that the system undergoes interactions with light pulses that come into or come out of the system. Each light

---

[1]   Small disclaimer: Since the double sided Feynman diagrams are the only Feynman diagrams I use in this thesis, so I might eventually abbreviate it to Feynman diagrams.

pulse is indicated by an arrow. Eq. 1.2.1 gives a few examples.

$$
\begin{array}{cccc}
& & \textbf{SFG} & \textbf{Raman} \\
& \textbf{Absorption} & \begin{vmatrix} 00 \\ 20 \\ 10 \\ 00 \\ |a\rangle\langle b| \end{vmatrix} & \begin{vmatrix} 00 \\ 10 \\ 00 \\ 10 \\ 00 \\ |a\rangle\langle b| \end{vmatrix} \\
\begin{vmatrix} 00 \\ 10 \\ 00 \\ |a\rangle\langle b| \end{vmatrix} & \begin{vmatrix} 11 \\ 10 \\ 00 \\ |a\rangle\langle b| \end{vmatrix} & &
\end{array}
\tag{Eq. 1.2.1}
$$

Absorption spectroscopy is linear spectroscopy, and is discussed in section 1.3.1. Adding a third pulse gives us sum frequency generation (SFG), which includes a stimulated emission step. This stimulated emission step is also used in conventional two dimensional electronic spectroscopy (2DES), see section 1.3.2. Adding a forth pulse unlocks a whole new realm of spectroscopies, like Raman, but also fluorescence detected two dimensional electronic spectroscopy (FD-2DES), see section 1.3.4.

In the above examples, all interactions (arrows) are on the ket ($|a\rangle$). For one moment, we will leave the bra ($\langle b|$) out of consideration, and tilt the diagrams 90° to create Figure 1.4.

What we are essentially doing is, we are looking at how the density matrix ρ changes under the influence of k interactions.
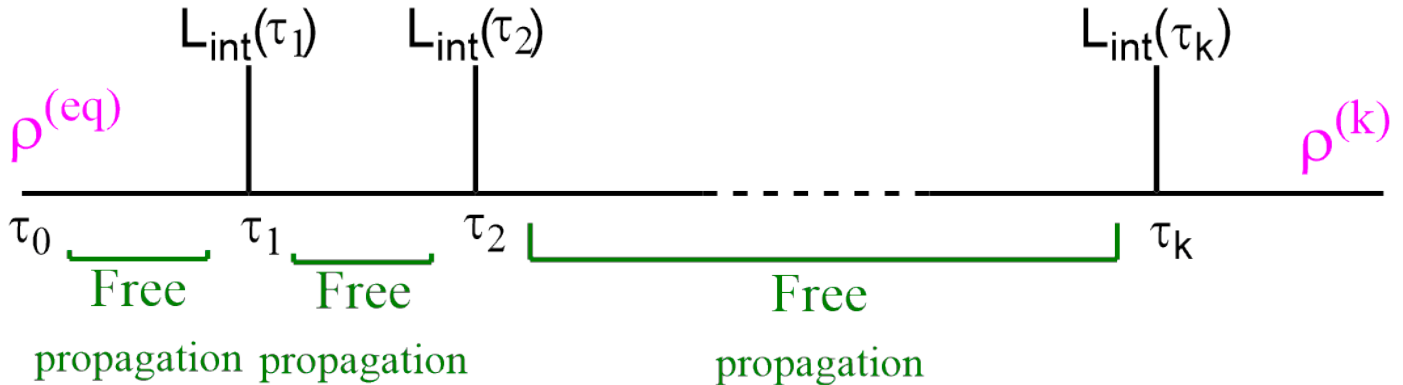
Figure 1.4: The density matrix ρ changes upon each interaction L_{interact}, and propagates according to $e^{iL_{\text{fr}} \cdot t_k}$.

If we look from a mathematical perspective, need to act with each of the operators on the electron density ρ.

$$
\frac{\mathrm{d}}{\mathrm{d}t}\hat{\rho}(t) = -iL\hat{\rho}(t)
\tag{Eq. 1.2.2}
$$

$$
= -\frac{i}{\hbar}[H, \rho(t)] + \Gamma\rho(t)
\tag{Eq. 1.2.3}
$$

This equation is solvable if the Hamiltonian is defined. Working it out is done elsewhere[13, 14]. The conclusion is that this will lead to Lorenzian line shapes. This will be elaborated in Chapter 3.

1.3 Multidimensional Spectroscopy

We can measure the Feynman diagrams of section 1.2 (previous page), with ultrafast spectroscopy methods. Depending on the number of light pulses or interactions, we can measure absorption, fluorescence, multidimensional spectroscopy (e.g. 2DES), or even flurescence detected multidimensional spectroscopy (e.g. FD-2DES).

There are many different kinds of multidimensional experiments. In this thesis, we try to predict and rationalize the results of FD-2DES spectra, a relatively new technique in which 4 laser-pulses are used., however, we cannot understand the 4-pulse experiment without understanding the 3-pulse experiment.

1.3.1 Absorption & Fluorescence

Absorption and fluorescence fall under linear spectroscopy, but they can also be a step in multidimensional spectroscopy. In order for light to have a chance of being absorbed, we need to have photons which are resonant with the states present in the sample, see Figure 1.5. Therefore, the spectrum of the pulsed laser used in multidimensional spectroscopy is tuned so that it is resonant with the states in our sample. In Figure 1.6 we see an example of a laser-spectrum which is used in an ultra fast spectroscopy experiment, to measure the kinetics between the B800/B850 bands within LH2. Also shown are the absorption spectra of B800/B850; the chlorophores in LH2.

If we were to do a 3-pulse experiment, we would need to measure the signal of our stimulated emission pulse above $\lambda \geq 875$ nm, else we would measure a lot of background intensity from the laser pulse used. Emission of B800 cannot be
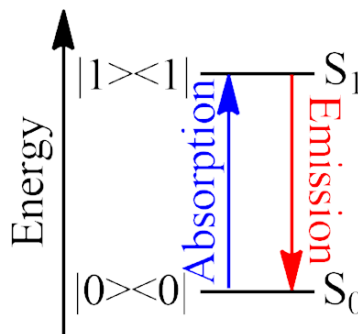
Figure 1.5: A two-level system, indicating a ground state ($\langle 00|$ in Dirac notation, S_0 in Jablonski-diagram notation) and the first excited state ($\langle 11|$ in Dirac notation, S_1 in Jablonski-diagram notation). The transition from the ground state to the first excited state are absorption and emission.
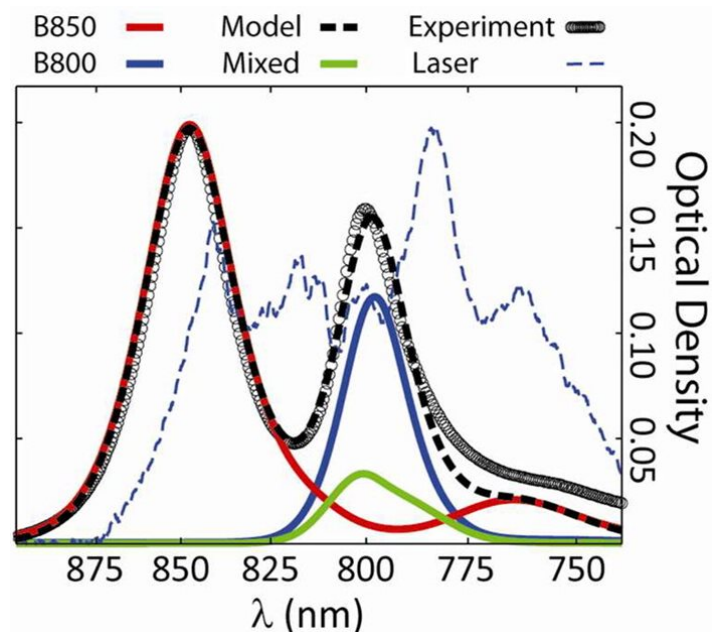
Figure 1.6: Experimental absorption spectrum (black circles) of the LH2 complex and model (black dashed). The theoretical model can be decomposed into contributions from the B850 pigments (red), B800 pigments (blue), and mixed character states (green). The experimental spectrum of the laser pulse is also shown (dashed blue). Reprinted with permission from Ref. [15]. Copyright 2013 American Chemical Society.

measured, as emission from B800 completely overlaps with the laser spectrum, see Figure 1.6.

1.3.2   2DES: The 3-pulse experiment

In the 3-pulse experiment, three light pulses enter the system at different time intervals, see Figure 1.7.

(a) The 3-pulse train experiment

(b) An example of a 2DES spectrum

Figure 1.7: The 3-pulse experiment.
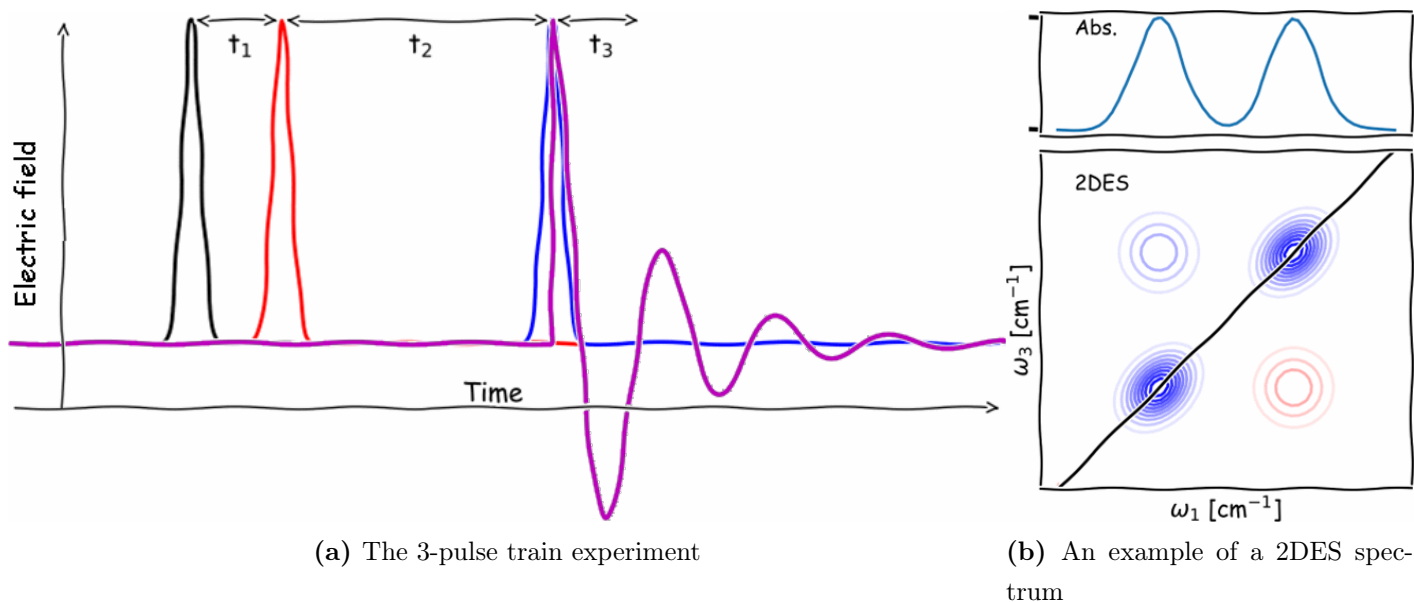**(A)** The 3-pulse train. The first pulse (**black**) brings the system in a electronic vibrating state, after which the electrons are oscillating during t_1. The second pulse (**red**) brings the system in a full excited state, in which the electrons are no longer rapidly oscillating. The third pulse (**blue**) brings the system in a electronic vibrating state again; but this time, we record the signal of this vibrating state (**purple**). Figures 1.8 and 1.9 explain the events in t_1 and t_3 in a more visually attractive way.
(B) When the measured stimulated emission intensity is plotted as a function of ω_1 (Fourier transform of t_1) and ω_3 (Fourier transform of t_3), one obtains a two dimensional electronic spectrum (2DES).

1. The first pulse brings the system in vibration with frequency ω_1.

2. The second pulse stops this oscillation by either bringing the molecule/system to the stable ground state ($|00\rangle$) or excited state ($|11\rangle$). Usually the second time delay (t_2) is fixed.

3. The third pulse is called the measurement. The third pulse leaves the system in an oscillating state, which will emit a photon (purple line in Figure 1.7a). This process is also called stimulated emission. Phase-wise, the electrons could either oscillate in the same phase, or in the other phase, this gives the difference between rephasing and nonrephasing, better explained on the next page.

The pulse sequence and the transitions within the system are best described by the double sided Feynman diagrams shown in Eq. 1.3.1.

(a) 6 runners start to run.

$$\text{Rephasing} \quad t_2 \left[\begin{array}{ccc} \textbf{GB} & \textbf{SE} & \textbf{EA} \\ \begin{array}{|c} 00 \\ 10 \\ 00 \\ 01 \\ 00 \end{array} & \begin{array}{|c} 00 \\ 10 \\ 11 \\ 01 \\ 00 \end{array} & \begin{array}{|c} 11 \\ 21 \\ 11 \\ 01 \\ 00 \end{array} \end{array} \right] t_2 \qquad \text{(Eq. 1.3.1a)}$$

$$\text{Nonrephasing} \quad t_2 \left[\begin{array}{ccc} \textbf{GB} & \textbf{SE} & \textbf{EA} \\ \begin{array}{|c} 00 \\ 10 \\ 00 \\ 10 \\ 00 \end{array} & \begin{array}{|c} 00 \\ 10 \\ 11 \\ 10 \\ 00 \end{array} & \begin{array}{|c} 00 \\ 21 \\ 11 \\ 10 \\ 00 \end{array} \end{array} \right] t_2 \qquad \text{(Eq. 1.3.1b)}$$

When a photon excites a molecule, an electron-hole pair is generated. This is also called an exciton.

The difference between rephasing and nonrephasing can best be described by looking at the system from the perspective of the electron-hole pairs. If this is difficult, just consider the electron. Picture them as runners. The first pulse initiates polarization in the sample, after which the electron-hole-pair starts oscillating. From a quantum mechanical point of view, the complex wavefunction starts rotating in the complex plane. The complex plane can be represented as a complex unit circle. Lets represent each oscillator with a runner (Figure 1.8a). The oscillation can visualized as that the runners start running in a circle. Not every electron is exactly in the same environment, so each electron will oscillate with a slightly different frequency. This can be visualized as that the runners have a slightly different running speed amongst each other, see Figure 1.8. The "start" and "stop" of the referee are the black and the red pulse of Figure 1.7a/1.11a. The stop-pulse also indicates the start of t_2, after which the runners will start changing their local environment, after which the resonance frequency changes. This is indicated by a change of color (compare Figure 1.8d with Figure 1.9a). Note that Figure 1.8 continues in Figure 1.9.
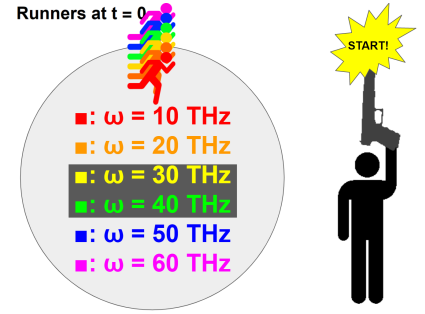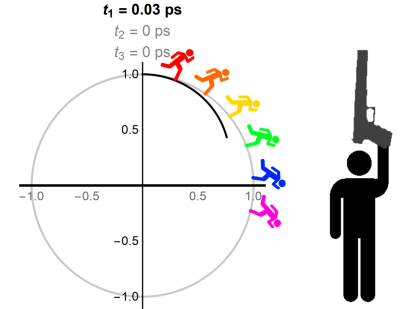
(b) They run at different speeds.
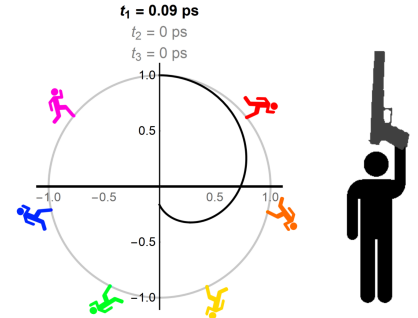
(c) We observe severe dephasing.

(d) When the second pulse arrives, the runners stop running; the system is in a stationary state.

Figure 1.8: All the events that occur during t_1 of Figures 1.7a/1.11a.

As indicated on page 7, the second time delay (t_2) is usually fixed, but in section 3.2, we will also show an experiment in which t_2 could 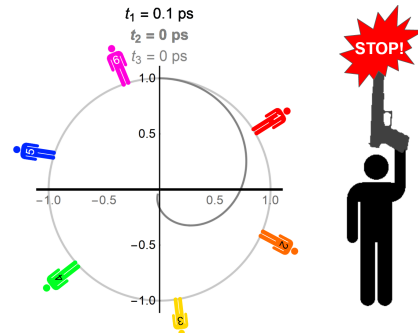be varied. This could be done to observe beating patterns, which happens if two molecules oscillate with a slightly different frequency.

During t_2, the electrons change their local environment a bit, which means that the standard frequency by which they oscillate will change a bit. This is indicated in Figure 1.9a by the fact that the runners change color. Note that the runners don't change position! The position (or identity) of the runners is labeled with a number on their chest (compare Figure 1.9a with Figure 1.8d).

After t_2, we have the third pulse (blue pulse of Figures 1.7a/1.11a), after which the system will be oscillating again.

1.3.3 Distinction between the 3-pulse experiment and the 4-pulse experiment

In the **3-pulse experiment**, the system will be left in the oscillating state, which by nature will emit photons. Since this oscillating state was induced by another photon or light pulse, this process is also called stimulated emission. Another name by which this goes is "the measurement", because the system will be emitting photons which we will collect for our measurement.

In the **4-pulse experiment**, we give the system another pulse (see green line in Figure 1.11a on page 11) at a time at which the bulk polarization is maximal again. This typically is around $t_3 = t_1$, see Figure 1.9d. After that, the system is allowed to spontaneously emit photons. t_4 isn't fixed; all photons after the 4th pulse are collected.
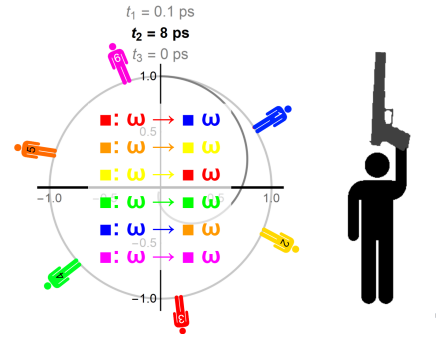
(a) During t_2, runners change color.
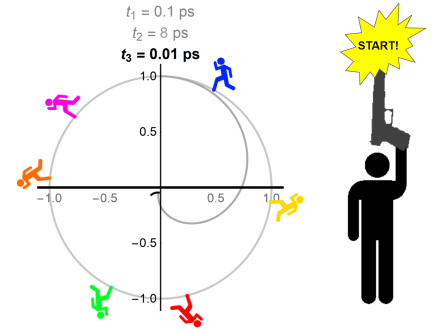
(b) For rephasing, the runners run in the opposite direction.
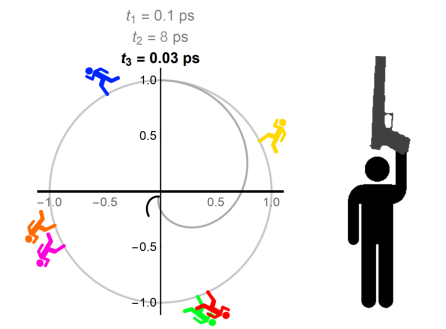
(c) A bulk polarization reappears!
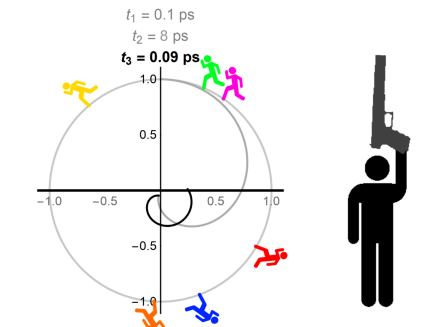
(d) Around the point $t_3 = t_1$, we sometimes observe a maximum in bulk polarization.

Figure 1.9: All the events that occur during t_3 of Figure 1.7a/1.11a.

1.3.4 The 4-pulse experiment

In the 4-pulse experiment, we stop the runners after t_3. The sample is then left undisturbed, and we measure the spontaneous emission of photons, see Figure 1.10. The signal-to-noise ratio of Fluorescence Detected two dimensional spectroscopy (FD-2DES) is remarkably higher than for conventional 2DES, because the measurement is done in the dark, without background noise of the 3rd pulse.

(a) The 4th pulse stops the oscillators from oscillating.

(b) Fluorescence of a molecule.

(c) Fluorescence of another molecule.
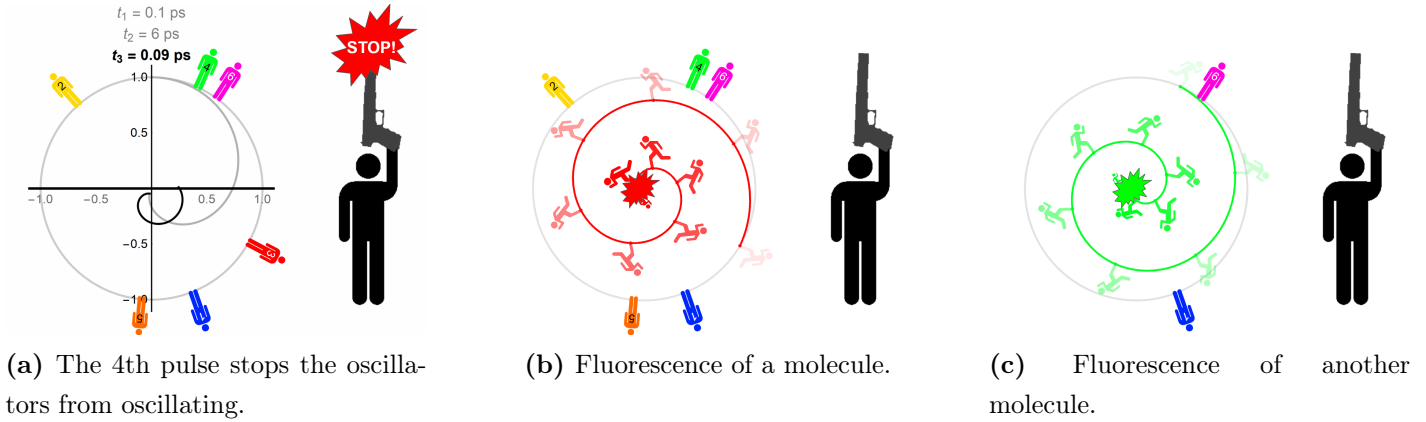
Figure 1.10: The events during t_4 of Figure 1.11. Note that each molecule which spontaneously emits a photon creates it's own wiggle in the electric field (purple line), after a distinct t_4.

The Feynman diagrams for FD-2DES is shown in Eq. 1.3.2.

(Eq. 1.3.2a)

(Eq. 1.3.2b)

We will refer to the Feynman diagrams with 4 laser-pulses (Eq. 1.3.2) again in the Theory chapter (Chapter 3). In section 3.1, we will discuss the spectral line-shapes which we can observe in FD-2DES

experiments. In 3.2, we fill in Eq. 1.3.2 for two molecules; instead of 1 and 2 we will use A or B and A^2 or B^2 to refer to excited states in different molecules.

(a) The pulse-train for a 4-pulse experiment.

(b) Schematic FD-2DES spectrum
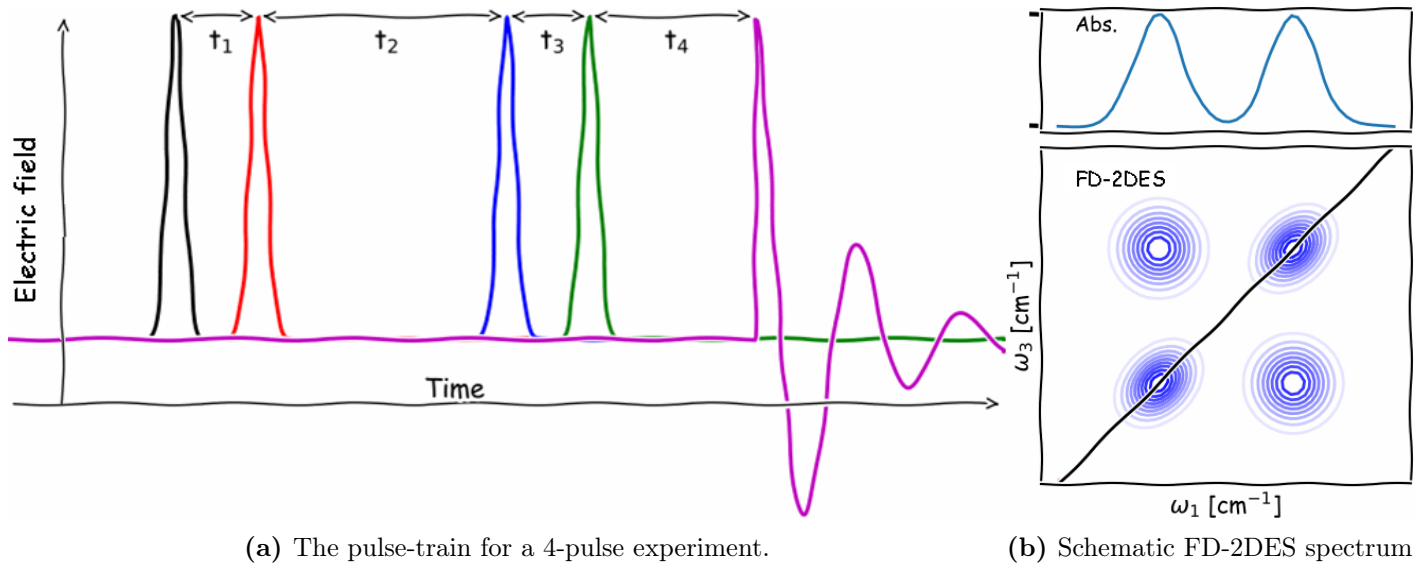
Figure 1.11: The 4-pulse experiment.

(A) The 4-pulse train. The first pulse (**black**) brings the system in a electronic vibrating state, after which the electrons are oscillating during t_1. The second pulse (**red**) brings the system in a full excited state, in which the electrons are no longer rapidly oscillating. The third pulse (**blue**) brings the system in a electronic vibrating state again; but this time, the signal is just partially rephased (or nonrephased), see Figure 1.9, until the oscillation is stopped with a fourth pulse (**green**). The system is now (during t_4 in a properly excited, non oscillating state. At rest, this system will spontaneously emit photons (indicated by the **purple** curve). Figures 1.8 and 1.9 explain the events in t_1 and t_3 in a more visually attractive way.

(B) When the measured fluorescence intensity as a function of ω_1 (Fourier transform of t_1) and ω_3 (Fourier transform of t_3) is plotted, one obtains a fluorescence detected two dimensional electronic spectrum (FD-2DES).

The signal pattern we get out of a Fluorescence Detected Two Dimensional Spectroscopy (FD-2DES) experiment, e.g. Figure 1.11b, is still not fully understood. This is the main reason why this thesis performs the theoretical analysis for the FD-2DES experiment.

1.4 Outline

Chapter 2 is the methods-chapter, which introduces the Master equations. For each component of the master equation, an example will be demonstrated, with as final product, a master-equation-matrix for a dimer. Of course, building these matrices manually would be tedious, therefore I've written some code which automatically generates the master-equation-matrix for any given/generated $n \times m$-LH-matrix. The documentation of the code is given in Appendix B, recommended for anyone who would like to redo these computational experiments.

The simulations spit out photon intensities for each different starting configuration. Unfortunately, these raw intensities barely make any sense when we try to compare it with an experiment: all intensities are dependent on how many photons are emitted from the system. Fortunately, experiments also give frequency information for which the system is sensitive. In order to make the connection between the diagrams and the measured spectra, we need theory on Feynman diagrams (Chapter 3) before we can build an equation for the relative intensities of the cross-peaks and the diagonal peaks. When we calculate this, we will be consider this the results (Chapter 4).

Chapter 2

Methods: Setting up Python and formulating the Master equations

This is the methods chapter. Besides the version declarations of Python, this chapter can best be read as a technical introduction: it will introduce all the exciton dynamics processes that are taken into account. Each dynamics process is like a small puzzle piece. In the end (section 2.2.5), we bring all the puzzle pieces together, and we can start building the Master equations. In section 2.2.4 we build a small test code in Mathematica, for the B800/B850 system within LH2. The results of that section allow us to generate some numbers for intensity for a doubly excited state, which we can use in our Theory chapter. This makes the theory a little less dusty, and a little more visual.

2.1 Setup

I'm using Python version 3.6.3[16]. Within Python, I use the `numpy` package, with version 1.14.3[17].

The two dimensional electronic spectroscopy (2DES) plots of Chapter 3 are made with Mathematica 12[18]. This version of Mathematica is used to perform the simulations on the B800/B850 system in section 2.2.4.

2.2 Formulating The Master equations

For this master thesis, the master equations are evaluated. This sounds more complicated than it actually is. The master equations are a set of equations which model the kinetics of excited states in our system. In the following section, the master equations is built up, step by step.

Before we start, I will define an example system. Imagine 2 molecules, molecule A and molecule B, which are close to each other. For each molecule, we can write a probability that the excited state is on that molecule. If we were dealing with only one exciton, for each molecule we can write the probability ρ that the exciton on that molecule. Since we will deal with multiple excitons later, we should label the states. Let's define these states rightaway:

- `AA` or A^2 (describing the $A^2 + B^0$ state),

- `BB` or B^2 (describing the $B^2 + A^0$ state),

- `AB` (describing the $A^1 + B^1$ state),

- `AG` (describing the $A^1 + B^0$ state),

- `BG` (describing the $B^1 + A^0$ state),

- `GG` (describing the $A^0 + B^0$ state).

The superscript indicates in which state each molecule is, 0 being the groundstate. We will solve differential equations with respect to time on these variables. If we call

$$\text{AG}(0) = 1, \text{ we mean that on t=0, we have } \rho(A) = 1 \text{ and } \rho(B) = 0 \qquad \text{(Eq. 2.2.1a)}$$

$$\text{BG}(0) = 1, \text{ we mean that on t=0, we have } \rho(A) = 0 \text{ and } \rho(B) = 1 \qquad \text{(Eq. 2.2.1b)}$$

The simulation tracks the probability that the system has evolved from one state to another.

2.2.1 Fluorescence.

When a molecule is in an excited state, there is a probability that the molecule spontaneously emits a photon[20]. This process, also known as fluorescence, takes both the radiative rate and the nonradiative rate into account as follows:

$$k_F = k_R + k_{NR} \qquad \text{(Eq. 2.2.2)}$$

The part of the rate equations dedicated to the spontaneous emission looks as follows:

$$\frac{\mathrm{d}(\mathtt{AG})}{\mathrm{d}t} = -\underbrace{k_{A \to G} \cdot \mathtt{AG}(t)}_{\mathbf{X^1 \; Fluorescence}} \qquad \text{(Eq. 2.2.3a)}$$

$$\frac{\mathrm{d}(\mathtt{BG})}{\mathrm{d}t} = -\underbrace{k_{B \to G} \cdot \mathtt{BG}(t)} \qquad \text{(Eq. 2.2.3b)}$$

If we consider molecule A to be LH1, with a fluorescence lifetime of 0.680 ns, and molecule B to be LH2, with a fluorescence lifetime of 0.986 ns[19], the numerical solution for these differential equations are:

Decay due to fluorescence

Figure 2.1: Population density according to a simulation which only includes fluorescence. The fluorescence lifetime is 0.680 ns for LH1 and 0.986 ns for LH2[19].

$$\textbf{LH1:} \; \mathtt{AG}(t) = e^{-\frac{t}{0.680 \text{ ns}}}, \qquad \text{(Eq. 2.2.4a)}$$

$$\textbf{LH2:} \; \mathtt{BG}(t) = e^{-\frac{t}{0.986 \text{ ns}}}, \qquad \text{(Eq. 2.2.4b)}$$

also see plot in Figure 2.1.

Eventually, we will do photon-counting, and we will need to take the radiative rate k_R into account. This is given in literature[10, 19]. For completeness, the Nonradiative lifetime k_{NR} can be calculated as follows:

$$k_{NR} = k_F - k_R = \frac{1}{\tau_F} - \frac{1}{\tau_R}, \qquad \text{(Eq. 2.2.5)}$$

and the results are listed in Table 2.1.

\	Fluorescence Lifetime τ_F	Radiative Lifetime τ_R	Radiative Rate k_R	Nonadiative Rate k_{NR}	Ref.
LH2	0.986 ns	10 ns	0.10 ns^{-1}	0.91 ns^{-1}	[19]
LH1	0.680 ns	8.4 ns	0.12 ns^{-1}	1.35 ns^{-1}	[19]

Table 2.1: Values for the LH1/LH2 (non)radiative rates. All numbers were found in Ref. [19].

2.2.2 Energy transfer.

The excited state or exciton can move from molecule A to molecule B and vise versa, see Eq. 2.2.6:

$$A + B^* \underset{k_{A \to B}}{\overset{k_{B \to A}}{\rightleftharpoons}} A^* + B, \quad \text{or} \quad BG \underset{k_{A \to B}}{\overset{k_{B \to A}}{\rightleftharpoons}} AG \quad \text{(Eq. 2.2.6)}$$
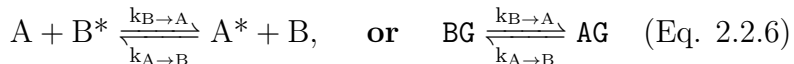
in standard notation. The ratio between the two rates $\frac{k_{A \to B}}{k_{B \to A}}$ is dependent on the energy difference between the two energy levels in the molecules, according to a Maxwell-Boltzmann distribution,

$$\frac{k_{B \to A}}{k_{A \to B}} = \frac{g_A}{g_B} \cdot e^{\frac{E_B - E_A}{k_B T}}, \quad \text{(Eq. 2.2.7)}$$

in which $\frac{g_A}{g_B}$ is the ratio between the number of molecules A and B in the system. This is relevant when we do simulations on the B800/B850 system within LH2; as there are twice as many B850 molecules than there are B800 molecules (recall Figure 1.2 on page 3). For now, however, I've decided to only focus on the LH1/LH2 system, and we will take $\frac{g_A}{g_B} = 1$, as the other Light Harvesting complexes will be added explicitly.

Eq. 2.2.7 is filled in (see Appendix Eq. A.1.3) to give:

$$\frac{k_{LH1 \to LH2}}{k_{LH2 \to LH1}} = 21.34\% \quad \text{(Eq. 2.2.8)}$$

Note that the absolute rate also depends on distance. The mean energy transfer rates are published in literature, see Table 2.2.

(a) Starting from LH1 (molecule A).
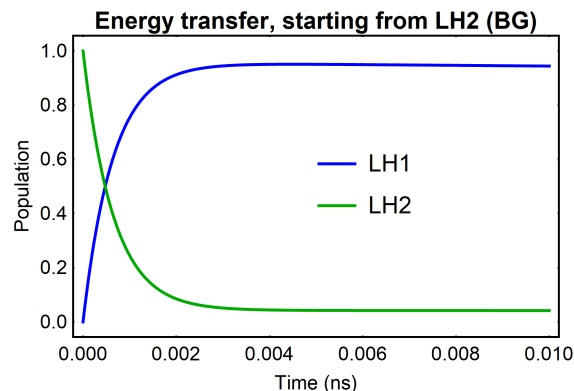
(b) Starting from LH2 (molecule B).

Figure 2.2: Exciton population density, according to a simulation on a LH1-LH2 dimer, with one excited state. The simulation includes energy transfer as described in Eq. 2.2.9, with rates from Rsp. photometricum[7]. Fluorescence is included but not visible on this time-scale.

Adding the energy transfer process to the rate equations, our master equations become as follows:

$$\frac{d(AG)}{dt} = \text{Eq. 2.2.3a} - \underbrace{k_{A \to B} \cdot AG(t)}_{A^1 \to B^1} + \underbrace{k_{B \to A} \cdot BG(t)}_{B^1 \to A^1} \quad \text{(Eq. 2.2.9a)}$$

$$\frac{d(BG)}{dt} = \text{Eq. 2.2.3b} + \underbrace{k_{A \to B} \cdot AG(t)}_{} - \underbrace{k_{B \to A} \cdot BG(t)}_{} \quad \text{(Eq. 2.2.9b)}$$

Species	LH2→LH1 rate constant	LH1→LH2	Reference
Rsp. photometricum	1.5 ps (670 ± 60 ns^{-1})	144 ± 10 ns^{-1}	[7]
Rps. acidophila	3-5 ps (250 ± 70 ns^{-1})	53 ± 14 ns^{-1}	[11]

Table 2.2: Values for LH2 $\rightleftharpoons$ LH1 exciton transfer rate. Calculations are done in Appendix section A.1 on page 70.

The differential equations of Eq. 2.2.9, for a LH1/LH2 dimer system, with the numbers of Rsp. photo-metricum, are solved with Mathematica, and gives Figure 2.2 on the preceding page.

Note that the energy transfer process between two Light Harvesting complexes is Förster Resonance Energy Transfer (FRET)[21]. The rate (k_{FRET}) and efficiency (η_{FRET}) of any FRET process is strongly dependent on distance, because it is dependent on the dipole-dipole coupling between the donor and the acceptor. The electric fields of a dipole scale as r^{-3}, and therefore, FRET scales as $(r^{-3})^2 = r^{-6}$.

$$\eta_{FRET} = \frac{k_{FRET}}{k_{FRET} + k_F + \sum k_i} = \frac{1}{1 + \left(\frac{r}{R_0}\right)^6} \qquad \leftrightarrow \qquad k_{FRET}(r) \propto \frac{k_{FRET}(R_0)}{r^6} \qquad \text{(Eq. 2.2.10)}$$

There are a lot more experiments published on the energy transfer process within LH2[22, 23, 24, 15] than there are known experiments between one LH1 and one LH2 light harvesting complexes. There is no experimental rate between two LH2 molecules, however, in 2014, Danielle E. Chandler and Klaus Schulten et al did manage to determine these transfer rates using Hierarchical equations of motion (HEOM) calculations[7], see Figure 2.3.
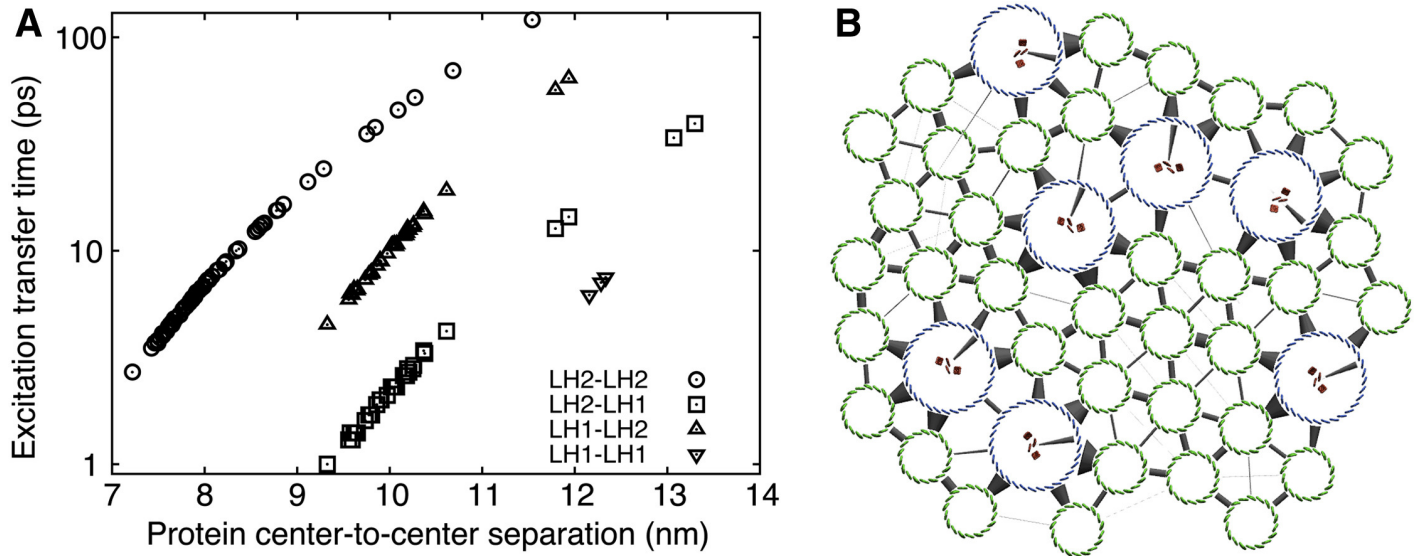
Figure 2.3: (A) Exciton transfer time as determined by Hierarchical equations of motion (HEOM) calculations performed in ref. [7]. Reprinted with permission from Ref. [7].

2.2.3 Nonlinear processes (Exciton annihilation).

Before I storm off with nonlinear optics, it's good to point out that nonlinear optics is only possible in systems with more than two states. In a real system with more than one electron, there is an infinite number of states, but this is over-kill, as most of the states are not optically relevant. For the light harvesting complexes, we typically only look at the ground state and the first excited state, but we now need at least one more state. There is not so much information available on the other energy-levels of the system, and therefore I assumed that the system only consisted of 3 energy-levels: ground state (0), first excited state (1) and second excited state (2), in which the second excited state has twice as much energy as the first excited state ($\omega_{02} \approx 2\omega_{01}$), similar to Figure 2.4. In reality, $\omega_{12} > \omega_{01}$, because there is a bit of anharmonicity[2], but this will be discussed further discussed in section 3.2.3.
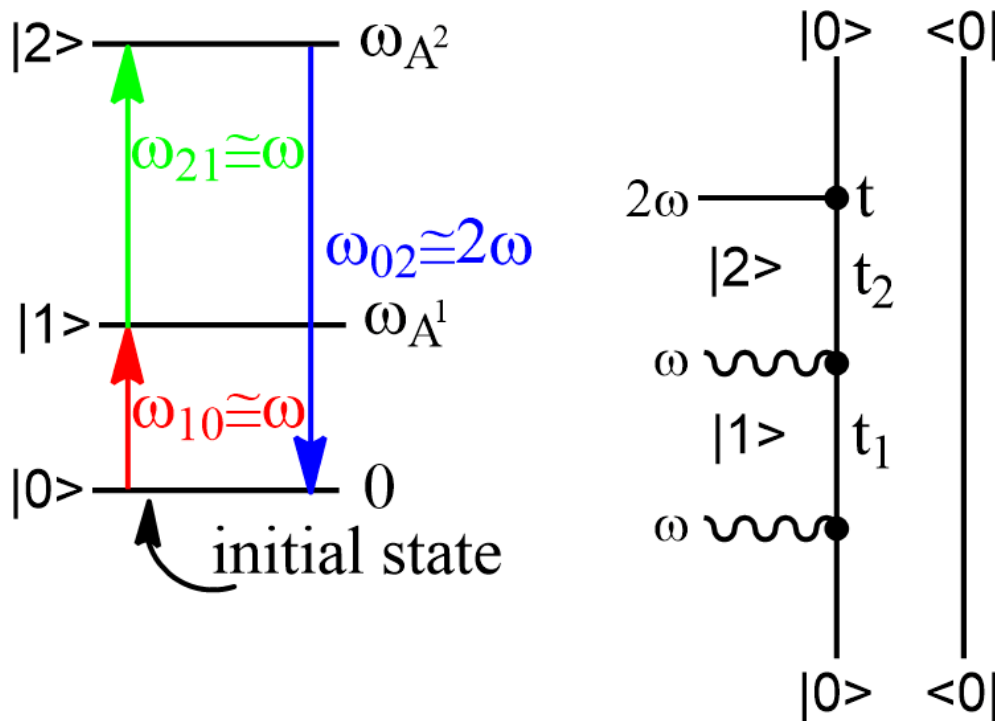
Figure 2.4: A 3-level-system with an example double sided Feynman diagram. The states $|0\rangle, |1\rangle$ and $|2\rangle$ resonate with frequencies $0, \omega_{A^1}$ and ω_{A^2}

Typically, a nonlinear process occurs when there are two or more photons interacting with a crystal at the same time. These interactions are indicated by the $\sim\!\!\sim\!\!\sim$ in the right-half of Figure 2.4. However, as we work with a medium which is pretty good at absorbing photons and temporally storing this excited state energy as a exciton, we could also take a look at the situation where there are more excitons instead of more photons.

These double sided Feynman diagrams are further explained and described in detail in Chapter 3 because they can tell us many things about how the two-dimension electronic spectroscopy (2DES)

---

[2]   The anharmonicity constant is measured in Fig. 4a of Ref. [10] and is approximately 233 cm^{-1}.

graphs look like.

When there are two (or more) excitons in a network of light harvesting molecules, there is a probability that the two excited states end up on the same molecule, generating a higher excited state on one molecule. When the energy levels are organized as in Figure 2.4, we will obtain the second excited state. For light harvesting systems, the second excited state is short lived[10], which basically means that this results in exciton annihilation. This process is outlined in Figure 2.5.
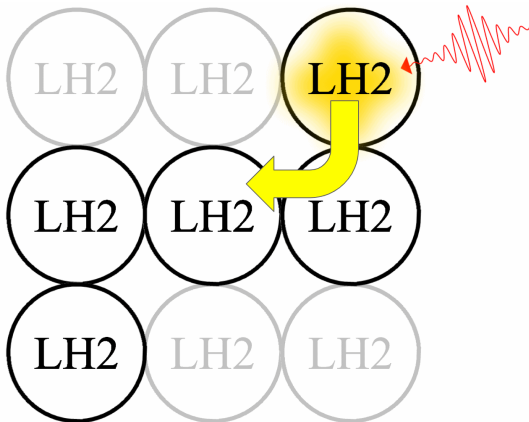
(a) When a photon is absorbed, an excited state is generated. The excited state (or exciton) migrates over the LH2 network.
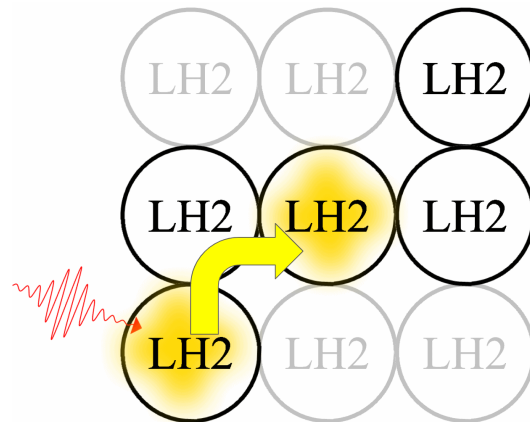
(b) Another exciton is generated by absorption of a second photon. The two excitons keep migrating over the LH2 network, until they encounter each other on the same LH2 unit.
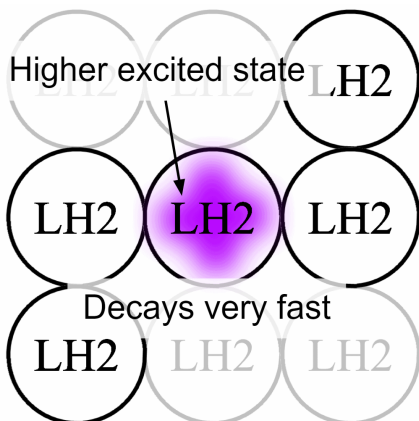
(c) When the two excited states $(|1\rangle + |1\rangle)$ end up on the same LH2 unit, a higher excited state $|2\rangle$ is generated.
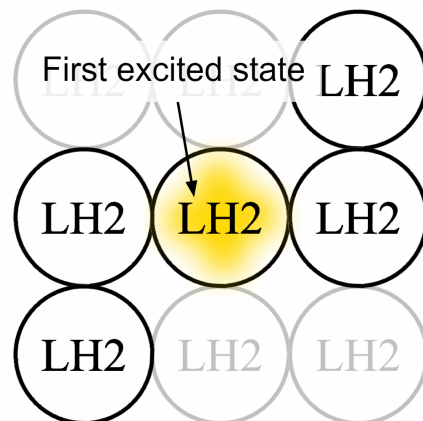
(d) The higher excited state $|2\rangle$ is unstable and very rapidly decays to the first excited state $|1\rangle$ without emitting a photon. The net effect is that one single excited state $|1\rangle$ is annihilated.

Figure 2.5: Key-processes which cause nonlinear optic effects in our system, where instead of multiple photons in the same femtosecond hitting the same light harvesting complex, we have multiple excitons.

As mentioned on page 14, for a dimer, we have 6 different states. The challenge is now to write out the pathways how one state is converted to the other state.

When we have both molecule A and B in the excited state, one excited state can hop from A to B with rate $k_{A \to B}$, or from B to A with rate $k_{B \to A}$. These rates ($k_{A \to B}$ and $k_{B \to A}$) are tabulated in Table 2.2 on page 16. When one exciton hops from one excited light harvesting complex to the other excited light harvesting complex, the 2nd excited state is generated on that other light harvesting complex. This could either be $A^1 + B^1 \to A^2 + B^0$ or $A^1 + B^1 \to A^2 + B^0$.

Another process which is present, is fluorescence. Fluorescence can either

Figure 2.6: The kinetic model for the A/B dimer, in which the key conversion rates between the states are indicated. The numbers filled in are for A and B being LH1 and LH2 respectively. For energy transfer, took the numbers of Rsp. photometricum, see Table 2.2[7]. For fluorescence, I took the numbers of Table 2.1[19].

occur from the A^1 or B^1 state, leaving the BG or AG states behind. It must be noted that, for a dimer, the fluorescence pathway is less dominant than second-excited state generation, e.g. see Figure 2.6, where the exciton diffusion pathways are at least 2 orders of magnitude greater than the fluorescence pathways.

$$\frac{\mathrm{d}(\mathtt{AB})}{\mathrm{d}t} = -(\underbrace{k_{A \to A^2} + k_{B \to B^2}}_{\mathbf{X^2 \ Formation}} + \underbrace{k_{A \to G} + k_{B \to G}}_{\mathbf{X^1 \ Fluorescence}}) \cdot \mathtt{AB}(t) \tag{Eq. 2.2.11}$$

That already makes the first differential equation that needs to be solved. Other differential equations are for the 2nd excited state:

$$\frac{\mathrm{d}(\mathtt{A^2})}{\mathrm{d}t} = \underbrace{k_{A \to A^2} \cdot \mathtt{AB}(t)}_{\mathbf{X^2 \ Formation}} - \underbrace{(k_{A^2 \to A} + k_{A^2 \to G})\mathtt{A}^2(t)}_{\mathbf{X^2 \ Annihilation}} \tag{Eq. 2.2.12a}$$

$$\frac{\mathrm{d}(\mathtt{B^2})}{\mathrm{d}t} = k_{B \to B^2} \cdot \mathtt{AB}(t) - (k_{B^2 \to B} + k_{B^2 \to G})\mathtt{B}^2(t) \tag{Eq. 2.2.12b}$$

and for the 1st excited state:

$$\frac{\mathrm{d}(\mathtt{AG})}{\mathrm{d}t} = \text{Eq. 2.2.9a} \underbrace{-k_{A \to G} \cdot \mathtt{AG}(t)}_{} \underbrace{+k_{B \to G} \cdot \mathtt{AB}(t)}_{} \underbrace{+k_{A^2 \to A}\mathtt{A}^2(t)}_{} \tag{Eq. 2.2.13a}$$

$$\frac{\mathrm{d}(\mathtt{BG})}{\mathrm{d}t} = \text{Eq. 2.2.9b} \underbrace{-k_{B \to G} \cdot \mathtt{BG}(t)}_{\mathbf{X^1 \ Fluorescence}} \underbrace{+k_{A \to G} \cdot \mathtt{AB}(t)}_{\mathbf{Y^1 \ Fluorescence}} \underbrace{+k_{B^2 \to B}\mathtt{B}^2(t)}_{\mathbf{X^2 \ Annihilation}} \tag{Eq. 2.2.13b}$$

For completeness, the full groundstate (GG) is expressed as:

$$\frac{\mathrm{d}(\mathtt{GG})}{\mathrm{d}t} = \underbrace{k_{B \to G} \cdot \mathtt{BG}(t) + k_{A \to G} \cdot \mathtt{AG}(t)}_{\mathbf{X^1 \ Fluorescence}} + \underbrace{k_{A^2 \to G}\mathtt{A}^2(t) + k_{B^2 \to G}\mathtt{B}^2(t)}_{\mathbf{X^2 \ Annihilation}} \tag{Eq. 2.2.14}$$

The only number I could find in literature for the rate at which the annihilation process takes place, is for the LH2 complex of Rhodobacter sphaeroides[10]:

$$k_{B^2 \to B} = \frac{1}{0.59 \text{ ps}} = \frac{1}{0.00059 \text{ ns}} = 1695 \text{ ns}^{-1}, \quad \text{(Eq. 2.2.15)}$$

but it's the only number known, so we will assume that this number is also representative for LH1 and for other species (e.g. acidophila strain 10050). We also assume that $k_{A^2 \to G} = k_{B^2 \to G} = 0$ (hence the red cross in Eq. 2.2.14). This assumption is supported by the experiments performed in Ref. [25].

The result of a simulation of a dimer, in which both LH1 and LH2 are excited is shown in Figure 2.7.
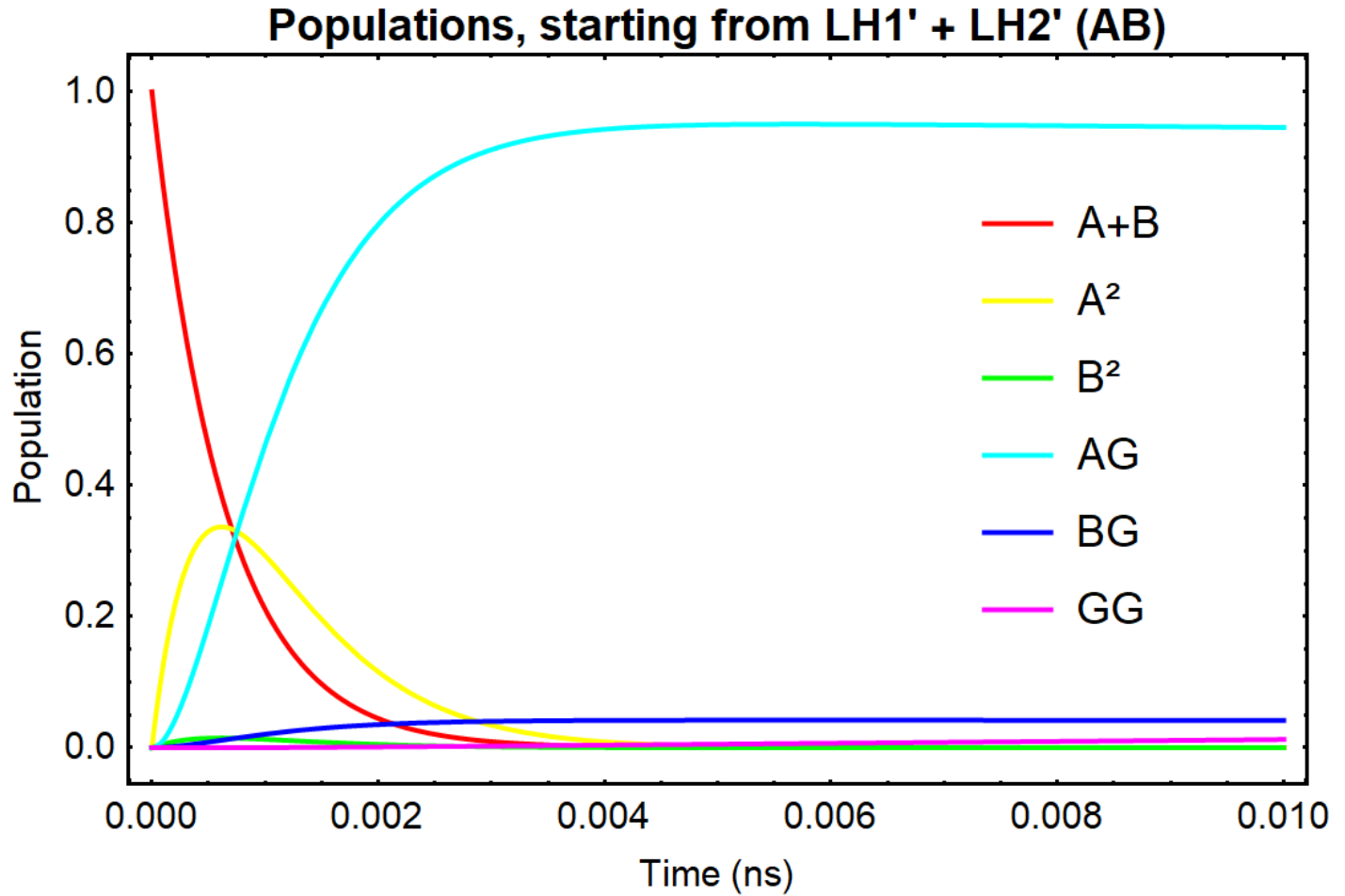
Figure 2.7: The first 10 picoseconds of the population density, according to a simulation of a LH1 - LH2 dimer. In this simulation, we start with an initial configuration in which both LH1 and LH2 hold one excited state. This model also incorporates kinetic equations Eq. 2.2.11 to Eq. 2.2.14. The first 10 picoseconds show how the population changes due to the nonlinear processes. After that, fluorescence takes over as the dominant process. After 10 nanoseconds, we obtain that only state populated is the ground state (**GG**). Figure 3.10a on page 35 shows a similar simulation, but then upto 10 nanoseconds, and for the B800/B850 system within LH2.

2.2.4   Building a Mathematica simulation for B800/B850 within LH2

Figure 2.7 was made using Mathematica. The same code used for the LH1/LH2 dimer could also be used (with a few modifications) to simulate the B800/B850 bands within LH2. Because the LH2 system can be considered as a closed system, it is easier to understand, and therefore these simulations are an easy introduction to the bigger simulations explained in the next section (Section 2.2.5).

In the Mathematica notebook, I use `DSolve` or `NDSolve`, depending on whether we want an equation or a numerical result. Both functions use the same differential equations defined throughout this section (Formulating The Master equations, starting on page 14) but with different settings for exciton dynamics. The exciton transfer rate is different because the energy of the B850/B800 bands is different from

Figure 2.8: The B800/B850 system within LH2. Reprinted from Ref. [10].

the B850/B875 bands. The transfer rates used here are tabulated in Table 2.3.

Species	B800→B850 rate constant	B850→B800	Reference
Rb. sphaeroides	0.7 ps (1430 ± 100 ns^{-1})	24 ± 2 ns^{-1}	[22] (via [26])
Rps. acidophila 10050	0.9 ps (1110 ± 60 ns^{-1})	19 ± 1 ns^{-1}	[23, 24] (via [26])

Table 2.3: Values for the B800 $\rightleftharpoons$ B850 exciton transfer rate.

We will be using the fluorescence lifetime for LH2 tabulated in Table 2.1 on page 15. The reason why there is no separate lifetime for the B800 and B850 bands is because the dynamics within the LH2 is faster than exciton decay, so the separate decay rates are simply impossible to measure experimentally.

The Mathematica simulation is available as a download[3]. The output of this notebook used throughout this entire thesis. I will refer to this section when use of the Mathematica code was made.

2.2.5 Building The Master equations

Now that I've described all relevant kinetic processes in a dimer, we can start writing out the Master equation. The Master equation can be expanded so that it describes the processes in a network of many molecules, so that we can describe the exciton dynamics taking place in an arbitrary or specific antenna network.

Actually it's quite easy: we put all the rate constants in a matrix $\mathbf{K}$ to find the time-derivative of the populations $\vec{P}$:

$$\frac{\mathrm{d}\vec{P}}{\mathrm{d}t} = \mathbf{K}\vec{P} \tag{Eq. 2.2.16}$$

Since the rate constants are time-independent, the equation for the population matrix one timestep ($\mathrm{d}t$) ahead can be calculated via an integral as follows:

$$\int_{t'}^{t'+\mathrm{d}t} \frac{\mathrm{d}\vec{P}(t)}{\mathrm{d}t} \, \mathrm{d}t = \int_{t'}^{t'+\mathrm{d}t} \mathbf{K} \cdot \vec{P} \, \mathrm{d}t \tag{Eq. 2.2.17}$$

$$\vec{P}(t + \mathrm{d}t) - \vec{P}(t) = (t' + \mathrm{d}t - t')\mathbf{K} \cdot \vec{P}(t) \tag{Eq. 2.2.18}$$

Note that we have $\vec{P}(t)$ both left and right. We can bring $\vec{P}(t)$ from left to right by adding $\mathbf{I} \cdot \vec{P}(t)$ to both sides.

$$\vec{P}(t + \mathrm{d}t) = \mathrm{d}t \cdot \mathbf{K} + \vec{P} = (\mathrm{d}t \cdot \mathbf{K} + \mathbf{I}) \cdot \vec{P}(t) \tag{Eq. 2.2.19}$$

Let's consider a dimer of one LH1 and one LH2 unit, and let's take one simplification step: assume $k_{A^2 \to A} = k_{B^2 \to B} = \infty$. This simplification applies, as the annihilation process is much faster than the other processes. This allows us to reduce the number of states to take into consideration to $n*(n-1)+3$ instead of $n^2 + 3$. For the dimer, this means 4 states (instead of 6), and it allows us to take bigger timesteps without introducing numerical errors or unphysical negative probabilities.

Before we can start to write out the $\mathbf{K}$ matrix, we need to decide the order of elements in the matrix. I made the decision to write the identity matrix as follows:

$$\mathbf{I} = \begin{pmatrix}
 & & fgs & A(LH1) & B(LH2) & AB & Ph(LH1) & Ph(LH2) \\
 & & \vdots & \vdots & \vdots & \vdots & \vdots & \vdots \\
fgs & \cdots & 1 & 0 & 0 & 0 & 0 & 0 \\
A(LH1) & \cdots & 0 & 1 & 0 & 0 & 0 & 0 \\
B(LH2) & \cdots & 0 & 0 & 1 & 0 & 0 & 0 \\
AB & \cdots & 0 & 0 & 0 & 1 & 0 & 0 \\
Ph(LH1) & \cdots & 0 & 0 & 0 & 0 & 1 & 0 \\
Ph(LH2) & \cdots & 0 & 0 & 0 & 0 & 0 & 1
\end{pmatrix} \tag{Eq. 2.2.20}$$

Next, we can start writing out the $\mathbf{K}$-matrix, or actually, it makes more sense to write out the $\mathrm{d}t \cdot \mathbf{K} + \mathbf{I}$ matrix, since this is the matrix which we can raise to a certain power to obtain the probability of finding

excitons there then. Since it becomes tedious and chaotic to write out $dt \cdot k...$ for each element, let's first define short hand notation for rate times timestep:

$$r = dt \cdot k \qquad\qquad (\text{Eq. 2.2.21})$$

With this little simplification step, we can write out two transformation matrices: one for exciton transfer $\mathbf{K}_{tr}$ (movement over the antenna network), and one for fluorescence $\mathbf{K}_F$.

$$\mathbf{K}_{tr} = \begin{pmatrix} & & fgs & A(LH1) & B(LH2) & AB & Ph(LH1) & Ph(LH2) \\ & & \vdots & \vdots & \vdots & \vdots & \vdots & \vdots \\ fgs & \cdots & 1 & 0 & 0 & 0 & 0 & 0 \\ A(LH1) & \cdots & 0 & 1-r_{A\to B} & r_{A\to B} & 0 & 0 & 0 \\ B(LH2) & \cdots & 0 & r_{B\to A} & 1-r_{B\to A} & 0 & 0 & 0 \\ AB & \cdots & 0 & r_{B\to A} & r_{A\to B} & 1-(r_{A\to B}+r_{B\to A}) & 0 & 0 \\ Ph(LH1) & \cdots & 0 & 0 & 0 & 0 & 1 & 0 \\ Ph(LH2) & \cdots & 0 & 0 & 0 & 0 & 0 & 1 \end{pmatrix}$$

$$(\text{Eq. 2.2.22a})$$

$$\mathbf{K}_F = \begin{pmatrix} & & fgs & A(LH1) & B(LH2) & AB & Ph(LH1) & Ph(LH2) \\ & & \vdots & \vdots & \vdots & \vdots & \vdots & \vdots \\ fgs & \cdots & 1 & 0 & 0 & 0 & 0 & 0 \\ A(LH1) & \cdots & r_{A\to G} & 1-r_{A\to G} & 0 & 0 & f_{LH1} & 0 \\ B(LH2) & \cdots & r_{B\to G} & 0 & 1-r_{B\to G} & 0 & 0 & f_{LH2} \\ AB & \cdots & 0 & r_{B\to G} & r_{A\to G} & 1-(r_{A\to G}+r_{B\to G}) & f_{LH1} & f_{LH2} \\ Ph(LH1) & \cdots & 0 & 0 & 0 & 0 & 1 & 0 \\ Ph(LH2) & \cdots & 0 & 0 & 0 & 0 & 0 & 1 \end{pmatrix}$$

$$(\text{Eq. 2.2.22b})$$

Equations Eq. 2.2.22a and b are shown in Figures 2.9a and b respectively. The values filled in to make the equation numerical, are exciton transfer rates from Rsp. photometricum (Table 2.2[7]) and exciton lifetimes from (Table 2.1[19]). The rates are listed here (for a time-step of 0.1 ps):

LH2 → LH1: 676 ns^{-1} → $r_{B\to A} = 0.0676$ per timestep. $\qquad\qquad (\text{Eq. 2.2.23})$

LH1 → LH2: 144 ns^{-1} → $r_{A\to B} = 0.0144$ per timestep $\qquad\qquad (\text{Eq. 2.2.24})$

LH1 fluorescence: $r_{A\to G} = 0.000\,147$ per timestep → $r_{A\to G,R} = 0.000\,012$ per timestep. $\quad (\text{Eq. 2.2.25})$

LH2 fluorescence: $r_{B\to G} = 0.000\,101$ per timestep → $r_{B\to G,R} = 0.000\,010$ per timestep. $\quad (\text{Eq. 2.2.26})$

The last step in converting Eq. 2.2.22 to Figure 2.9 is applying some gradient-color-coding from Excel: `0 = cyan`, `0.07 = yellow`, `1 = orange`. This color scheme is used all over this Master-thesis.

Transport

	fgs	A/LH1	B/LH2	AB	Ph(LH1)	Ph(LH2)
fgs	1.000E+00	0.000E+00	0.000E+00	0.000E+00	0.000E+00	0.000E+00
A/LH1	0.000E+00	9.856E-01	1.443E-02	0.000E+00	0.000E+00	0.000E+00
B/LH2	0.000E+00	6.760E-02	9.324E-01	0.000E+00	0.000E+00	0.000E+00
AB	0.000E+00	6.760E-02	1.443E-02	9.180E-01	0.000E+00	0.000E+00
Ph1	0.000E+00	0.000E+00	0.000E+00	0.000E+00	1.000E+00	0.000E+00
Ph2	0.000E+00	0.000E+00	0.000E+00	0.000E+00	0.000E+00	1.000E+00

(a) The matrix describing exciton transfer (or transport).

Fluorescence

	fgs	A/LH1	B/LH2	AB	Ph(LH1)	Ph(LH2)
fgs	1.000E+00	0.000E+00	0.000E+00	0.000E+00	0.000E+00	0.000E+00
A/LH1	1.471E-04	9.999E-01	0.000E+00	0.000E+00	1.190E-05	0.000E+00
B/LH2	1.014E-04	0.000E+00	9.999E-01	0.000E+00	0.000E+00	1.000E-05
AB	0.000E+00	1.014E-04	1.471E-04	9.998E-01	1.190E-05	1.000E-05
Ph1	0.000E+00	0.000E+00	0.000E+00	0.000E+00	1.000E+00	0.000E+00
Ph2	0.000E+00	0.000E+00	0.000E+00	0.000E+00	0.000E+00	1.000E+00

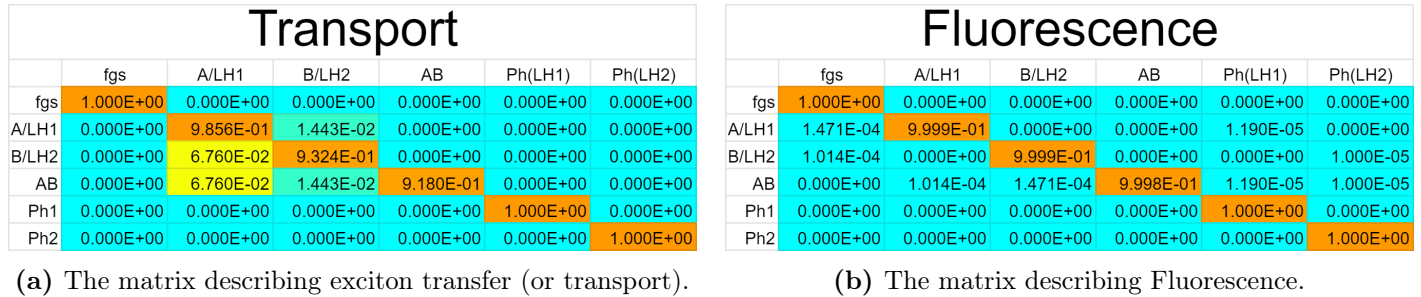**(b)** The matrix describing Fluorescence.

Figure 2.9: We are building the Master equations for LH1-LH2 dimer. Here we see the 2 components which together build up one complete timestep: exciton transfer (or transport) and fluorescence.

Each of the matrices above represent half of a complete timestep. If we multiply the two matrices (via matrix multiplication), we obtain the complete master equations for a dimer. The master-equations will appear different if we first take a time-step in exciton transfer and then take a time-step in fluorescence, or the other way around. Hiërarchically, it makes most sense to do the fastest step first, and then do the slowest step, so exciton transfer first, and then fluorescence.
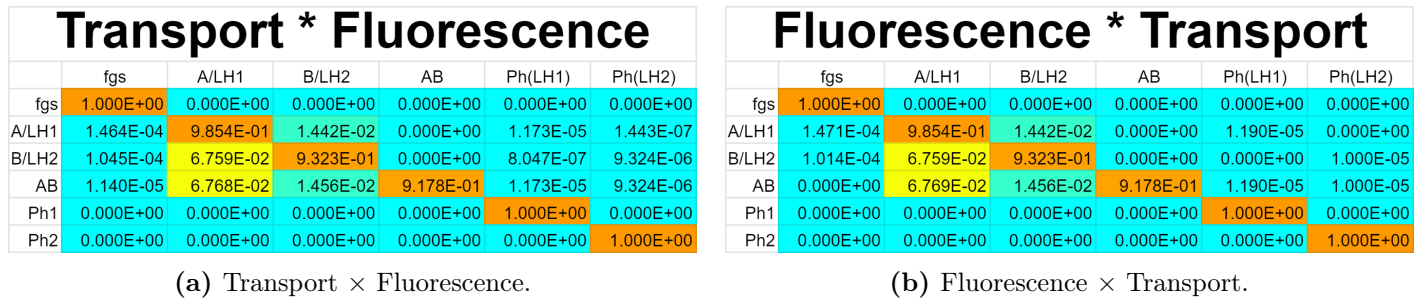
Transport * Fluorescence

	fgs	A/LH1	B/LH2	AB	Ph(LH1)	Ph(LH2)
fgs	1.000E+00	0.000E+00	0.000E+00	0.000E+00	0.000E+00	0.000E+00
A/LH1	1.464E-04	9.854E-01	1.442E-02	0.000E+00	1.173E-05	1.443E-07
B/LH2	1.045E-04	6.759E-02	9.323E-01	0.000E+00	8.047E-07	9.324E-06
AB	1.140E-05	6.768E-02	1.456E-02	9.178E-01	1.173E-05	9.324E-06
Ph1	0.000E+00	0.000E+00	0.000E+00	0.000E+00	1.000E+00	0.000E+00
Ph2	0.000E+00	0.000E+00	0.000E+00	0.000E+00	0.000E+00	1.000E+00

(a) Transport × Fluorescence.

Fluorescence * Transport

	fgs	A/LH1	B/LH2	AB	Ph(LH1)	Ph(LH2)
fgs	1.000E+00	0.000E+00	0.000E+00	0.000E+00	0.000E+00	0.000E+00
A/LH1	1.471E-04	9.854E-01	1.442E-02	0.000E+00	1.190E-05	0.000E+00
B/LH2	1.014E-04	6.759E-02	9.323E-01	0.000E+00	0.000E+00	1.000E-05
AB	0.000E+00	6.769E-02	1.456E-02	9.178E-01	1.190E-05	1.000E-05
Ph1	0.000E+00	0.000E+00	0.000E+00	0.000E+00	1.000E+00	0.000E+00
Ph2	0.000E+00	0.000E+00	0.000E+00	0.000E+00	0.000E+00	1.000E+00

(b) Fluorescence × Transport.

Figure 2.10: There are two ways to build the Master equations, as there can only be one first process: it either is exciton transfer (or transport) or fluorescence. Note that for visualization purpose, only 4 significant numbers are shown, while the actual calculation considers 7 significant numbers.

If we raise this matrix to the power of 100,000, we obtain the situation after 10 nanoseconds. Figure 2.11 shows that the differences between taking the one or the other half-timestep first becomes negligible.

V17*: Excel-generated Transport * Fluorescence

	n=	100,000	t=	10	ns		Transport * fluorescence	
	fgs	A/LH1	B/LH2	AB	Ph(LH1)	Ph(LH2)
fgs	1.000E+00	0.000E+00	0.000E+00	0.000E+00	0.000E+00	0.000E+00
A/LH1	1.000E+00	7.543E-07	1.611E-07	0.000E+00	7.058E-02	1.263E-02
B/LH2	1.000E+00	7.547E-07	1.611E-07	0.000E+00	7.048E-02	1.275E-02
AB	1.000E+00	7.555E-07	1.613E-07	0.000E+00	7.069E-02	1.277E-02
Ph1	0.000E+00	0.000E+00	0.000E+00	0.000E+00	1.000E+00	0.000E+00
Ph2	0.000E+00	0.000E+00	0.000E+00	0.000E+00	0.000E+00	1.000E+00

(a) Transport × Fluorescence.

V18: Script generated Fluorescence * Transport

	n=	100,000	t=	10	ns;	wall-time= 0	Fluorescence * Transport	
	fgs	A/LH1	B/LH2	AB	Ph(LH1)	Ph(LH2)
fgs	1.000E+00	0.000E+00	0.000E+00	0.000E+00	0.000E+00	0.000E+00
A/LH1	1.000E+00	7.543E-07	1.611E-07	0.000E+00	7.058E-02	1.263E-02
B/LH2	1.000E+00	7.547E-07	1.611E-07	0.000E+00	7.047E-02	1.276E-02
AB	1.000E+00	7.557E-07	1.613E-07	0.000E+00	7.071E-02	1.278E-02
Ph1	0.000E+00	0.000E+00	0.000E+00	0.000E+00	1.000E+00	0.000E+00
Ph2	0.000E+00	0.000E+00	0.000E+00	0.000E+00	0.000E+00	1.000E+00

(b) Fluorescence × Transport.

Figure 2.11: There is very little difference between the final results, whether we simulate the fluorescence- or exciton transfer-timestep first.

Which way is right? For the dimer, the difference in final result is negligible (∼4 orders of magnitude less). For bigger systems, however, it turns out that the differences are larger, but this discussion will quickly involve comparing different versions of working code, which will be discussed in Appendix B.6.

2.3   Concluding the methods

Now that we have built the Master equations for a dimer, we know which essential processes will be going on, under the hood of our computational model. In the next chapter, we discuss some theory which we need to interpret our computational results.

Chapter 3

Theory

In this Chapter, I will introduce and discuss double sided Feynman diagrams. In order to be able to interpret our computational results, we need to determine which diagrams are responsible for which peak in our two dimensional electronic spectroscopic (2DES) images.

Note that 2DES and 2DIR and 2D-NMR are all related by the fact that they are two dimensional spectroscopy techniques, which can be used to determine the coupling, connectivity or dynamics between two (or more) states.
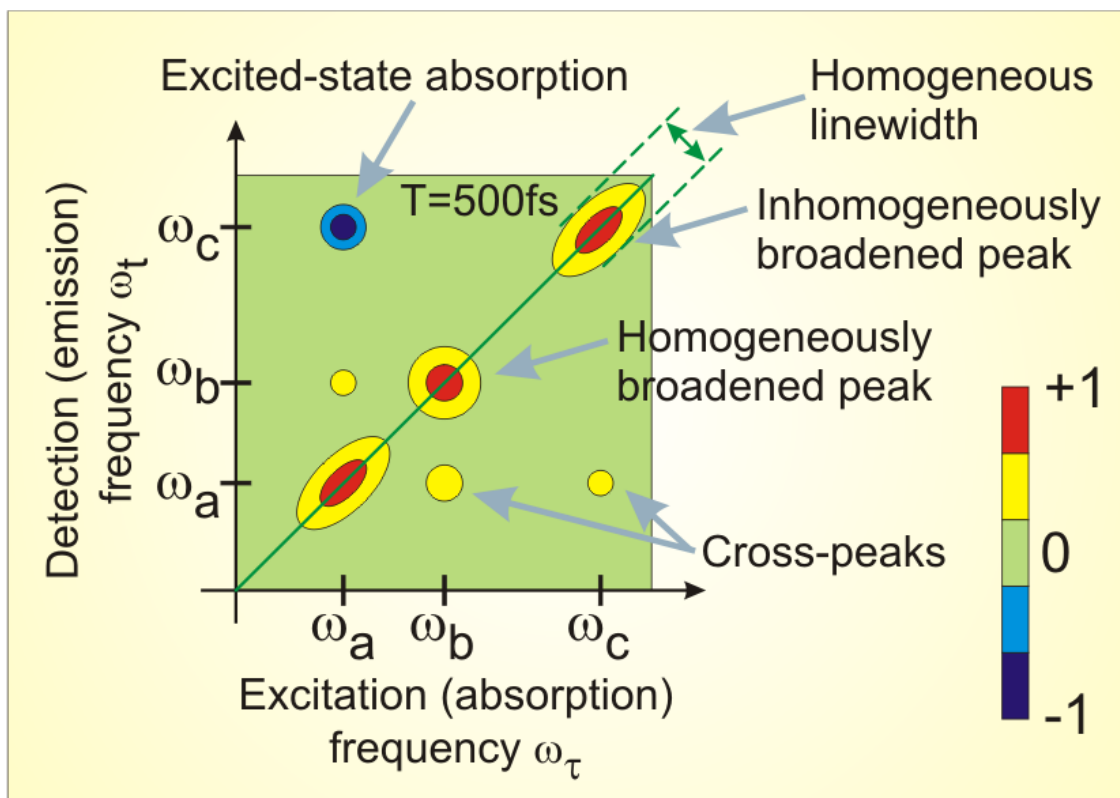
Figure 3.1: Figure explaining the key-observations possible with two dimensional electronic spectroscopy (2DES). Figure copied from the NIREOS website: `https://nireos.com/2des/`. Peaks I will commonly refer to in this chapter are:

Lower cross peak (LCP) for peaks in the lower right quadrant.

Upper cross peak (UCP) for peaks in the top left quadrant.

Lower diagonal peak (LDP) the peak on the diagonal (green line) with a lower frequency.

Upper diagonal peak (UDP) the peak on the diagonal (green line) with a higher frequency.

3.1 Fluorescence detected Two dimensional Feynman diagrams

This masterthesis looks into the fluorescence detected 2D spectroscopy. In this spectroscopy, we send 4 laser pulses to the sample. Then we wait and measure the photons emitted.

The way the laser pulses interact with the matter is summarized in Feynman diagrams. Each light-matter interaction is indicated with an arrow, after which either the ket $\langle a|$ or the bra $\langle b|$ changes state. Emission is indicated by $\nwarrow \begin{vmatrix} 00 \\ 11 \end{vmatrix} \nearrow$, which is short for both $\nwarrow \begin{vmatrix} 00 \\ 10 \\ 11 \end{vmatrix} \nearrow$ and $\nwarrow \begin{vmatrix} 00 \\ 01 \\ 11 \end{vmatrix} \nearrow$. A state for which the bra and the ket are in different excited states, is an oscillating electric dipole, which allows the molecule (or system) to absorb or emit a photon. Except for the emission interactions, all other 4 interactions can give rise to $2^4 = 16$ interaction diagrams, but not all diagrams are resonant with states. For Fluorescence detected 2D spectroscopy, we only need to consider the diagrams given in Eq. 3.1.1 [27].

$$
\text{Rephasing} \quad
\begin{array}{ccccc}
 & \textbf{GB} & \textbf{SE} & \textbf{EA1} & \textbf{EA2} \\
t_3 \begin{bmatrix} \\ \\ \\ \end{bmatrix} & \begin{matrix} \nwarrow\,00\,\nearrow \\ 11 \\ 10\,\nwarrow \\ \nearrow 00\,\nearrow \end{matrix} & \begin{matrix} \nwarrow\,00\,\nearrow \\ 11 \\ 10 \\ 11 \end{matrix} & \begin{matrix} \nwarrow\,00\,\nearrow \\ \nwarrow\,11 \\ 21 \\ \nearrow 11 \end{matrix} & \begin{matrix} \nwarrow\,11\,\nearrow \\ 22 \\ 21\,\nwarrow \\ \nearrow 11 \end{matrix} \\
t_1 \begin{bmatrix} \\ \\ \end{bmatrix} & \begin{matrix} 01 \\ 00\,\nwarrow \end{matrix} & \begin{matrix} \nearrow\,01 \\ 00\,\nwarrow \end{matrix} & \begin{matrix} \nearrow\,01 \\ 00\,\nwarrow \end{matrix} & \begin{matrix} \nearrow\,01 \\ 00\,\nwarrow \end{matrix}
\end{array}
\quad \begin{matrix}\,]\,t_3 \\ \,]\,t_1\end{matrix}
\qquad \text{(Eq. 3.1.1a)}
$$

$$
\text{Nonrephasing} \quad
\begin{array}{ccccc}
 & \textbf{GB} & \textbf{SE} & \textbf{EA1} & \textbf{EA2} \\
t_3 \begin{bmatrix} \\ \\ \\ \end{bmatrix} & \begin{matrix} \nwarrow\,00\,\nearrow \\ 11 \\ 10\,\nwarrow \\ \nearrow 00 \end{matrix} & \begin{matrix} \nwarrow\,00\,\nearrow \\ 11 \\ 10 \\ 11 \end{matrix} & \begin{matrix} \nwarrow\,00\,\nearrow \\ \nwarrow\,11 \\ 21 \\ \nearrow 11 \end{matrix} & \begin{matrix} \nwarrow\,11\,\nearrow \\ 22 \\ 21\,\nwarrow \\ \nearrow 11 \end{matrix} \\
t_1 \begin{bmatrix} \\ \\ \end{bmatrix} & \begin{matrix} 10 \\ \nearrow 00 \end{matrix} & \begin{matrix} 10\,\nwarrow \\ \nearrow 00 \end{matrix} & \begin{matrix} 10\,\nwarrow \\ \nearrow 00 \end{matrix} & \begin{matrix} 10\,\nwarrow \\ \nearrow 00 \end{matrix}
\end{array}
\quad \begin{matrix}\,]\,t_3 \\ \,]\,t_1\end{matrix}
\qquad \text{(Eq. 3.1.1b)}
$$

As discussed in section 1.3 on page 6, the spectrum of the pulse is tuned to be resonant with the states in the system. In a 2D electronic spectroscopy experiment, the waiting times t_1 and t_3 are varied. The Fourier transform of t_1 and t_3 give rise to ω_1 and ω_3, which are the two axes of our image.

A common misconception is that we would be able to select a diagram we want to measure. t_1 and t_3 are the only two knobs we can turn, and nature will reply with an adequate response for the intensity at that point. By scanning both over t_1 and t_3 and collecting the intensity in each point, a 2D spectrum can be measured.

"So, how does the 2D IR spectrum look like?", Peter Hamm and Martin Zanni asked on page 72 of their "Concepts and Methods of 2D IR Spectroscopy" book[14][4]. They derived the response functions

---
[4]   Note that we are not looking at 2DIR but at 2DES, but these two techniques are very similar, and the response

to be as follows:

$$\textbf{Rephasing:} \qquad R_1(\omega_1, \omega_3) \propto \frac{1}{i(-\omega_1 + \omega_{01}) - \Gamma_2} \cdot \frac{1}{i(\omega_3 - \omega_{01}) - \Gamma_2} \qquad \text{(Eq. 3.1.2)}$$

$$\textbf{Non-rephasing:} \qquad R_4(\omega_1, \omega_3) \propto \frac{1}{i(\omega_1 - \omega_{01}) - \Gamma_2} \cdot \frac{1}{i(\omega_3 - \omega_{01}) - \Gamma_2} \qquad \text{(Eq. 3.1.3)}$$

For the ground state bleach (GB) diagrams, it is just as likely that a photon is emitted from the rephasing GB diagram as from the nonrephasing GB diagram. The total intensity is therefore given by summing the contributions of both the rephasing and the nonrephasing diagram. This can be written as a complex sum, but it's actually more elegant to simplify this equation a bit.

$$R_1 + R_4 \propto \underbrace{\left(\frac{1}{i(-\omega_1 + \omega_{01}) - \Gamma_2} + \frac{1}{i(-\omega_1 + \omega_{01}) - \Gamma_2} \right)}_{\textbf{We will work this part out in Eq. 3.1.6}} \cdot \frac{1}{i(\omega_3 - \omega_{01}) - \Gamma_2} \qquad \text{(Eq. 3.1.4)}$$

Next, we use Eq. 3.1.5 to simplify the part between brackets[5].

$$\frac{1}{i\delta\omega - \Gamma} = \frac{1}{i\delta\omega - \Gamma} \cdot \frac{-i\delta\omega - \Gamma}{-i\delta\omega - \Gamma} = \frac{-i\delta\omega - \Gamma}{(i\delta\omega - \Gamma) \cdot (-i\delta\omega - \Gamma)} = \frac{-\Gamma - i\delta\omega}{-i^2(\delta\omega)^2 + \Gamma^2} = \frac{\overbrace{-\Gamma}^{\textbf{Real}} \overbrace{-i\delta\omega}^{\textbf{Imaginary}}}{(\delta\omega)^2 + \Gamma^2}$$

$$\text{(Eq. 3.1.5)}$$

$$\frac{1}{i\delta\omega - \Gamma} + \frac{1}{-i\delta\omega - \Gamma} = \frac{\overbrace{-\Gamma}^{\textbf{Real}}\overbrace{-i\delta\omega}^{\textbf{Imaginary}}}{(\delta\omega)^2 + \Gamma^2} + \frac{\overbrace{-\Gamma}^{\textbf{Real}}\overbrace{+i\delta\omega}^{\textbf{Imaginary}}}{(-\delta\omega)^2 + \Gamma^2} = \frac{\overbrace{-\Gamma}^{\textbf{Real}}\overbrace{-i\delta\omega}^{\textbf{Imaginary}}\overbrace{-\Gamma}^{\textbf{Real}}\overbrace{+i\delta\omega}^{\textbf{Imaginary}}}{(\delta\omega)^2 + \Gamma^2} = \frac{\overbrace{-2\Gamma}^{\textbf{Real}}}{(\delta\omega)^2 + \Gamma^2}$$

$$\text{(Eq. 3.1.6)}$$

This makes

$$R_1 + R_4 \propto \underbrace{\left(\frac{1}{i(-\omega_1 + \omega_{01}) - \Gamma} + \frac{1}{i(-\omega_1 + \omega_{01}) - \Gamma} \right)}_{\textbf{This part was worked out in Eq. 3.1.6}} \cdot \frac{1}{i(\omega_3 - \omega_{01}) - \Gamma} \qquad \text{(Eq. 3.1.4)}$$

$$= \frac{\overbrace{-2\Gamma}^{\textbf{Real}}}{(\delta\omega)^2 + \Gamma^2} \cdot \frac{1}{i(\omega_3 - \omega_{01}) - \Gamma} \qquad \text{(Eq. 3.1.7)}$$

We now have 3 equations: for rephasing (Eq. 3.1.2), for nonrephasing (Eq. 3.1.3), and for rephasing+nonrephasing (Eq. 3.1.7). The real part of these equations is plotted in Figure 3.2 on the next page.

---

functions are identical.

[5] I dropped the subscript 2 on Γ_2. Officially, this is to declare that it's the dephasing constant during t_2, however, currently t_2 is the only time interval for which dephasing is relevant, so suffices to say that $\Gamma_2 = \Gamma$.

(a) Rephasing, R_1, Eq. 3.1.2   **(b)** Nonrephasing, R_4, Eq. 3.1.3   **(c)** Rephasing + Nonrephasing, $R_1 + R_4$, Eq. 3.1.7
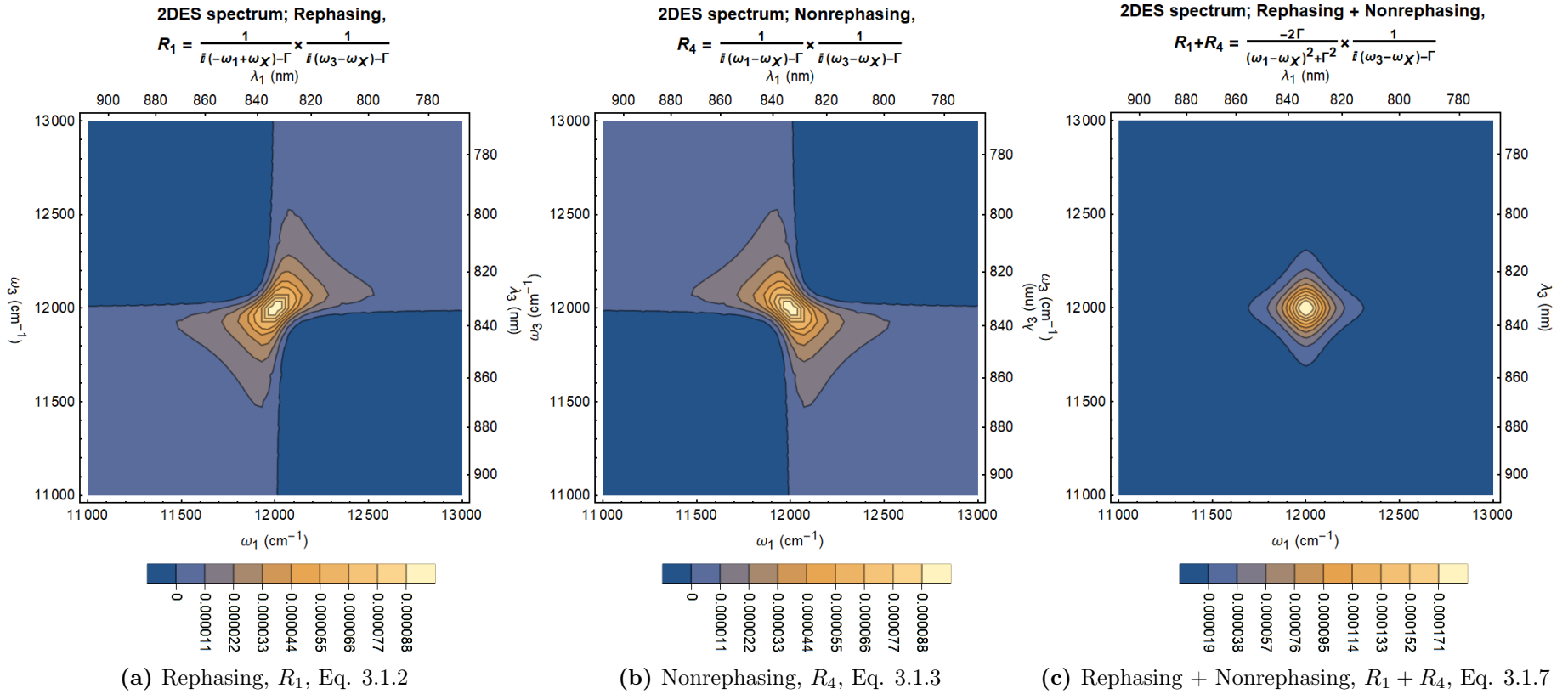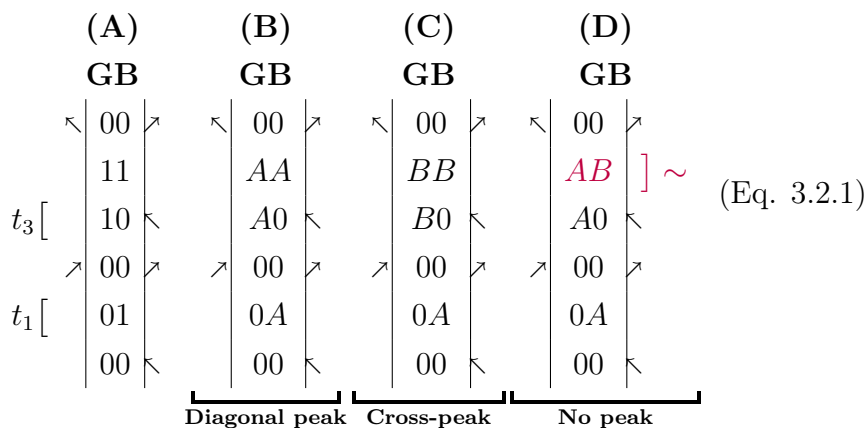
Figure 3.2: Spectral shapes observed in 2DES spectroscopy. Ref. [14] shows similar graphs for 2DIR spectroscopy. In the example above, the spectroscopic region is 800 nm is near infrared, and therefore the above isn't infrared spectroscopy. Note that I chose ω_X to be 12 000 cm^{-1}, which is arbitrary, except for the fact that we will use this plot region more frequently, and this is exactly the middle of the graph.

3.2   Double Sided Feynman diagrams for 2 molecules

We can fill out an Feynman diagram with numbers to indicate how the excited states are probed of one molecule, recall Eq. 3.1.1 on page 28. Next step is to fill in these diagrams for two molecules, however, we use A and B for first excited state, and A^2 and B^2 for the second excited state.

3.2.1   Groundstate Bleach (GB)

The first diagram to discuss is Groundstate Bleach (GB).

	(A)	(B)	(C)	(D)
	GB	GB	GB	GB
	00	00	00	00
	11	AA	BB	AB
t_3	10	$A0$	$B0$	$A0$
	00	00	00	00
t_1	01	$0A$	$0A$	$0A$
	00	00	00	00

$$\sim \quad \text{(Eq. 3.2.1)}$$

Diagonal peak   **Cross-peak**   **No peak**

I wrote a Mathematica script which can show the two dimensional electronic spectrum (2DES) for isolated Feynman diagrams. Because I just want to have a system with two energy-states, I've chosen to perform these simulations on the B800/B850 system within LH2, recall section 2.2.4. The resulting Groundstate Bleach (GB) spectrum is shown in Figure 3.3.

Diagram **(GB.B)** gives rise to the lower diagonal peak, and has the fluorescence intensity of one molecule of A. For the upper diagonal peak, all A's must be replaced by B's, and therefore, that peak has the fluorescence intensity of one molecule of B.

Diagram **(GB.C)** gives rise to the upper cross peak, and has the fluorescence intensity of one molecule of B. Similarly, the diagram for the lower cross peak has A's must be replaced by B's and vise versa, and therefore has the fluorescence intensity of one molecule of A.
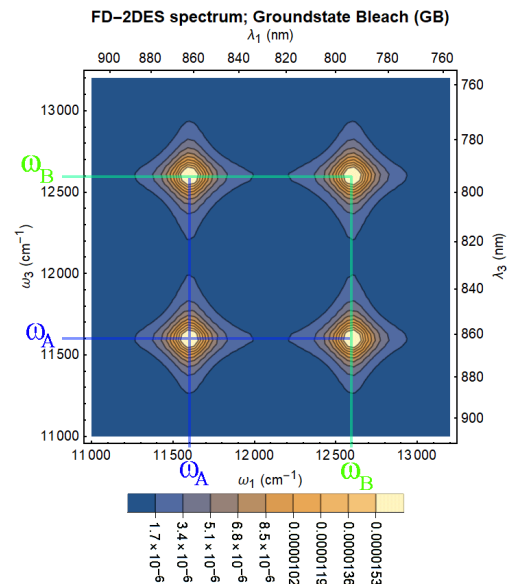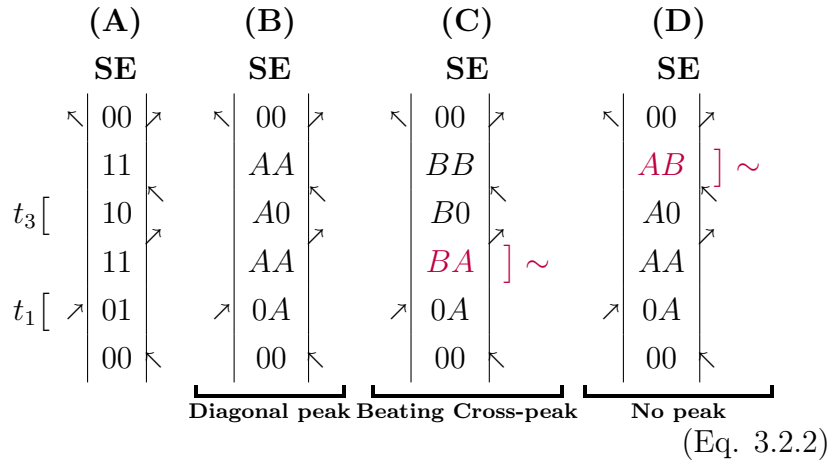
Figure 3.3:   Weighted 2DES intensity profile of the Groundstate Bleach (GB) Feynman diagrams (Eq. 3.2.1). The intensities for the AA and BB states are calculated with the Mathematica script outlined in section 2.2.4.

3.2.2 Stimulated Emission (SE)

The next diagram to discuss is Stimulated Emission (SE).
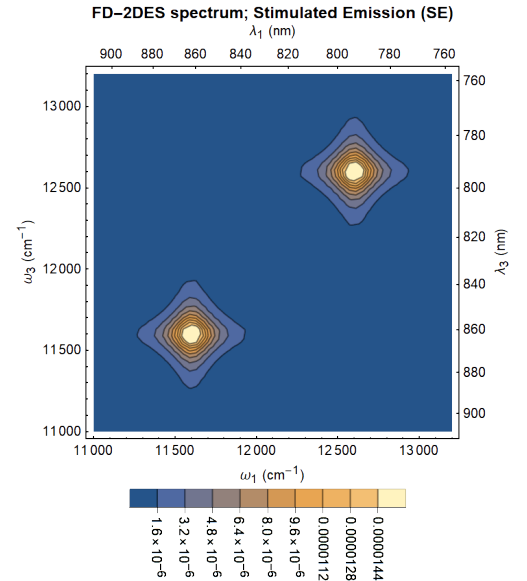

$$\text{(Eq. 3.2.2)}$$

Figure 3.4: Weighted 2DES intensity profile of the Stimulated Emission (SE) Feynman diagrams (Eq. 3.2.2). This Figure was produced by the Mathematica script described in section 2.2.4.
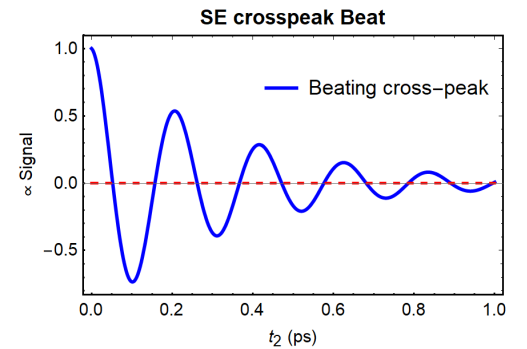
Stimulated Emission (SE) only gives diagonal peaks, see Figure 3.4. Diagram **SE.C** is in an oscillating state ($|AB|$ or $|BA|$) during t_2. These oscillating states have strong tendency to dephase to an incoherent state. The dephasing isn't instantaneous, but is proportional to

$$\text{signal} \propto \cos\left(t_2 \cdot (\omega_B - \omega_A)\right) \cdot e^{-t_2 \cdot \Gamma} \qquad \text{(Eq. 3.2.3)}$$

Note that ω and Γ are typically given in cm^{-1}, and therefore, in we need to convert the frequency from cm^{-1} to Hz. We can convert from cm^{-1} to Hz via the energy:

$$E = hf = \frac{hc}{\lambda} = hc\tilde{\omega} \qquad \text{(Eq. 3.2.4)}$$

$$f = c\tilde{\omega} = 299\,792\,458\,\frac{\text{m}}{\text{s}} \times \tilde{\omega}(\text{in m}^{-1}) \qquad \text{(Eq. 3.2.5)}$$

$$f = c\tilde{\omega} = 29\,979\,245\,800\,\frac{\text{cm}}{\text{s}} \times \tilde{\omega}(\text{in cm}^{-1}) \qquad \text{(Eq. 3.2.6)}$$

Eq. 3.2.3 is plotted in Figure 3.5.

The next diagrams to test are Excited State Absorption (EA) diagrams. There are two types of EA diagrams:

- **EA1:** with an excited-state bleach step, after which the system is in either one of the two first-excited states.

- **EA2:** in which both the bra- and the ket-side absorb two photons, after which the system is in a double-excited state.

These two diagrams are discussed on the next two pages!

Figure 3.5: Beating intensity of the crosspeaks in the stimulated emission (SE) diagram. Plotted is Eq. 3.2.3.

3.2.3 Excited State Absorption 1 (EA1)

Next, let's discuss Feynman diagrams for excited-state absorption #1, see Eq. 3.2.7 and Figure 3.6.
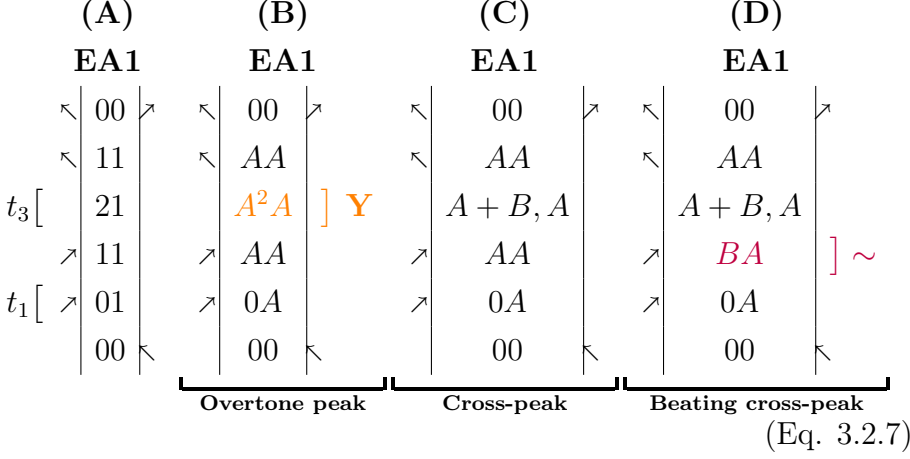

(A)	(B)	(C)	(D)
EA1	**EA1**	**EA1**	**EA1**

$$
\begin{array}{llll}
\text{(A)} & \text{(B)} & \text{(C)} & \text{(D)} \\
\text{EA1} & \text{EA1} & \text{EA1} & \text{EA1}
\end{array}
$$

(Eq. 3.2.7)

Diagram **EA1.B** gives rise to overtone peaks. Diagram **EA1.C** gives rise to normal cross-peaks[7], and diagram **EA1.D** contributes to the blinking of the same cross peaks. Together, **EA1.C** and **EA1.D** make the intensity of these cross-peaks to beat as follows:

$$
\text{signal} \propto \overset{\text{(EA1.C)}}{1} + \overbrace{\cos\left(t_2 \cdot (\omega_B - \omega_A)\right) \cdot e^{-t_2 \cdot \Gamma}}^{\text{(EA1.D)}}, \quad \text{(Eq. 3.2.8)}
$$

Recall how we changed frequency ω in cm^{-1} to frequency f in Hz via Eq. 3.2.6). Eq. 3.2.8 is plotted in Figure 3.7.

The overtone peak (due to the $|A^2, A|$ state, see **EA1.B**) resonates with a similar (but not the same) frequency as the $|A, 0|$ state; the difference in frequency is caused by the fact that the second excited state is not exactly twice the energy of the first excited state. This is due to anharmonicity. This was shortly touched upon in section 2.2.3. The frequency at which this $|A^2\rangle$ state vibrates is:

$$
\omega_{A^2} = 2\omega_A + \Delta \quad \text{(Eq. 3.2.9)}
$$

in which Δ is the anharmonicity constant. In this section, Δ is assumed to be 233 cm^{-1}, which is based on a measurement in Fig. 4a of Ref. [10]. The frequency at which the $|A^2, A|$ state resonates is

$$
\omega_{A^2} - \omega_A = 2\omega_A + \Delta - \omega_A = \omega_A + \Delta \quad \text{(Eq. 3.2.10)}
$$

As a result, the overtone peak is located $\Delta = 233$ cm^{-1} above the diagonal peak in the 2DES diagram,
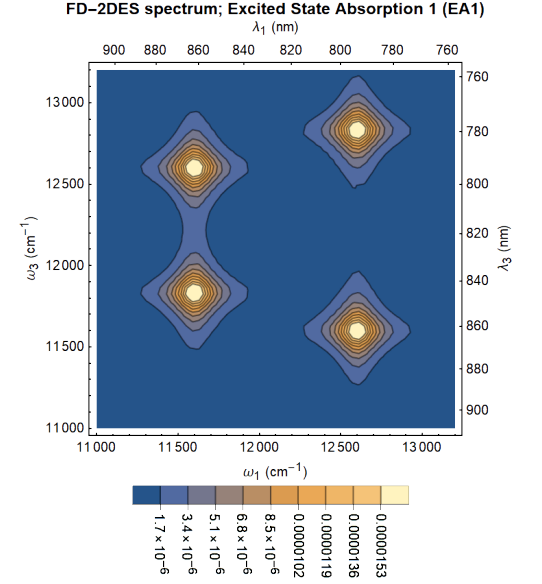

Figure 3.6: Weighted 2DES intensity profile of Excited State Absorption 1 (EA1) Feynman diagrams (Eq. 3.2.7). This Figure was produced by the Mathematica script described in section 2.2.4.
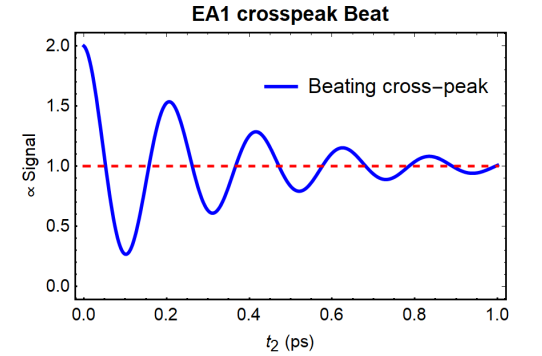

Figure 3.7: Beating intensity of the crosspeaks in the EA1 diagram, as described by Eq. 3.2.8.

see Figure 3.6. To make reading the Feynman diagrams a bit easier, overtone peaks will be marked with an **Y** (similar to that oscillating states will be marked with $\sim$).

3.2.4 Excited State Absorption 2 (EA2)

The next Feynman diagrams to discuss are those for excited-state absorption #2, see Eq. 3.2.11 and Figure 3.8.
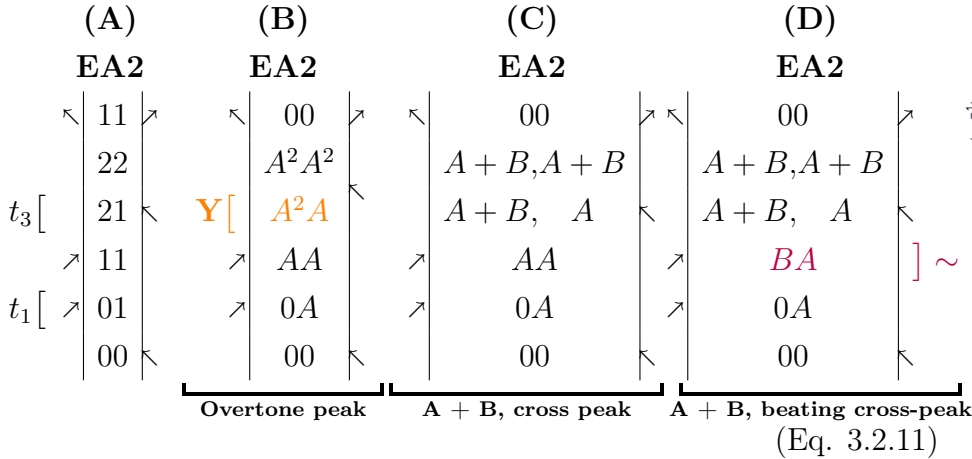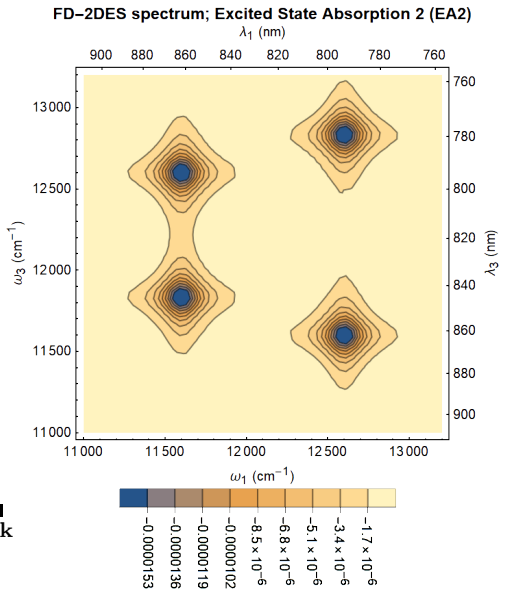
FD–2DES spectrum; Excited State Absorption 2 (EA2)

Figure 3.8: Weighted 2DES intensity profile of Excited State Absorption 2 (EA2) Feynman diagrams (Eq. 3.2.11). This Figure was produced by the Mathematica script described in section 2.2.4.

Diagram **EA2.B** puts one molecule in the second excited state. Diagrams **EA2.C** and **EA2.D** put both molecules in the first excited state.

The diagram that brings one molecule to the second excited state (Diagram **EA2.B**), gives rise to an overtone peak. The second excited state quickly decays towards the first exited state[6], so the overtone intensity can be calculated by integrating the intensity emitted by the first excited state.

The diagram that brings both molecules to the first excited state (**EA2.C**[7]), gives rise to cross-peaks. However, since both excited states are present, the intensity must be calculated via a kinetic model. For now I will which is of course done with the Mathematica notebook of section 2.2.4.

---

[6]   Although it is theoretically possible that a fraction of the second exited state decays directly towards the groundstate, we assumed the rate for this process to be 0.

[7]   Note that the $|A+B, A|$ state in **EA1.C**, **EA1.D**, **EA2.C** and **EA2.D** are relatively as stable as the $0, B$ state, because molecule A completely in the first excited state ($|A, A| = A^1$).

3.2.4.1 Note on sign

The sign of the diagram is calculated as

$$\text{sign} = (-1)^n \qquad \text{(Eq. 3.2.12)}$$

in which n is the number of photons on the bra side of the diagram.

The EA1 diagram (Eq. 3.2.7) has 2 arrows on the bra-side, meaning that the sign is $+$. The EA2 diagram (Eq. 3.2.11) has 3 arrows on the bra-side, meaning that the sign is negative.

Now we know that the lower overtone peak (LOP) has positive fluorescence intensity of B850' or A (see EA1 Eq. 3.2.7B), and negative fluorescence intensity of B850'' or A² (see EA2 Eq. 3.2.11). We know the intensities from the Mathematica simulation, see Figure 3.10. If we subtract the numbers, we come to:

$$LOP(\texttt{EA1}) = +\texttt{AG} = -\,0.0985962 \qquad \text{(Eq. 3.2.13)}$$
$$LOP(\texttt{EA2}) = -\texttt{A^{2}} = -\,\underline{0.0985961}_{+} \qquad \text{(Eq. 3.2.14)}$$
$$-\,0.0000001, \qquad \text{(Eq. 3.2.15)}$$

which is impossible to measure. This outcome isn't surprising: we discussed that the `A²` state decays very rapidly to the `AG` state.
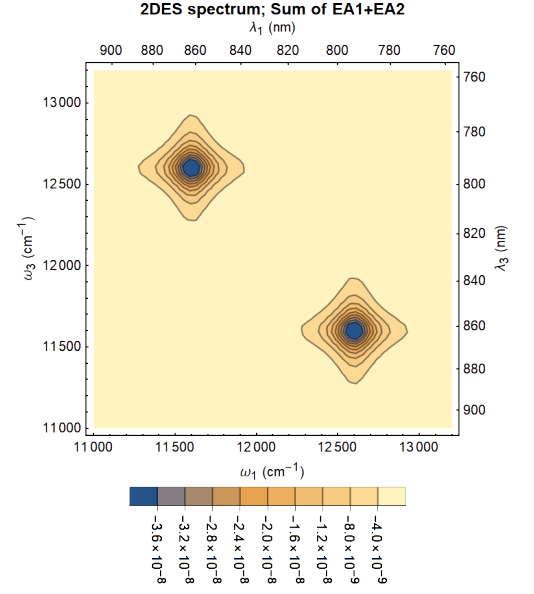
Figure 3.9: When Figures 3.6 (EA1) and 3.8 (EA2) are added, they merely entirely cancel each other, because they display the same peaks with almost the same intensity, but with opposite sign, see discussion in leading text.
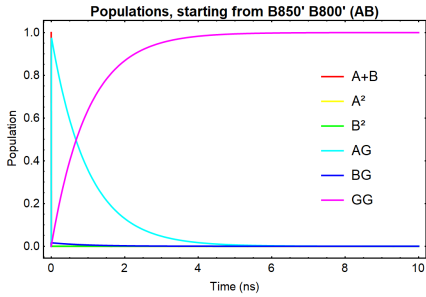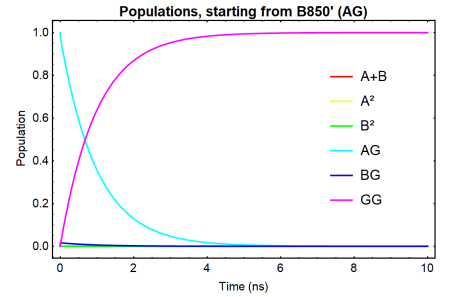

(a) Starting from AB:
TotalIntensityA = 0.097113
TotalIntensityB = 0.00171871
TotalPhotons = 0.0988317
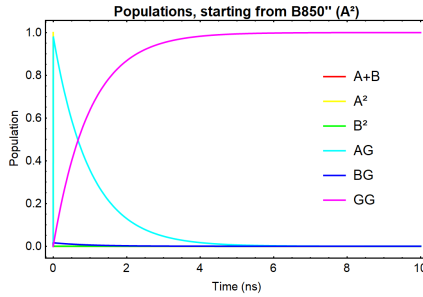
(b) Starting from A²:
TotalIntensityA = 0.0969972
TotalIntensityB = 0.00159889
TotalPhotons = 0.0985961

(c) Starting from A:
TotalIntensityA = 0.0969973
TotalIntensityB = 0.00159889
TotalPhotons = 0.0985962

Figure 3.10: Relevant simulations from the Mathematica model of Section 2.2.4.

For the cross-peaks, it is a similar story:

$$LOP(\texttt{EA1}) = +\texttt{AG} = +\,0.0985962 \qquad \text{(Eq. 3.2.16)}$$
$$LOP(\texttt{EA2}) = \texttt{AB} = -\,\underline{0.0988317}_{+} \qquad \text{(Eq. 3.2.17)}$$
$$-\,0.0002355. \qquad \text{(Eq. 3.2.18)}$$

This means that EA1 and EA2 will almost completely cancel each other, see Figure 3.9. Note that Figure 3.9 is a factor 500 less intense than Figures 3.6 & 3.8.

But then the story gets a twist: when we switch to the LH1/LH2 system, it is not longer always true that the two molecules 'A' and 'B' are neighbors, so the intensity from the 'A+B' state might actually give significantly more photons than the single exciton A state.

And then the discussion still isn't complete yet, because we have way more diagrams that give cross peaks. Let's analyze/summarize all the contributions to the crosspeaks!

3.3 Analyzing the contributions to the crosspeaks

Let's start by analyzing how much each diagram contributes to the intensity to either of the two crosspeaks. The diagrams that give a **permanent** upper cross-peak (UCP) contribution are given by:

Rephasing

(Eq. 3.2.1C)	(Eq. 3.2.7C)	(Eq. 3.2.11C)
GB	**EA1**	**EA2**

$$
\begin{array}{c|c}
 & 00 \\
 & BB \\
t_3 & B0 \\
 & 00 \\
t_1 & 0A \\
 & 00
\end{array}
\qquad
\begin{array}{c}
00 \\
AA \\
A+B,A \\
AA \\
0A \\
00
\end{array}
\qquad
\begin{array}{c}
00 \\
A+B,A+B \\
A+B,\ \ A \\
AA \\
0A \\
00
\end{array}
$$

(Eq. 3.3.1)

Nonrephasing

(Eq. 3.2.1C*)	(Eq. 3.2.7C*)	(Eq. 3.2.11C*)
GB	**EA1**	**EA2**

$$
\begin{array}{c}
00 \\
BB \\
B0 \\
00 \\
A0 \\
00
\end{array}
\qquad
\begin{array}{c}
00 \\
AA \\
A+B,A \\
AA \\
A0 \\
00
\end{array}
\qquad
\begin{array}{c}
00 \\
A+B,A+B \\
A+B,\ \ A \\
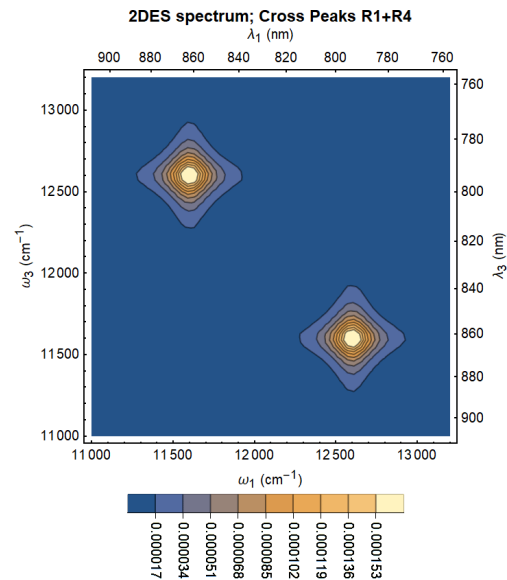AA \\
A0 \\
00
\end{array}
$$

(Eq. 3.3.2)

Figure 3.11: 2DES intensity profile of $R_1 + R_4$ cross peaks, coming from diagrams Eq. 3.3.1 and Eq. 3.3.2. Shape defined by Eq. 3.1.7.

As the rephasing diagrams (with 2D intensity profile R_1) and nonrephasing diagrams (with 2D intensity profile R_4) have the same intensity $(BB, AA, A+B)$, we know that the peaks will appear with the shape as shown in Figure 3.11.

The diagrams that give a **beating** upper cross-peak (UCP) are:

$$
\text{Rephasing}
\begin{array}{ccc}
\textbf{(Eq. 3.2.2C)} & \textbf{(Eq. 3.2.7D)} & \textbf{(Eq. 3.2.11D)} \\
\textbf{SE} & \textbf{EA1} & \textbf{EA2} \\
\begin{array}{l}
00 \\
BB \\
t_3 \Big[\; B0 \\
\qquad BA \;\Big] \sim \\
t_1 \Big[\; 0A \\
\qquad 00
\end{array}
&
\begin{array}{l}
00 \\
AA \\
A+B,A \\
\qquad BA \;\Big] \sim \\
0A \\
00
\end{array}
&
\begin{array}{l}
00 \\
A+B,A+B \\
A+B,\quad A \\
\qquad BA \;\Big] \sim \\
0A \\
00
\end{array}
\end{array}
$$

(Eq. 3.3.3)

An attempt to convert the rephasing beating cross-peak diagrams (Eq. 3.3.3) into nonrephasing diagrams resulted in beating diagonal peaks, see Eq. 3.3.4 below.

$$
\text{Nonrephasing}
\begin{array}{ccc}
\textbf{(Eq. 3.2.2C*)} & \textbf{(Eq. 3.2.7D*)} & \textbf{(Eq. 3.2.11D*)} \\
\textbf{SE} & \textbf{EA1} & \textbf{EA2} \\
\begin{array}{l}
00 \\
AA \\
t_3 \Big[\; A0 \\
\qquad AB \;\Big] \sim \\
t_1 \Big[\; A0 \\
\qquad 00
\end{array}
&
\begin{array}{l}
00 \\
BB \\
A+B,B \\
\qquad AB \;\Big] \sim \\
A0 \\
00
\end{array}
&
\begin{array}{l}
00 \\
A+B,A+B \\
A+B,\quad B \\
\qquad AB \;\Big] \sim \\
A0 \\
00
\end{array}
\end{array}
$$

(Eq. 3.3.4)

The diagrams which give rise to intensity for the lower right cross-peak (LCP) are given by similar diagrams as Eq. 3.3.1, Eq. 3.3.2 and Eq. 3.3.3, except that all A's are replaced by B's and vise versa. This means that, there where the diagrams for the upper cross peak (UCP) have intensity of $\text{int}(AA)$, LCP has intensity of $\text{int}(BB)$, and where UCP has intensity of $\text{int}(BB)$, LCP has intensity of $\text{int}(AA)$, see Table 3.1 on the next page.

Now if we want to know the total intensity of each cross-peak, we need to sum the intensity of all diagram. All the intensities are calculated via a kinetic simulation, which can be from an isolated LH2 molecule (this Chapter) or from an entire Light Harvesting network (see Results, Chapter 4).
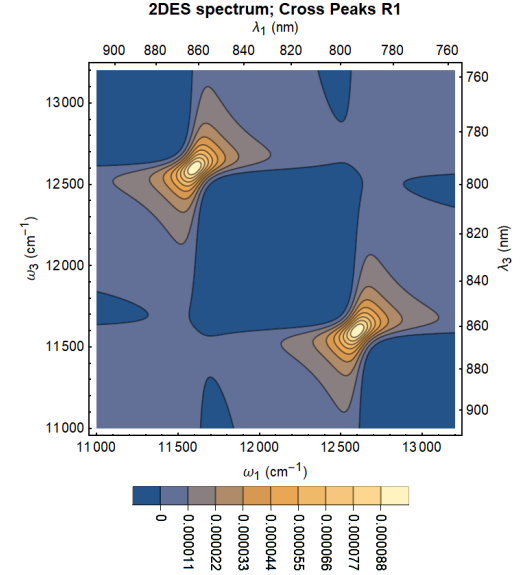

Figure 3.12: 2DES intensity profile of R_1 rephasing cross-peaks, coming from diagram Eq. 3.3.3 (shape defined by Eq. 3.1.2).
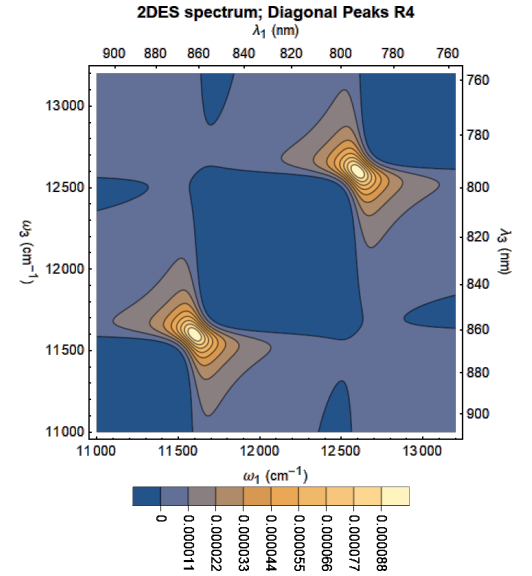

Figure 3.13: 2DES intensity profile of R_4 nonrephasing diagonal-peaks, coming from diagram Eq. 3.3.4 (shape defined by Eq. 3.1.3).

Note that the sign depends on the number of interactions n with the bra $\langle A|$.

$$\text{sign} = (-1)^n$$

$$\text{sign}(\mathbf{GB}) = (-1)^4 = +1 \qquad \text{sign}(\mathbf{SE}) = (-1)^4 = +1 \qquad \text{(Eq. 3.3.5)}$$

$$\text{sign}(\mathbf{EA1}) = (-1)^2 = +1 \qquad \text{sign}(\mathbf{EA2}) = (-1)^3 = -1$$

The total intensity of the cross peaks is summarized in Table 3.1

$\dfrac{-2\Gamma}{(\omega_1 - \omega_A)^2 + \Gamma^2} \cdot$ $\dfrac{1}{i(\omega_3 - \omega_B) - \Gamma}$	**The upper left cross-peak (UCP)**				
	Type	Static	Beating	(1+Beat)	(1+Beat)
	Origin	GB	SE	EA1	EA2
	Intensity	+BB	+BB	+AA	-(A+B)
$\dfrac{-2\Gamma}{(\omega_1 - \omega_B)^2 + \Gamma^2} \cdot$ $\dfrac{1}{i(\omega_3 - \omega_A) - \Gamma}$	**The lower right cross-peak (LCP)**				
	Type	Static	Beating	(1+Beat)	(1+Beat)
	Origin	GB	SE	EA1	EA2
	Intensity	+AA	+AA	+BB	-(A+B)

Table 3.1: The components of the two cross-peaks. Note that "AA" means that the diagram is in state AA after 4 interactions, meaning that only molecule A is in the excited state.

Now we can sum all the contributions to calculate the upper-to-lower cross-peak ratio in Eq. 3.3.6.

$$\boxed{\text{UCP}} = \mathtt{BG} + \mathtt{BG} \cdot \text{Beat} + \mathtt{AG} \cdot (1 + \text{Beat}) - \mathtt{AB} \cdot (1 + \text{Beat})$$

$$= \mathtt{BG} \cdot (1 + \text{Beat}) + \mathtt{AG} \cdot (1 + \text{Beat}) - \mathtt{AB} \cdot (1 + \text{Beat})$$

$$= (\mathtt{AG} + \mathtt{BG} - \mathtt{AB}) \cdot (1 + \text{Beat}) \qquad \text{(Eq. 3.3.6a)}$$

$$\boxed{\text{LCP}} = \mathtt{AG} + \mathtt{AG} \cdot \text{Beat} + \mathtt{BG} \cdot (1 + \text{Beat}) - \mathtt{AB} \cdot (1 + \text{Beat})$$

$$= \mathtt{AG} \cdot (1 + \text{Beat}) + \mathtt{BG} \cdot (1 + \text{Beat}) - \mathtt{AB} \cdot (1 + \text{Beat})$$

$$= (\mathtt{AG} + \mathtt{BG} - \mathtt{AB}) \cdot (1 + \text{Beat}) = \boxed{\text{UCP}} \qquad \text{(Eq. 3.3.6b)}$$

According to this calculation, the upper cross peak intensity (Eq. 3.3.6a) is by definition equal to the lower cross peak intensity (Eq. 3.3.6b). However, we could look closer at the ratio between the cross-peak and the diagonal peak. In order to do so, we first need to sort out which Feynman diagrams give intensity to the diagonal peaks. This is discussed in the next section.

3.4 Analyzing the contributions to the diagonal peaks
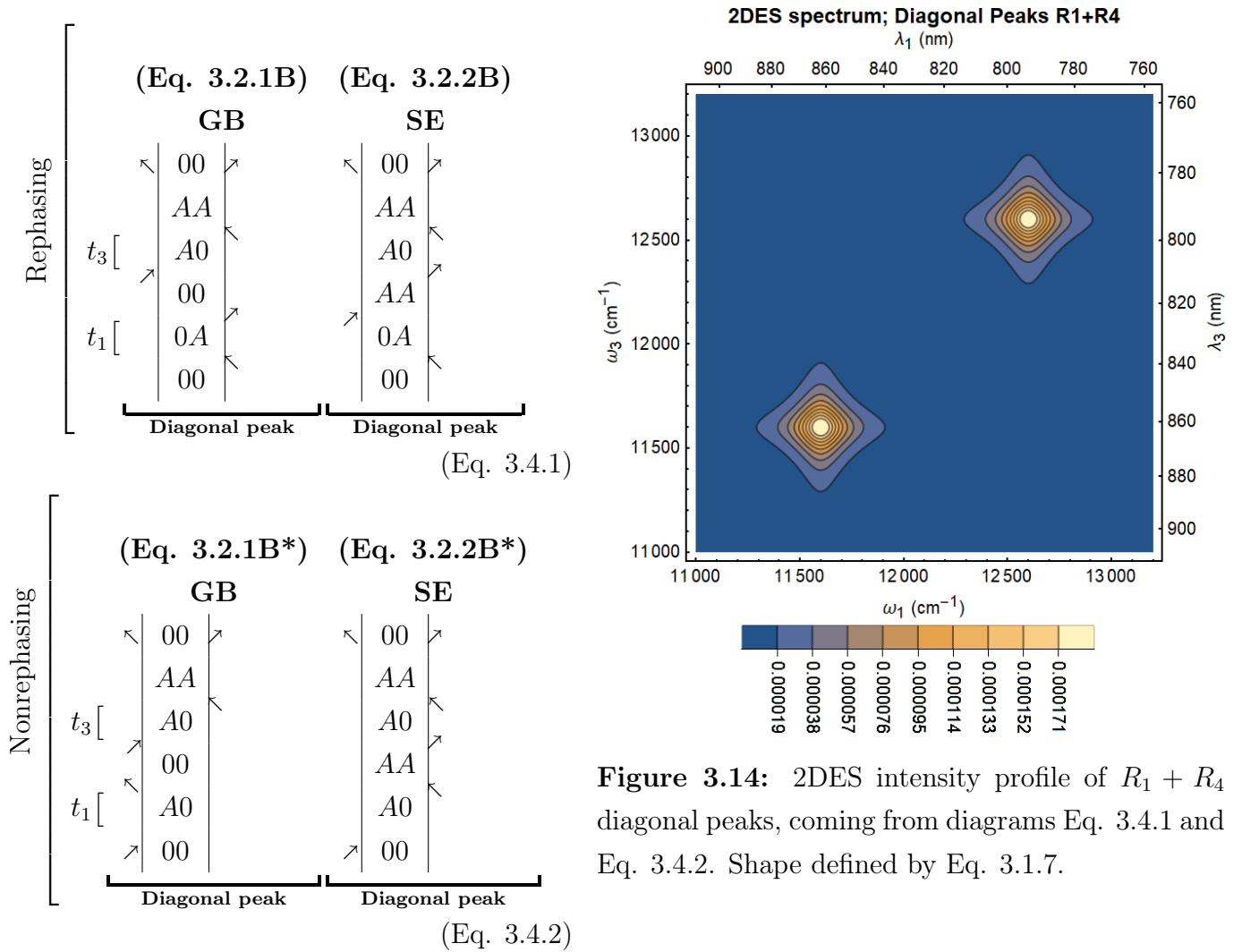

(Eq. 3.4.1)

(Eq. 3.4.2)

Figure 3.14: 2DES intensity profile of $R_1 + R_4$ diagonal peaks, coming from diagrams Eq. 3.4.1 and Eq. 3.4.2. Shape defined by Eq. 3.1.7.

As the rephasing diagrams (with 2D intensity profile R_1) and nonrephasing diagrams (with 2D intensity profile R_4) have the same intensity (AA), we know that the peaks will appear with the shape as shown in Figure 3.14.

$$\text{Stationary Lower Diagonal Peak (LDP)} = \texttt{AG} + \texttt{AG} = 2\texttt{AG} \qquad (\text{Eq. 3.4.3})$$

$$\text{Stationary Upper Diagonal Peak (UDP)} = \texttt{BG} + \texttt{BG} = 2\texttt{BG} \qquad (\text{Eq. 3.4.4})$$

$$\text{Beating diagonal peaks} = \texttt{AG} + \texttt{BG} - \texttt{AB} = \frac{\texttt{UCP}}{(1 + \text{Beat})} \qquad (\text{Eq. 3.4.5})$$

3.5   Calculating the cross-peak : diagonal peak ratio

The intensity is also proportional to the dipole moment.

$$\textbf{For the diagonal peaks:} \qquad I_A \propto \mu_A^4 \quad \textbf{and} \quad I_B \propto \mu_B^4 \qquad \text{(Eq. 3.5.1)}$$

$$\textbf{For the cross peaks:} \qquad I_{cp} \propto \mu_A^2 \cdot \mu_B^2 \qquad \text{(Eq. 3.5.2)}$$

The values of μ_A and μ_B can be determined by linear absorption spectroscopy, but I'm not sure if this is relevant right now. We could also take a look at the relative intensity, as in:

$$\frac{\boxed{\text{LCP}} * \boxed{\text{UCP}}}{\boxed{\text{LDP}} * \boxed{\text{UDP}}} = \frac{(\texttt{AG} + \texttt{BG} - \texttt{AB})^2}{2\texttt{AG} * 2\texttt{BG}} = \frac{(\texttt{Ph(Ex.1)} + \texttt{Ph(Ex.2)} - \texttt{Ph(Ex.12)})^2}{4 * \texttt{Ph(Ex.1)} * \texttt{Ph(Ex.2)}} \qquad \text{(Eq. 3.5.3)}$$

Then we know for sure that the contribution of dipole moments will all cancel.

Small spoiler

If we use the photon counter values from a simulation of a trimer (see section 4.1 on the next page), we would obtain:

$$\frac{\boxed{\text{LCP}} * \boxed{\text{UCP}}}{\boxed{\text{LDP}} * \boxed{\text{UDP}}} = \frac{(\texttt{AG} + \texttt{BG} - \texttt{AB})^2}{2\texttt{AG} * 2\texttt{BG}} = \frac{(7.541 + 7.535 - 7.619)^2}{(2 * 7.541) * (2 * 7.535)} = \frac{\boxed{7.457} * \boxed{7.457}}{\boxed{15.081} * \boxed{15.070}} = 24.47\%$$

$$\text{(Eq. 3.5.4)}$$

Chapter 4

Results

With the simulation code written in Chapter 3, we are able to simulate all possible starting configurations for a certain LH1/LH2-configuration at once. Certain configurations are highlighted here.

Color-coding: In this chapter, the following color-coded abbreviations are used: Exciton = `yellow`

LH1 = `LH1` = `1`   Trimer matrix identity with exciton on A: `A`-B-C

LH2 = `LH2` = `2`   Trimer with excitons on A and B: `A`-`B`-C = AB

4.1   Trimers: LH1-LH2-LH1 and LH1-LH2-LH2

As the dimer was already studied intensively in Chapter 1, the first notably different simulation we could perform is a trimer. Because the rate constant between two LH1 units is unknown, the only well-defined trimer-systems are `LH1`-`LH2`-`LH1` and `LH1`-`LH2`-`LH2`. My hypothesis for these two simulations would be that the `LH1`-`LH2`-`LH1` simulation is much better at keeping two excited states separate than `LH1`-`LH2`-`LH2`. This will lead to a higher photon-count than `LH1`-`LH2`-`LH2`, and subsequently lead to a lower cross-peak intensity.

A few frames of the simulation are shown in Figure 4.1 on the following page.

The way how we convert photon intensity in the last frame (n = 100k or t = 10 ns), to cross-peak-to-diagonal-peak ratio was explained in Eq. 3.5.3 on the preceding page. We can apply Eq. 3.5.3 to each of the double excited states (e.g. AB, AC and BC) to calculate the cross-peak to diagonal-peak ratio, see Table 4.1 and Table 4.2. It turns out my hypothesis is wrong. Apparently the gradient which causes the excited state(s) to accumulate on `LH1` is because diffusion from `LH1` towards the central `LH2` is slowed down, but more because the diffusion from `LH2` towards `LH1` is speed up.

Another thing is that the simulation was set to be symmetrical, with no fluctuations in the rates. This means that, when we look at the simulation of `LH1`-`LH2`-`LH1` and start from exciton distrubution AC (`LH1`-LH2-`LH1`), that the same amount of exciton flows from the left `LH1` to the central `LH2` as from the right `LH1` unit, always causing the central `LH2` unit to receive two excitons, which immediately decays to the ground state. Probably the excited states are easier to keep apart if we introduce more spacers between the left and the right `LH1` unit. This experiment is done in the next section.

Figure 4.1: Selection of frames from the simulations on trimers (LH1-LH2-LH1 vs LH1-LH2-LH2).

Ex.12	Ph(Ex.1)	Ph(Ex.2)	Ph(Ex.12)	LCP = UCP	LDP	UDP	ratio*
AB	7.541E-02	7.535E-02	7.619E-02	7.457E-02	1.508E-01	1.507E-01	24.47%
AC	7.541E-02	7.541E-02	7.697E-02	7.385E-02	1.508E-01	1.508E-01	23.97%
BC	7.535E-02	7.541E-02	7.619E-02	7.457E-02	1.507E-01	1.508E-01	24.47%

Table 4.1: Calculating the cross peak to diagonal peak ratio for the LH1-LH2-LH1 trimer. The numbers I use here are for the photon counters on LH1 after 10 ns of collecting time.

Ex.12	Ph(Ex.1)	Ph(Ex.2)	Ph(Ex.12)	LCP = UCP	LDP	UDP	ratio*
AB	6.263E-02	6.244E-02	6.282E-02	6.225E-02	1.253E-01	1.249E-01	24.78%
AC	6.263E-02	6.207E-02	6.318E-02	6.152E-02	1.253E-01	1.241E-01	24.34%
BC	6.244E-02	6.207E-02	6.287E-02	6.164E-02	1.249E-01	1.241E-01	24.51%

Table 4.2: Calculating the cross peak to diagonal peak ratio for the LH1-LH2-LH2 trimer. Again I use the photon counters on LH1 after 10 ns of simulated time. The ratio is calculated via Eq. 3.5.3.

4.2   Linear chains

The next simulation I did was on 6 different types of Light Harvesting chains, depicted in Figure 4.2.
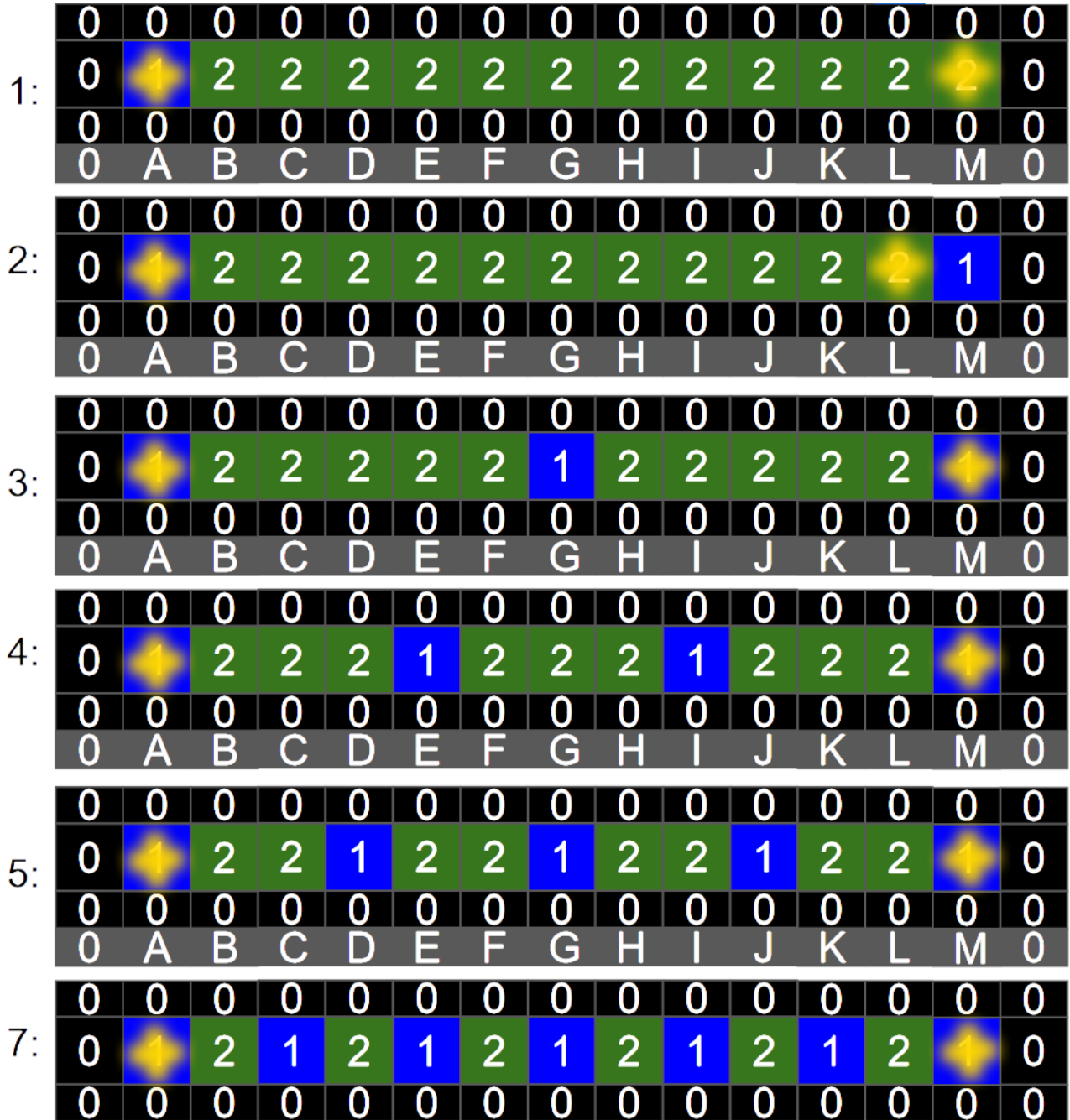
Figure 4.2: Chain configurations used for simulations in this section. The simulation results are depicted in Figure 4.3 on the facing page. The number on the left indicates the amount of LH1 units in that simulation.

The chains are designed to test the what the influence of LH1 concentration is.

I applied Equation Eq. 3.5.3 on page 40 to calculate the ratio between the cross-peaks and the

diagonal peaks intensity, and plotted the ratio as a function of exciton-exciton distance, see Figure 4.3. This ratio is measurable in 2DES experiments.

(a) According to photon counter measuring LH1.

(b) According to photon counter measuring LH2.

Figure 4.3: Cross-peak to Diagonal-peak ratio according to photon counters measuring either the fluorescence intensity on LH1 or LH2. This Figure is the result of simulating the chains defined in Figure 4.2 on the preceding page.

4.3 Embedded chains

I taught that the previous simulation (on linear chains) might not have been very realistic, since these simulations were one dimensional, and one can easily imagine that the probability that two excitons annihilate in a one-dimensional system is much higher than in a two dimensional system. Therefore, the linear chains (Figure 4.2) were embedded in a bath of LH2 molecules.

The first exciton is placed in the top left corner, but the second exciton can be placed anywhere, so I developed some algorithm which determines the distance of the second exciton with respect to the first exciton. The distance in units of LH1 or LH2, but this would only give a distance in integers. Since we have many more data points (3x15=45) than we have distance-points (15), the plot points got on top of each other, which made very ugly graphs. In order to make it nicer, I've decided to subtract some scoring $\frac{1}{n}$ if there are multiple (n) pathways of getting from the first to the second exciton. The offset is little, and it causes saw-toothed-graphs, which are still not the nicest looking graphs, but it's better than stick-figures.

Again, I applied Equation Eq. 3.5.3 on page 40 to calculate the ratio between the cross-peaks and the diagonal peaks intensity, and plotted the ratio as a function of exciton-exciton distance, see Figure 4.5 on the next page.

Figure 4.4: Embedded chain configurations used for simulations in this section. These are same chains as in Figure 4.2 but with one LH2 unit of padding around it. The number on the left of each simulation indicates the number of LH1 units in this simulation. The simulation results are depicted in Figure 4.5 on the next page.

(a) According to photon counter measuring LH1.

(b) According to photon counter measuring LH2.

Figure 4.5: Cross-peak to Diagonal-peak ratio according to photon counters measuring either the fluorescence intensity on LH1 or LH2. This Figure is the result of simulating the embedded chains defined in Figure 4.4 on the preceding page.

4.4 Squares

I thought that the embedded chains were a bit unrealistic, and I thought of a little fix to get rid of the saw-toothed graphs (Figure 4.5): let's try a square simulation box in which the configuration of LH1's/LH2 is symmetrical with respect to the diagonal on which the first exciton is placed. Since the previous simulation was starting to get slow, I didn't want to add much more molecules, as it might mean that the simulations would be running forever.

The simulated square configurations are shown in in Figure 4.6. One small note: I represented these configurations as squares, because I use square grids in `numpy`, as square grids are cheaper than hexagonal grids. In reality, however, I use a mathematical trick which cause the squares to sense 6 neighbors, just like a hexagonal grid. This is better explained in Figures B.2 and B.3 on page 74 of the Appendix.

#1

	1	2	3	4	5	6	7	
	0	0	0	0	0	0	0	0	0
1	0	2	2	2	2	2	2	2	0
2	0	2	2	2	2	2	2	2	0
3	0	2	2	2	2	2	2	2	0
4	0	2	2	2	1	2	2	2	0
5	0	2	2	2	2	2	2	2	0
6	0	2	2	2	2	2	2	2	0
7	0	2	2	2	2	2	2	2	0
	0	0	0	0	0	0	0	0	0

(a) Square 1.

#2

	1	2	3	4	5	6	7	
	0	0	0	0	0	0	0	0	0
1	0	2	2	2	2	2	2	2	0
2	0	2	1	2	2	2	2	2	0
3	0	2	2	2	2	2	2	2	0
4	0	2	2	2	2	2	2	2	0
5	0	2	2	2	2	2	2	2	0
6	0	2	2	2	2	2	1	2	0
7	0	2	2	2	2	2	2	2	0
	0	0	0	0	0	0	0	0	0

(b) Square 2.

#3

	1	2	3	4	5	6	7	
	0	0	0	0	0	0	0	0	0
1	0	2	2	2	2	2	2	2	0
2	0	2	1	2	2	2	1	2	0
3	0	2	2	2	2	2	2	2	0
4	0	2	2	2	2	2	2	2	0
5	0	2	2	2	2	2	2	2	0
6	0	2	1	2	2	2	2	2	0
7	0	2	2	2	2	2	2	2	0
	0	0	0	0	0	0	0	0	0

(c) Square 3.

#4

	1	2	3	4	5	6	7	
	0	0	0	0	0	0	0	0	0
1	0	2	2	2	2	2	2	2	0
2	0	2	1	2	2	2	1	2	0
3	0	2	2	2	2	2	2	2	0
4	0	2	2	2	2	2	2	2	0
5	0	2	2	2	2	2	2	2	0
6	0	2	1	2	2	2	1	2	0
7	0	2	2	2	2	2	2	2	0
	0	0	0	0	0	0	0	0	0

(d) Square 4.

#5

	1	2	3	4	5	6	7	
	0	0	0	0	0	0	0	0	0
1	0	1	2	2	2	2	2	1	0
2	0	2	2	2	2	2	2	2	0
3	0	2	2	2	2	2	2	2	0
4	0	2	2	2	1	2	2	2	0
5	0	2	2	2	2	2	2	2	0
6	0	2	2	2	2	2	2	2	0
7	0	1	2	2	2	2	2	1	0
	0	0	0	0	0	0	0	0	0

(e) Square 5.

#6

	1	2	3	4	5	6	7	
	0	0	0	0	0	0	0	0	0
1	0	1	2	2	1	2	2	2	0
2	0	2	2	2	2	2	2	2	0
3	0	2	2	2	2	2	2	2	0
4	0	1	2	2	2	2	2	1	0
5	0	2	2	2	2	2	2	2	0
6	0	2	2	2	2	2	2	2	0
7	0	2	2	2	1	2	2	1	0
	0	0	0	0	0	0	0	0	0

(f) Square 6.

Figure 4.6: Simulated square configurations. Note that the first excitation will always be placed in the top left corner. The second excitation will be placed everywhere, and the cross-peak to diagonal-peak ratio will be calculated and plotted as a function of distance, see Figure 4.7 on the facing page.
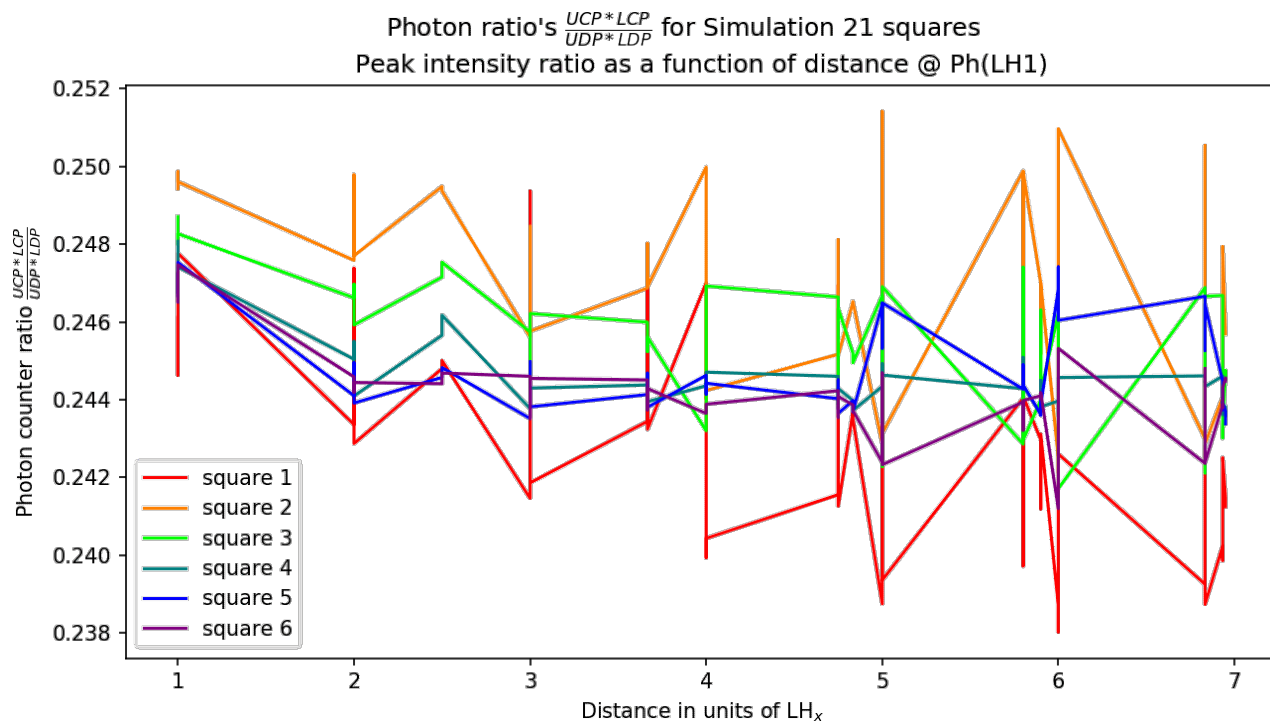
(a) According to photon counter measuring LH1.
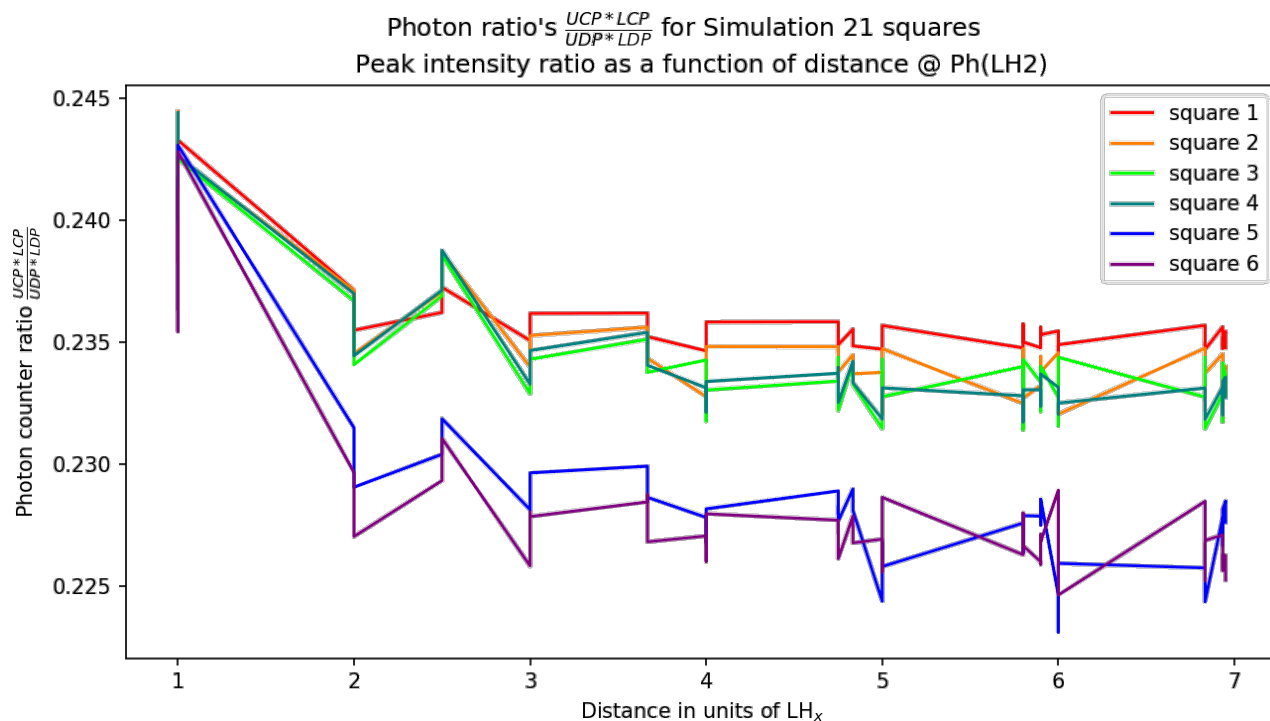
(b) According to photon counter measuring LH2.

Figure 4.7: Cross-peak to Diagonal-peak ratio $\left(\frac{UCP*LCP}{UDP*LDP}\right)$ according to photon counters measuring either the fluorescence intensity on LH1 or LH2. This Figure is the result of simulating the squares defined in Figure 4.6 on the facing page.
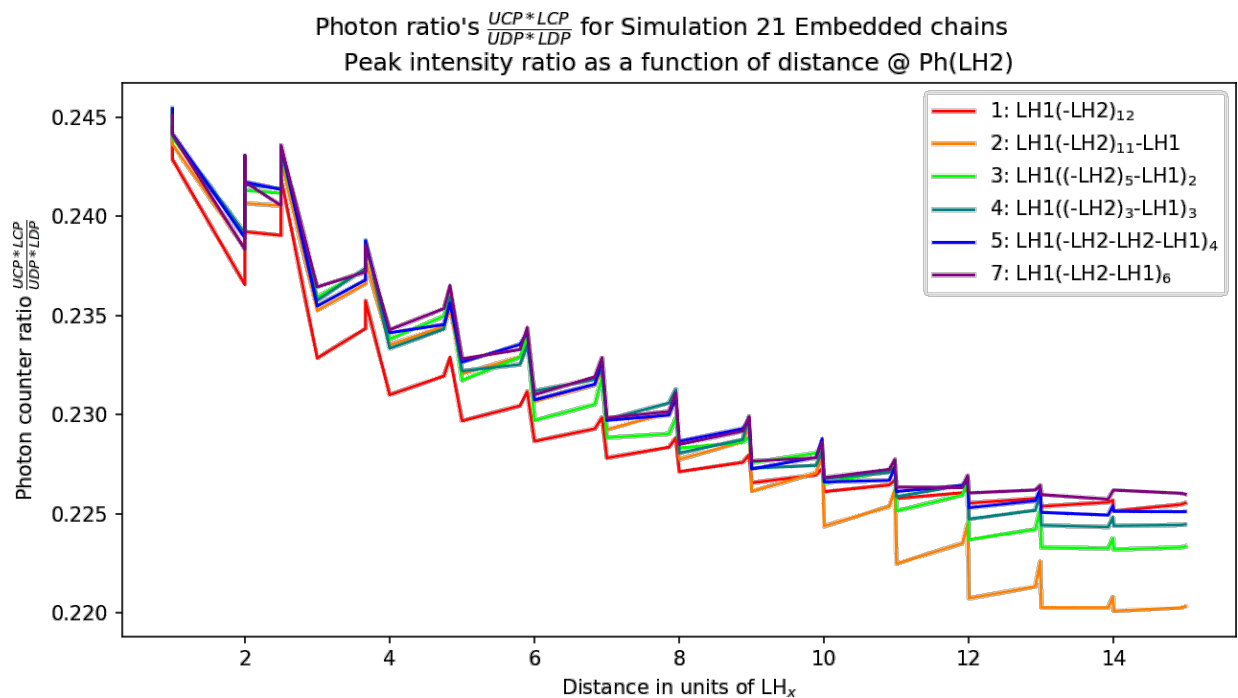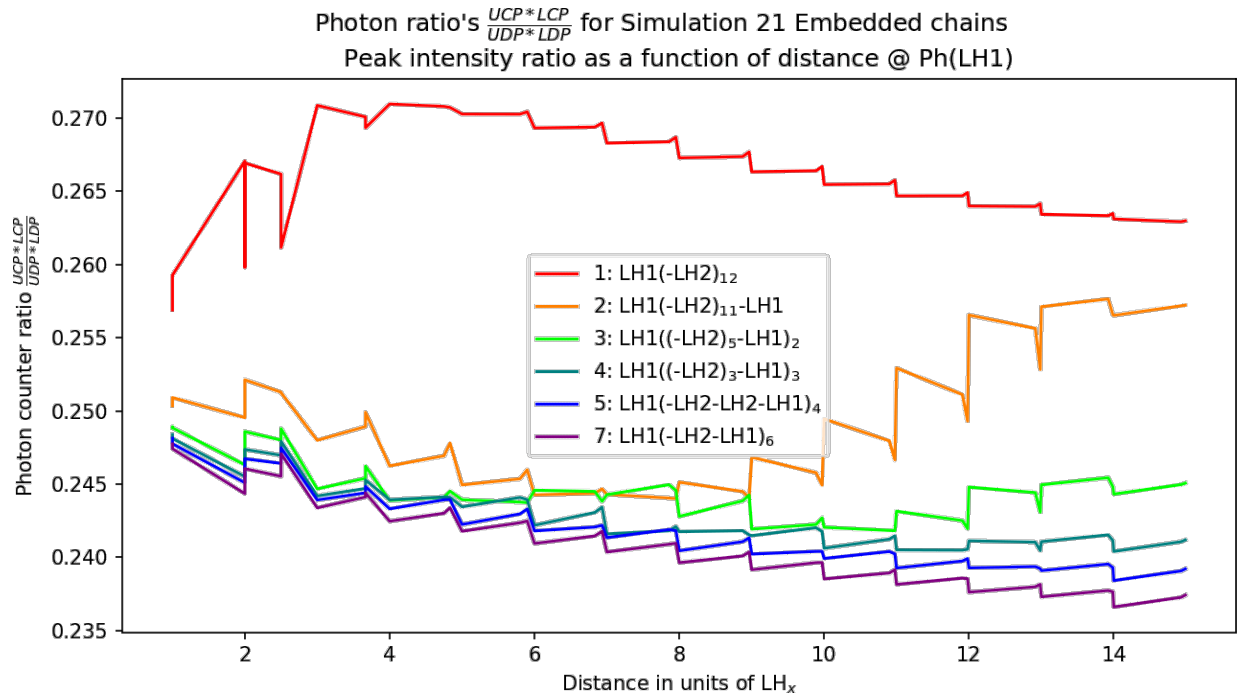
Unfortunately, it's very hard to find a trend which correlates to either distance or LH1 concentration, and it is more dependent on whether in the first frame, LH1 or LH2 is excited. This claim is underwritten by the fact that square 5 and 6 are significantly different to squares 1-4 in Figure 4.7b.

It becomes easier to find the trends if we calculate the $\frac{UCP*LCP}{UDP*LDP}$ photon counter ratio's between all pairs of Light Harvesting unit's, and display the mean $\pm$ standard deviation, see Figure 4.8

(a) According to photon counter measuring LH1.

(b) According to photon counter measuring LH2.
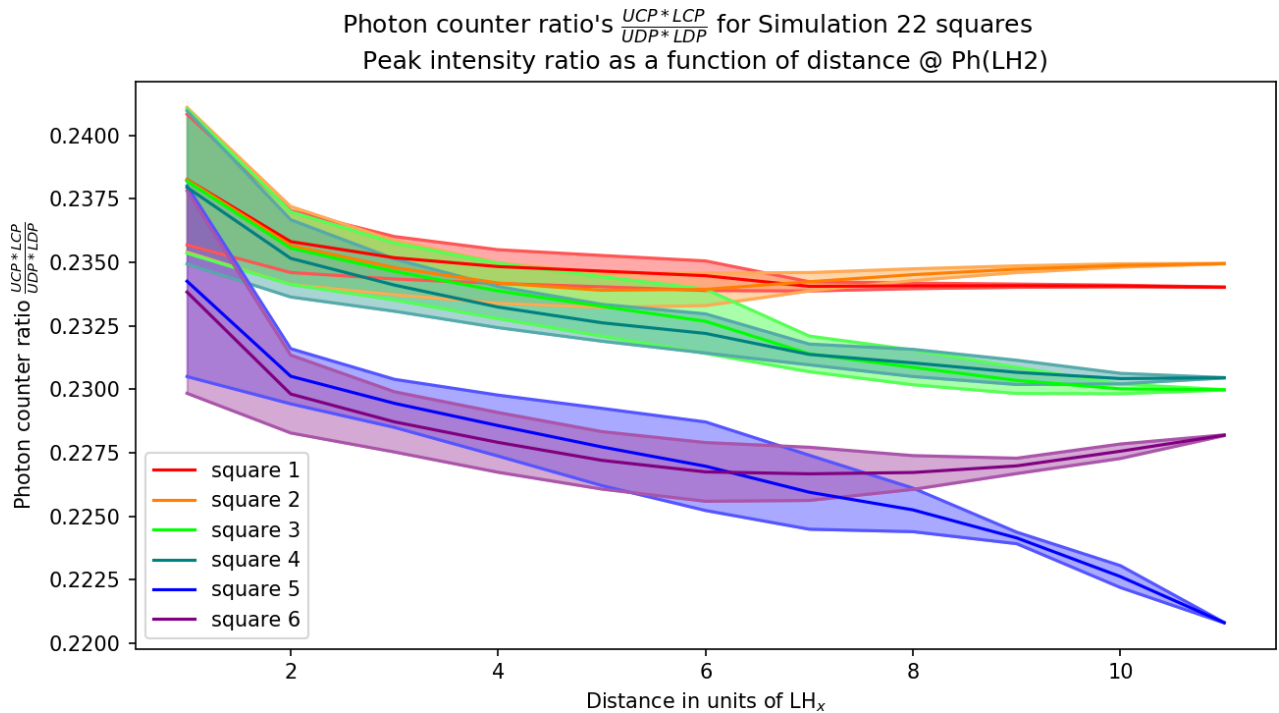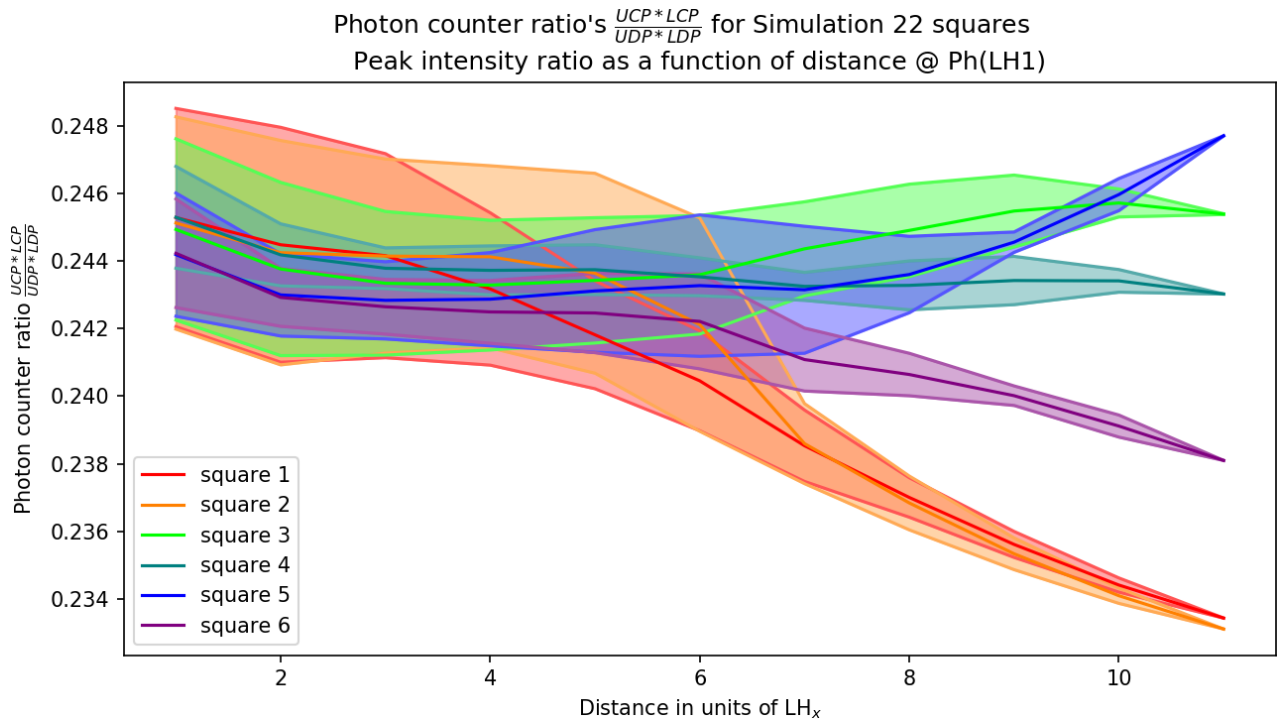
Figure 4.8: Cross-peak to Diagonal-peak ratio, averaged over all double excitations possible in the Light Harvesting antenna. This Figure is the result of simulating the squares defined in Figure 4.6.

Since experimentalists cannot select the distance at which the two excited states are placed, I decided to also make a graph in which all simulation data that comes out of one simulated square of Figure 4.6 will be reduced to one data-point: a mean peak ratio ± a standard deviation, see Figure 4.9.
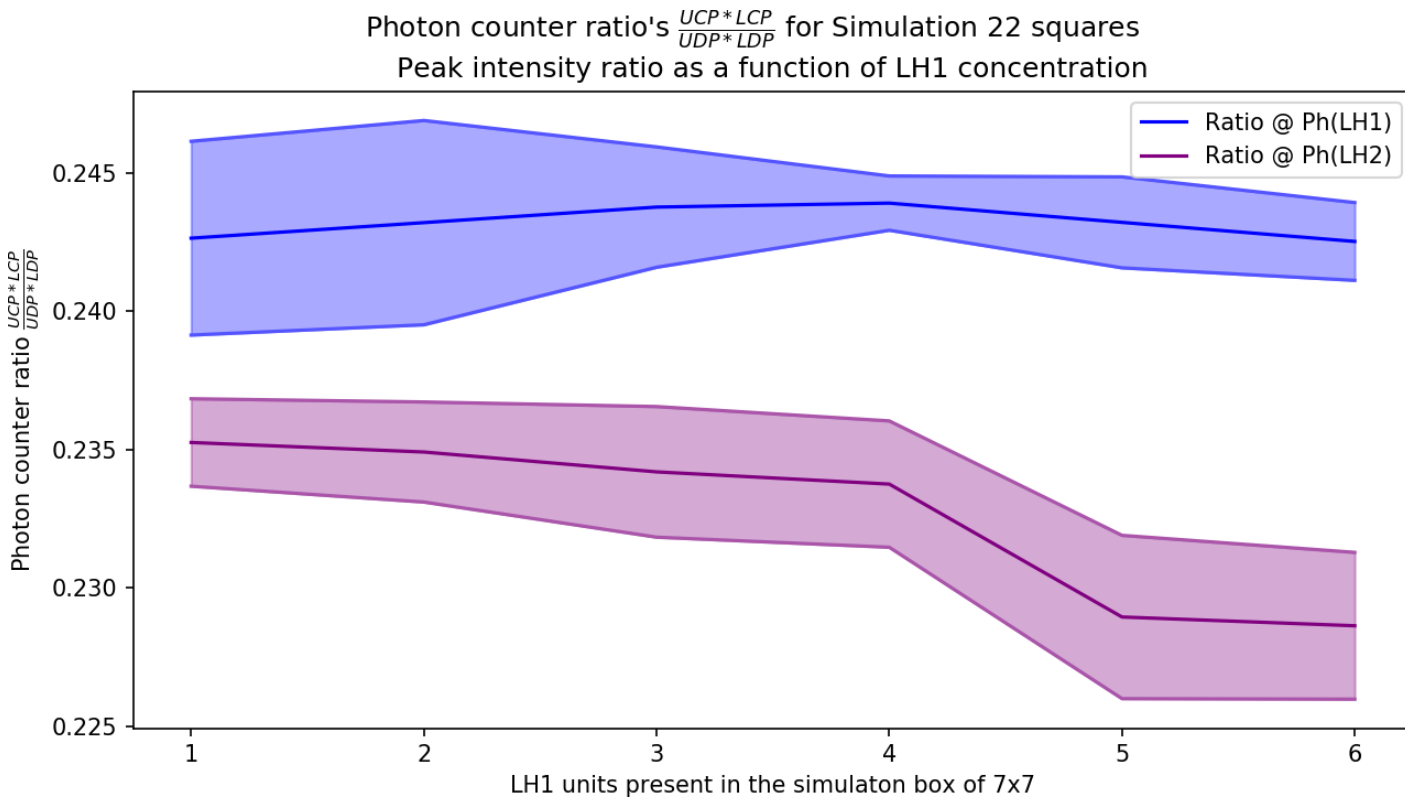
Figure 4.9: Cross-peak to Diagonal-peak ratio, as a function of LH1 concentration.

4.5 Introducing vacancies

The simulation from the previous section is nice, but it only shows 6 cherry picked simulations, and it says nothing about the $\sum_{nLH1=0}^{nLH1=49} \frac{49!}{(49-nLH1)! \times (nLH1)!} \approx 5.6295 \times 10^{14}$ other configurations in which the system could have been arranged. Therefore I decided to test more randomly generated configurations. These simulated configurations will look a lot more like those which could be encountered in nature.

As I will later point out in the discussion (section 5.2), we cannot perform experiments in which we explicitly put two excitons on different locations in the light harvesting network. Therefore the distance dependence graphs will be omitted. Which is actually great, since graphs containing more than 10 lines are typically a mess anyways.

Natural light harvesting systems change their LH1/LH2 concentrations based on the amount of light available. Under very low light conditions, the organism can survive with very little reaction centers (LH1), as long as it has plenty of light antenna (LH2) to catch the light. When there is more light, more reaction centers are required. I already demonstrated in the previous sections that I can easily model this by replacing an LH2 unit with an LH1 unit. When there is too much light, however, vacancies are introduced. This reduces the amount of light that will be captured.

I added the vacancy option in the simulation code by introducing the "nLH0" option in the `makeLH1LH2grid()` module. This introduces more "0" elements, which act as walls, placed at random positions in the `LHgrid`.
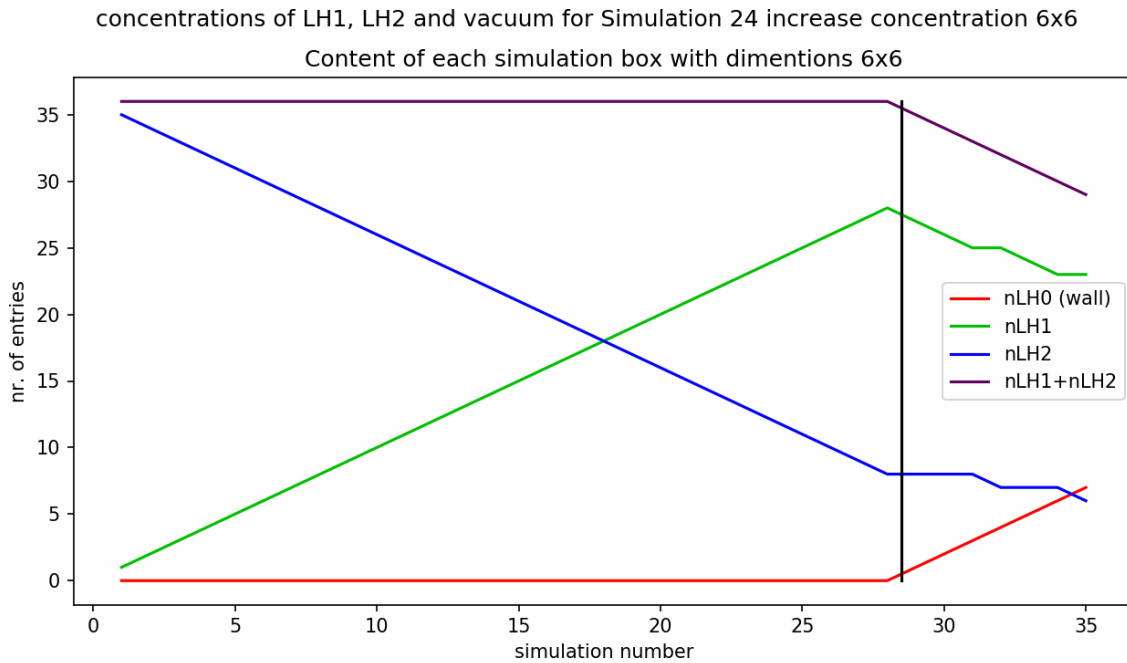
Figure 4.10: The content of each simulation. Left of the black line, the simulation number corresponds to the number of LH1 units in the 6x6 light harvesting network. After the black line, vacancies are introduced, deleting either an LH1 or an LH2 entity. `nLH1 = max_nLH2 - int(nLH0 / 1.4)`.
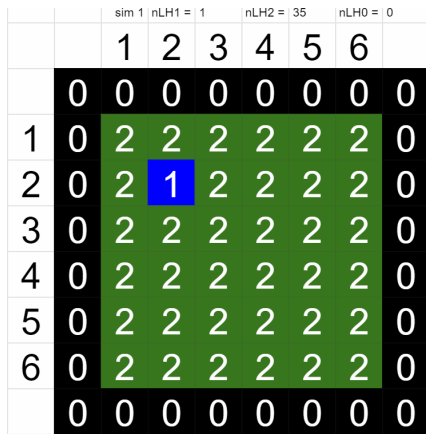
(a) Configuration 1.
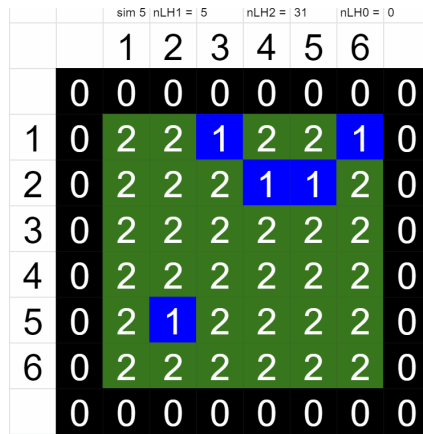
(b) Configuration 5.
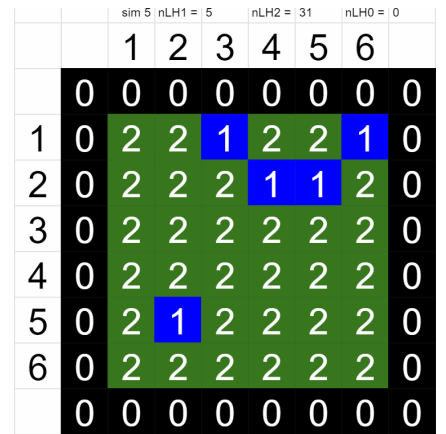
(c) Configuration 10.
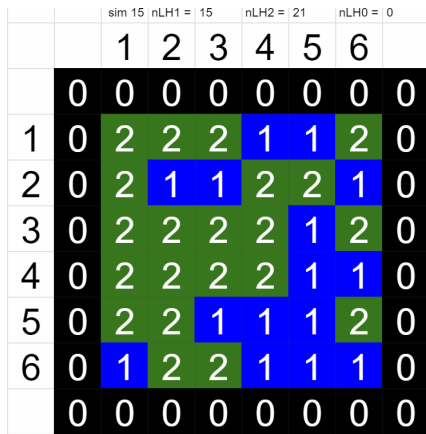
(d) Configuration 15.
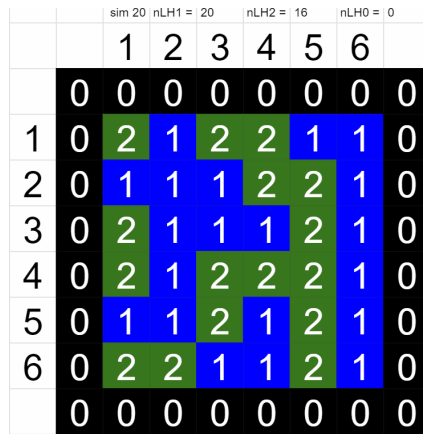
(e) Configuration 20.
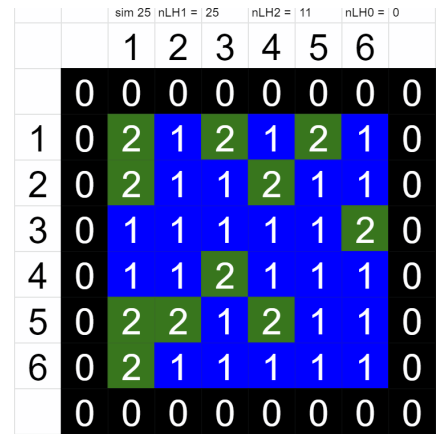
(f) Configuration 25.
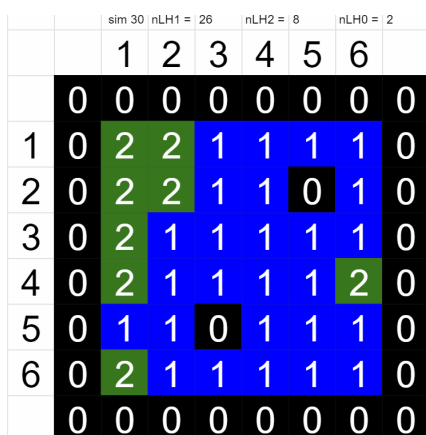
(g) Configuration 30.
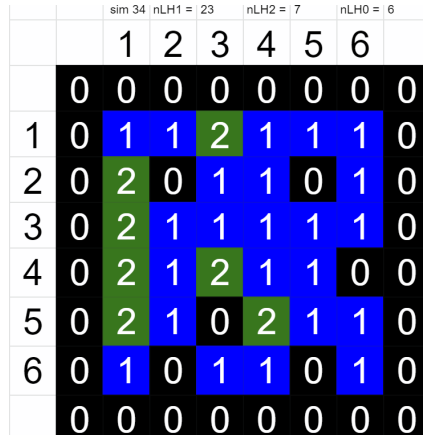
(h) Configuration 34.
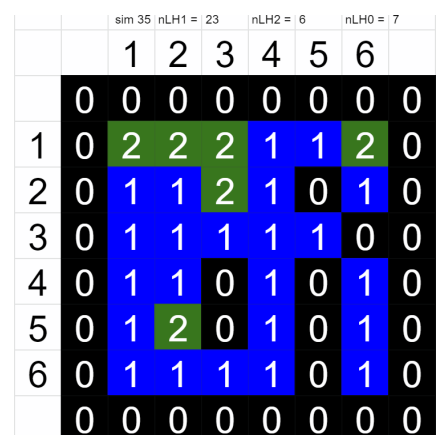
(i) Configuration 35.

Figure 4.11: The configurations of a few simulations of the experiment in which we continuously change the LH1/LH2 concentration, over a very wider range than we did in previous experiments.
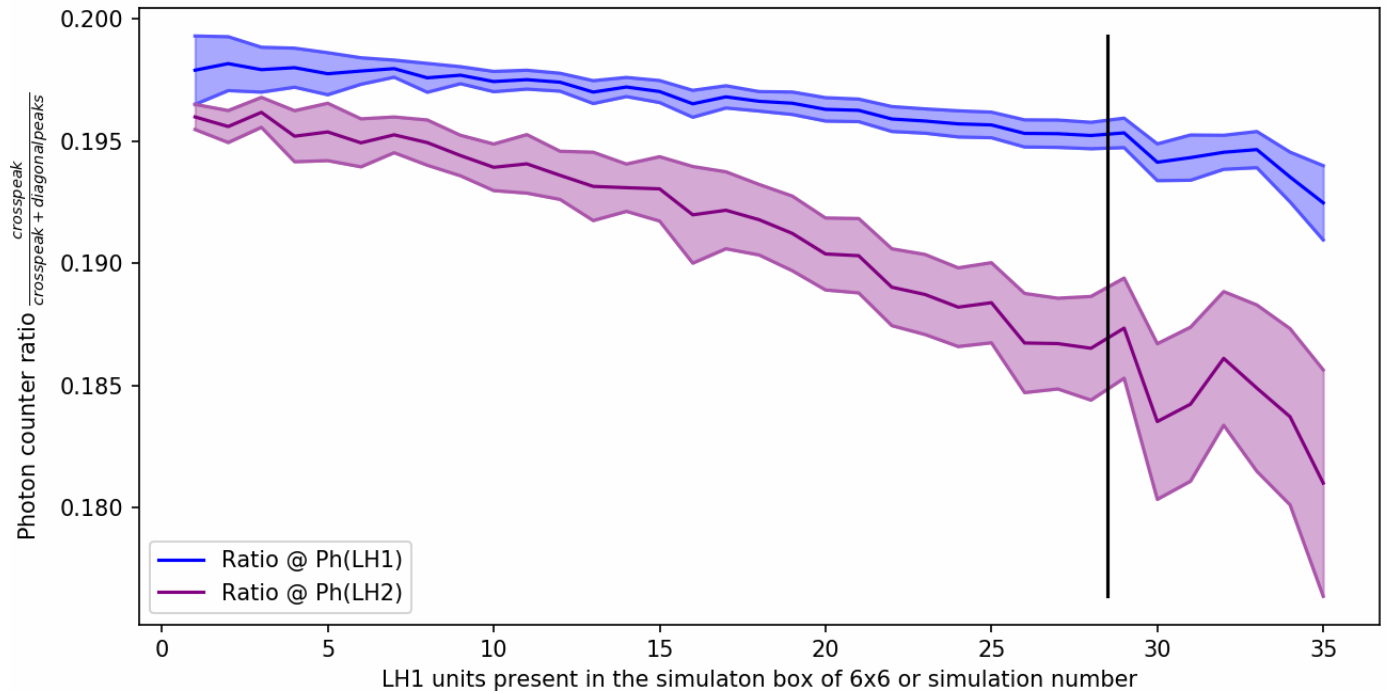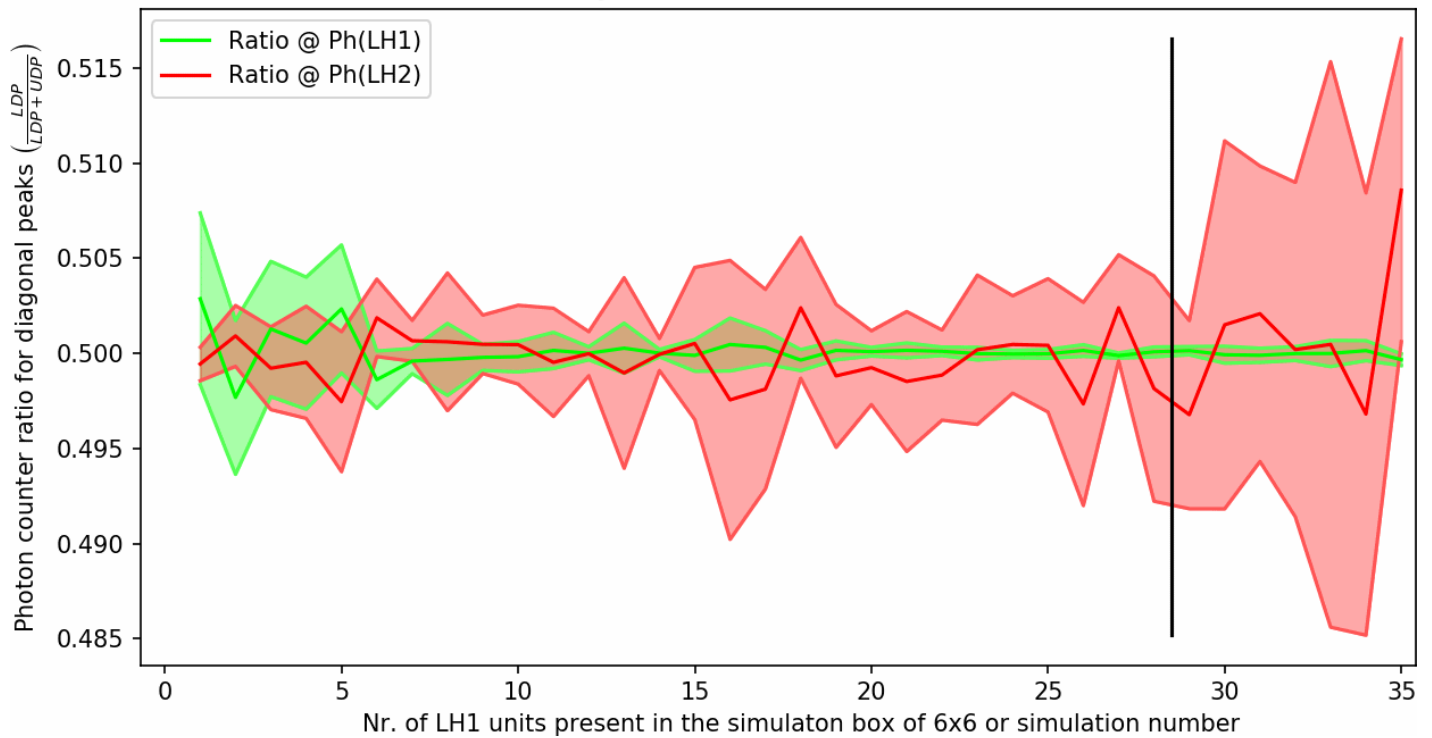
(a) Cross peak data

(b) Diagonal peak data

Figure 4.12: The **(A)** cross peaks and **(B)** diagonal peaks, both as a function of LH1/LH2 concentration. Similar to indicated in Figure 4.10, the black line indicates where the simulations switch from replacing LH2 with LH1 to introducing vacancies.

We can see a clear trend between increasing the LH1 concentration and a decreasing cross peak intensity, irrispective of whether we measure

Now, ideally, I would include even more simulations with even more vacancies. Unfortunately however, these simulations have the tendency to not generate stable information on the cross peaks. One of the ways it would crash was by having islands on which only one LH1 or LH2 would be found, which causes an $1/0$ error in the previous way we calculated the cross peak ratio.

$$\frac{\text{LCP} * \text{UCP}}{\text{LDP} * \text{UDP}} = \frac{(\text{AG} + \text{BG} - \text{AB})^2}{2\text{AG} * 2\text{BG}} \quad \leftarrow \text{ If either AG or BG} = 0, \text{ we encounter the } \tfrac{1}{0} \text{ problem}$$

This is why I have implemented the less scientifically accurate, but more robust

$$\text{Cross peak ratio} = \frac{\text{LCP}}{\text{LDP} + \text{UDP} + \text{LCP}} = \frac{(\text{AG} + \text{BG} - \text{AB})}{3\text{AG} * 3\text{BG} - \text{AB}} \qquad \text{(Eq. 4.5.2)}$$

Although the above equation is more robust, the $\tfrac{1}{0}$-issue will still occur at very low light harvester concentration (so when a simulation box contains a lot of vacancies). The most robust thing is to add some very small number, say 1E-99 to the denominator. This will ensure that the $\tfrac{1}{0}$-issue will be gone forever, regardless of the value in the nominator or denominator. Unfortunately, the author didn't have time to implement this idea before the deadline of this thesis.

Chapter 5

Discussion & Conclusion & Outlook

This is the concluding chapter of this thesis. We will start with a small summary, then postulate the limitations, emphasize what we can do, and then finish with a conclusion and an outlook.

5.1   In short

Fluorescence Detected Two Dimensional electronic Spectroscopy (FD-2DES) is a new multidimensional spectroscopy technique which allows for the detection of 2D electronic spectra, with a higher signal to noise ratio than obtained in regular 2DES experiments. Both normal 2DES and FD-2DES images are hard to interpret, but FD-2DES is still a very new spectroscopy technique, therefore, it makes sense to develop a model which predicts the outcome of the FD-2DES experiment.

The FD-2DES experiment is quite advanced. It's increased signal-to-noise ratio allows this technique to measure light sensitive photobacteria before they photo-bleach. It allows to measure and compare the light harvesting systems in bacteria grown under low light (LL) and high light (HL) conditions. This comparison is done in Section 5.4.

5.2 What <u>cannot</u> be measured? (Limitations)

As you can see from Figures 4.3, Fig. 4.5 and Fig. 4.7, the diagonal/cross-peak ratio is very sensitive to the initial double exciton configuration. It's so sensitive to the configuration, that it became hard to see the trend versus LH1 concentration.

Unfortunately, 2DES experiments are currently unable to repeat the experiments performed in those simulations, because the volume probed by the laser is approximately 1 µm³, which is much greater than one LH1 (∅ of ∼10 nm) or one LH2 (∅ of ∼5-6 nm). This is because the resolution in a fluorescence microscope is diffraction limited:

$$r = \frac{\lambda}{2 \cdot \textbf{N.A.}} = \frac{\lambda}{2n\sin(\alpha)}, \qquad \text{(Eq. 5.2.1)}$$

where r is the maximum resolution, λ is the wavelength of light and **N.A.** is the numerical aperture. The numerical aperture is calculated as n (the index of refraction of the imaging medium; typically immersion oil, n = 1.51) times $\sin(\alpha)$ (in which α is the half-angle by which light still hits the lens). A good first guess of the maximum resolutions is $r \approx \frac{\lambda}{2} \approx 500$nm. Much larger than an LH1 or LH2 anyways.

There is a technique which allows to for higher resolution: stimulated emission depletion (STED) fluorescence microscopy. This uses one pulse to excite the molecules, and then a second pulse with a doughnut-shaped light beam, see Figure 5.2. The second pulse induces stimulated emission, thus, photobleaching the molecules which are not in the center of the doughnut. The problem of STED is that it's probably not compatible with 2DES, because STED is a time-resolved experiment itself already.
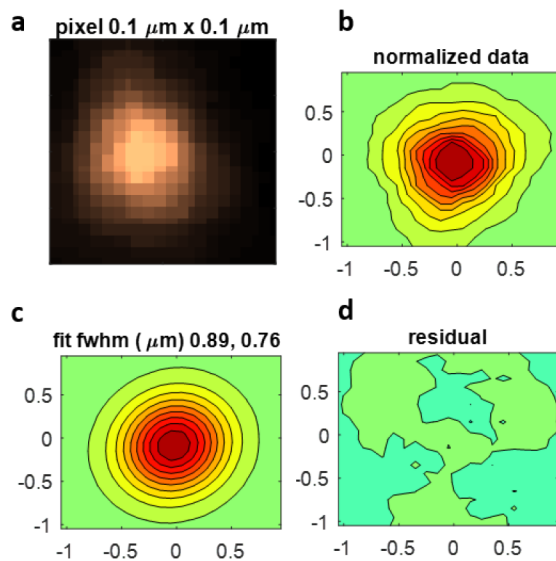
Figure 5.1: Confocal fluorescence image of a 0.5 µm fluorescent bead in the SR-FD-2DES setup[9]. This experiment is typically done in fluorescence microscopes to demonstrate the maximum resolution one can achieve with that microscope. The resolution is diffraction limited, see discussion in the leading text. Creative commons licence applies[8].
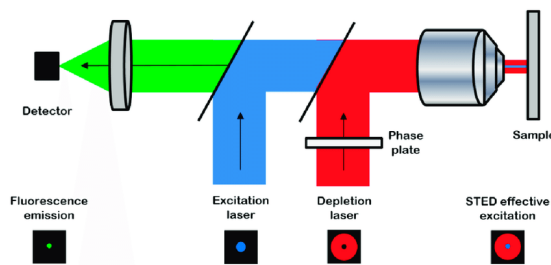
Figure 5.2: Schematic diagram of an optical stimulated emission depletion (STED) microscope. The phase plate shapes the depletion beam (red) into a doughnut-shape. This depleation beam then depletes the excited state (induced by the excitation beam (blue), to leave only fluorescence emission (green) from a small spot. Reprinted with permission from Ref. [28].

5.3 What <u>can</u> we measure?

Experimentally, it's most easy to measure one dimensional absorption spectra, see middle part of Figure 5.3.
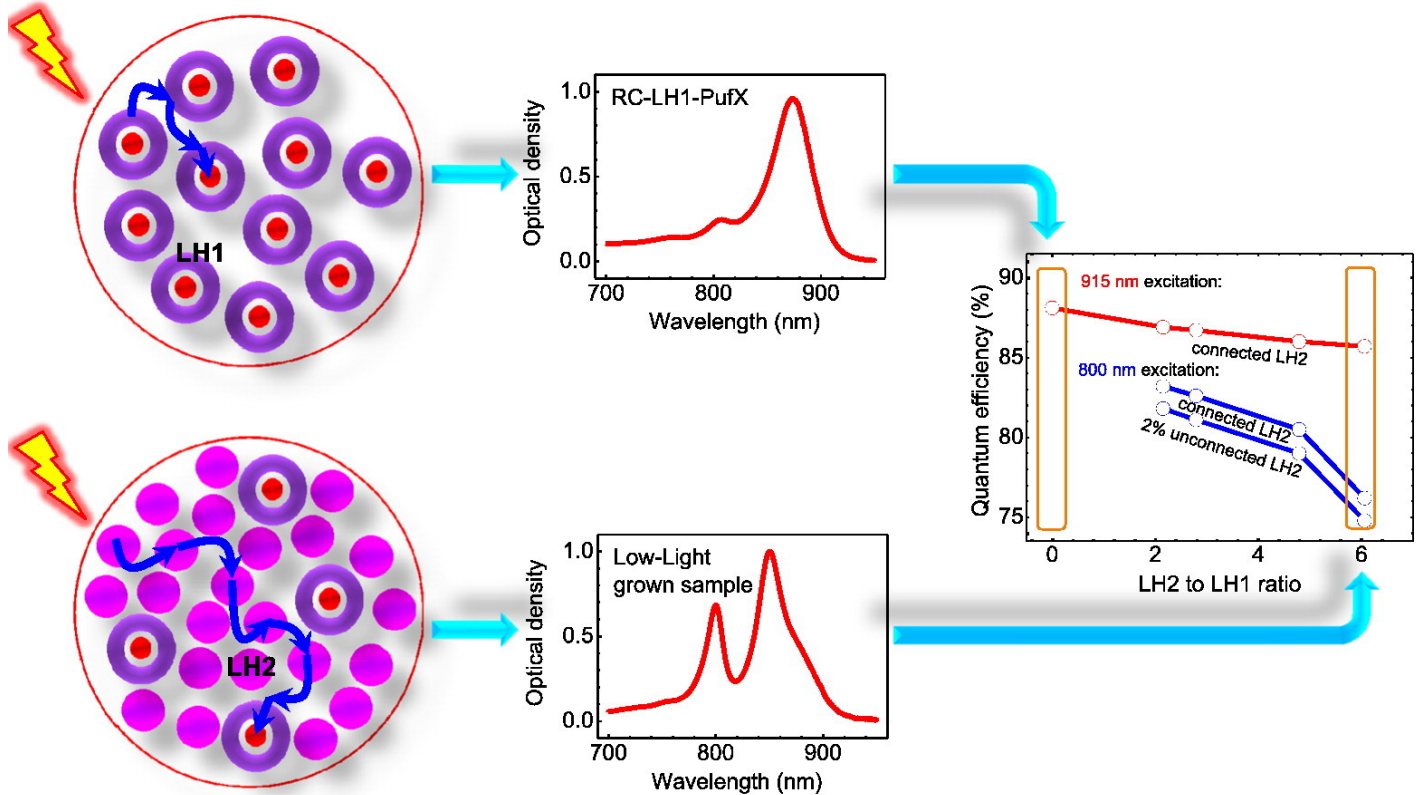
Figure 5.3: High light vs low light experiment. Figure reprinted with permission from Ref. [6].

The thing I concluded from Figure 5.3 is actually the two discs on the left. The main difference is that samples grown under high light (HL) samples contain more reactive centers (LH1), whihe samples grown under low light (LL) samples contain more light antenna's (LH2). Intuitively this makes sense.

For a two dimensional spectroscopy technique like 2DES or FD-2DES, it is experimentally possible to measure the average spectroscopy image of the volume probed. This is also what is simulated in Figure 4.8 on page 50 and Figure 4.12 on page 54. When all $\frac{UCP*LCP}{UDP*LDP}$ peak ratio's for all double exciton configurations are calculated, as done in Figure 4.12a, we can observe a trend of lower $\frac{UCP*LCP}{UDP*LDP}$ peak ratio at higher LH1 concentration. The correlation is stronger when LH2 is measured, but it is also there when LH1 is measured.

Another limitation. When we are introducing vacancies (which are present in high light samples, see Figure 5.3), the simulation becomes less reliable, because sometimes there is an island with no LH1 or LH2 entity. The photon counter for that molecule (either LH1 or LH2) will be 0. When applying Eq. 3.5.3, $\frac{1}{0}$ or $\frac{0}{0}$ might occur. This could be resolved by adding a very small number, e.g. `1E-99` to the denominator Unfortunately, the author didn't have time to implement this simple solution. For now, I

just don't perform the simulations with very low light harvesting concentation. The observation remains that that the same trend continues; higher LH1 concentration results in lower cross peak intensity, see Figure 4.12a on page 54.

5.4   Comparison with an FD-2DES experiment

As the signal-to-noise ratio for FD-2DES is higher than for the conventional 2DES experiment, FD-2DES allows us to measure photobacteria grown under low light (LL) conditions. We can now compare the spectroscopy images of these bacteria with bacteria grown under high light (HL) conditions, see Figure 5.4[8].

When I saw Figure 5.4 for the first time, it struck me that there is more upper diagonal peak in the high light sample than in the low light sample, while Figure 4.12b on page 54 predicted that there was no relation between the ratio between the two diagonal peaks, and the LH1:LH2 and vacancy ratio.

The thing with Figure 5.4 is that the samples only contained Light Harvesting system 2 (LH2). The main discovery of Ref. [9] is that LH2 changes upon different light conditions. This is something I did not include in my model.

5.5   Conclusion

Fluorescence detected two dimensional electronic spectroscopy (FD-2DES) is a relatively new spectroscopy technique. With the help of the code developed in this thesis, one can predict various observables from FD-2DES images, like cross-peak to diagonal peak ratio or the ratio at which the two diagonal peaks occur. These observables can be simulated and correlated with any adjustable parameter at choice, which gives the simulation operator infinite possibilities for simulations. This makes it hard to demonstrate the full potential of the code in just a few pages.

---

[8]   Figures 5.1 and 5.4 are from Ref. [9] with creative commons licence, see `https://creativecommons.org/licenses/by/4.0/`.
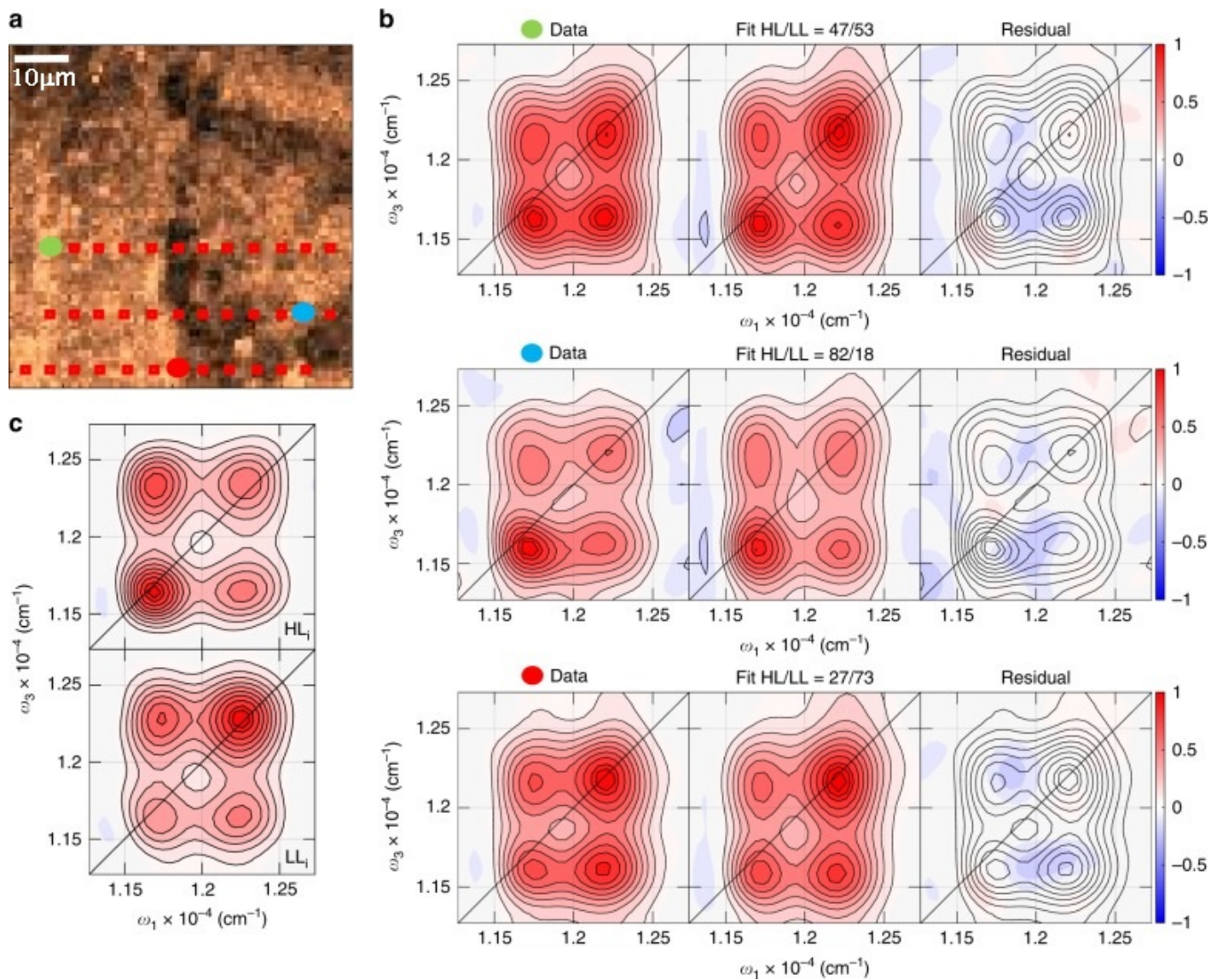
Figure 5.4: Spatially-resolved fluorescence-detected two-dimensional electronic spectroscopy (SR-FD-2DES)[9]. The red dots in (**a**) are the places where the 2D spectrum are measured. The maximum resolution of SR-FD-2DES is measured in Figure 5.1. Creative commons licence applies[8].

5.6 Outlook

The code can easily be adjusted for experiments with different light harvesting systems. The code is not limited by the boundaries of what nature has to offer. With a few adaptations, the code can be used to simulate exciton dynamics in a PN-heterojunction in an organic solar cell.
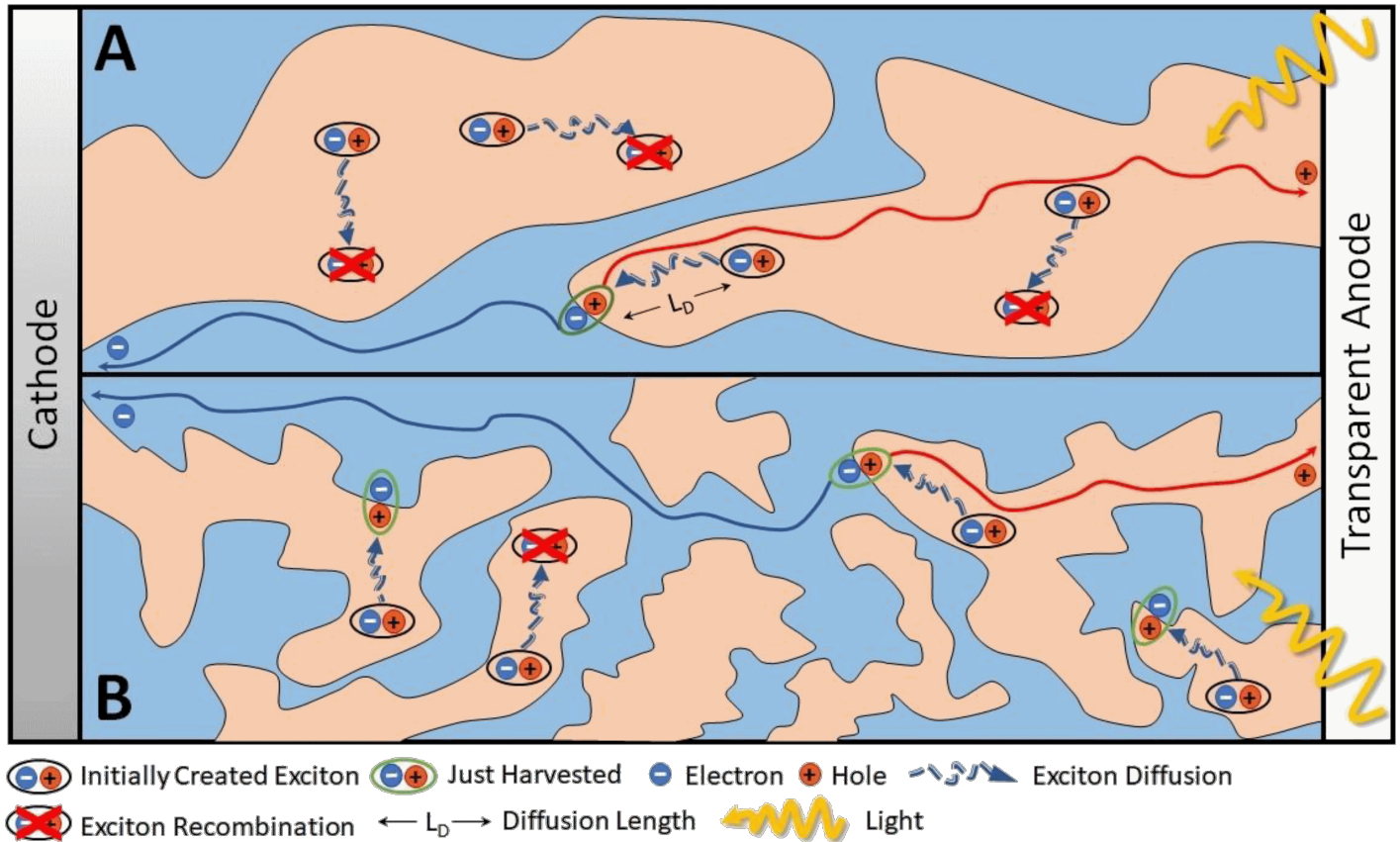
Figure 5.5: Photocurrent generation processes in two bulk heterojunctions with very different morphologies: a bad morphology (A) and a good morphology (B). Figure reprinted from Ref. [29]. This Figure was published under the Creative Common CC BY licence.

Together with the knowledge gained by studying natural light harvesting systems, we might be able to optimize organic solar cells.

Chapter 6

Contributions

The author proposed the research question and designed the research together with T.L.C. Jansen. Simulations were done using Python[16] and Mathematica from Wolfram Research[18]. The author wrote the code for all simulations and performed all debugging themselves. The conclusions presented in the conclusion section were all drawn by the author with feedback from T.L.C. Jansen.

Chapter 7

Acknowledgement

Appendices

Appendix A

Energy transfer rates rates

In this appendix-chapter, I will elaborate on the energy transfer rate. There are many interesting things going on, e.g. between equivalent light harvesting complexes (LH2*+LH2 $\rightleftharpoons$ LH2+LH2*), between unequal light harvesting complexes (LH2*+LH1 $\rightleftharpoons$ LH2+LH1*), and within light harvesting complex 2 (LH2: B800*+B850 $\rightleftharpoons$ B800+B850*).

In this appendix-chapter, I will elaborate a bit on how the numbers of are derived, and what further implications there are for the spectroscopic measurement.
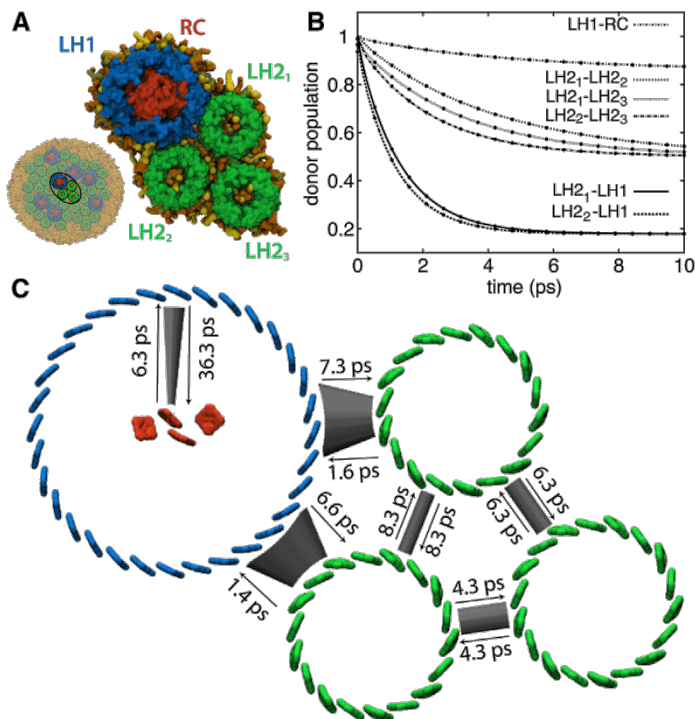
Figure A.1: (A) Schematic representation of an antenna network. The subsystem of one RC-LH1 (with B875 in blue) and three LH2 units (with B850 in green) is later used in (C) to illustrate the transfer rates. Reprinted with permission from [7].

A.1 Calculating asymmetric kinetic rates

As discussed in section 2.2.2 on page 16, the energy transfer rates between molecules A and B is asymmetric if A and B have a different HOMO-LUMO energy gap.

$$A + B^* \underset{k_{A \to B}}{\overset{k_{B \to A}}{\rightleftharpoons}} A^* + B \qquad \text{(Eq. A.1.1)}$$
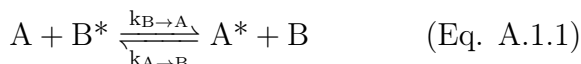
$$\frac{k_{A \to B}}{k_{B \to A}} = e^{\frac{E_A - E_B}{k_B T}} \qquad \text{(Eq. A.1.2)}$$

The diffusion between LH2 (B850) and LH1 (B875) is shown in Figure A.2.

Unfortunately, literature often only reports the rate for the most dominant process. To make our simulations more complete, however, we want to include diffusion in the opposite direction as well. The reverse rate is easily calculated from the forward rate by scaling the rate down by the $\frac{k_{A \to B}}{k_{B \to A}}$ ratio. We calculate these ratios for both the LH1/LH2 system and for the B800/B850 system. The calculation is performed as follows:
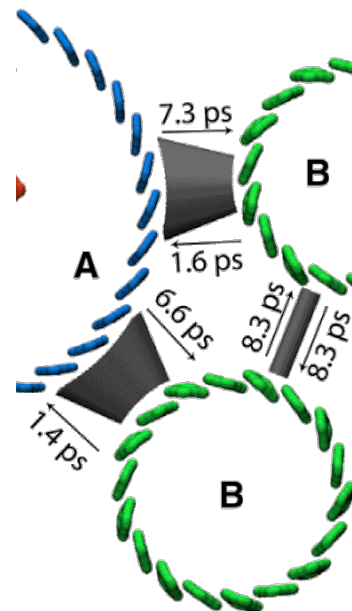
Figure A.2: A zoomed snapshot of Figure A.1 on the previous page. Note that the kinetics is symmetric between two molecules of B (B850 in green), but asymmetric between a molecule of A (B875 in blue) and a molecule of B. The ratio $\frac{k_{A \to B}}{k_{B \to A}}$ is described by the Maxwell-Boltzmann equations, however, the absolute rate also depends on distance and relative orientation.

$LH2 \longrightarrow LH1$	$B800 \longrightarrow B850$	
$E_A = E_{B875} = \frac{hc}{875 \text{ nm}} = 1.417 \text{ eV}$	$E_A = E_{B850} = \frac{hc}{850 \text{ nm}} = 1.459 \text{ eV}$	
$E_B = E_{B850} = \frac{hc}{850 \text{ nm}} = 1.459 \text{ eV}$	$E_B = E_{B800} = \frac{hc}{800 \text{ nm}} = 1.550 \text{ eV}$	
$E_B - E_A = 0.042 \text{ eV}$	$E_B - E_A = 0.091 \text{ eV}$	
At T=313K (40°C), $k_B T = 0.027$ eV	At T=313K (40°C), $k_B T = 0.027$ eV	(Eq. A.1.3)
$\frac{E_B - E_A}{k_B T} = \frac{0.042 \text{ eV}}{0.027 \text{ eV}} = 1.545$	$\frac{E_B - E_A}{k_B T} = \frac{0.091 \text{ eV}}{0.027 \text{ eV}} = 3.379$	
$\frac{k_{LH2 \to LH1}}{k_{LH1 \to LH2}} = e^{1.545} = 4.686$	$\frac{k_{B800 \to B850}}{k_{B850 \to B800}} = \frac{18}{9} \times e^{3.379} = 2 \times 29.33 = 58.67$	
$\frac{k_{LH1 \to LH2}}{k_{LH2 \to LH1}} = e^{-1.545} = 21.34\%$	$\frac{k_{B850 \to B800}}{k_{B800 \to B850}} = \frac{9}{18} \times e^{-3.527} = \frac{1}{2} \times 3.4\% = 1.7\%$	

These are the conversion factors used to build Table 2.2 on page 16.

From Figure A.1 on page 69, we can also determine what the mean and standard deviation of the rate constant for hopping from one LH2 to another LH2 is, by calculating the kinetic rate three times between LH2 complexes. Actually we are not really interested in the individual rates, but more so in the mean and standard deviation of the population of rates.

```python
kLH2LH2min = 1/0.0083
kLH2LH2meh = 1/0.0063
kLH2LH2max = 1/0.0043
kLH2LH2mean = np.mean([kLH2LH2meh,kLH2LH2min,kLH2LH2max])
kLH2LH2stdef = np.std([kLH2LH2meh,kLH2LH2min,kLH2LH2max])
print("kdif(LH2LH2) = ", kLH2LH2mean, " +- ", kLH2LH2stdef)
```

(Eq. A.1.4)

which prints

$$\text{kdif(LH2LH2)} = 170.59 \text{ +- } 46.517 \qquad \text{(Eq. A.1.5)}$$

in unit's of ns^{-1}, just like Eq. B.1.3e on page 77.

Appendix B

Explaining the code

In Chapter 2 (Methods), the Master equations are given. In this Appendix chapter, I demonstrate a few ideas how to program the Master equations in Python.

B.1 Initialization

Before we can run any simulation, we need to define a system. In the end, wanted to perform simulations which resemble the antenna networks encountered in nature as close as possible. See Figure B.1 for an AFM picture of the light harvesting antenna network. I make the following observations:

1. LH1 typically has 7 neighbors and LH2 typically has 6 neighbors.

2. There are more LH2 complexes (about $2 \sim 6\times$[6]) than there are LH1 molecules.

3. Sometimes, two LH1 complexes are neighbors.
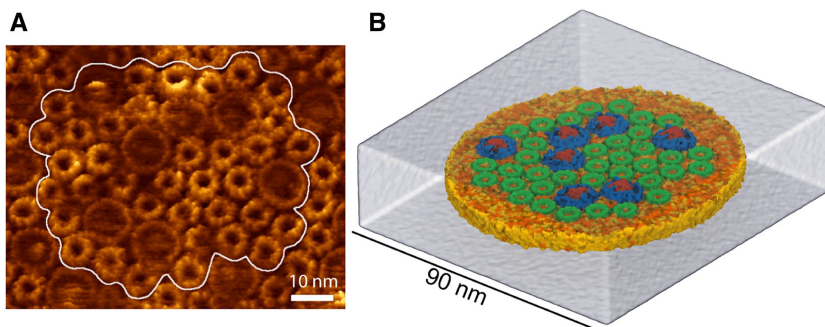
Figure B.1: (A) AFM topograph of the native Rhodospirillum photometricum photosynthetic membrane. (B) is a schematic representation, with LH1 in blue (with red reaction center) and LH2 in green. Reprinted with permision from [7].

B.1.1 Hexagonal grids

In our model, let's make a first simplification: let's assume that both LH1 and LH2 have 6 neighbors. This simplification allows us to use a honeycomb-like lattice with 6-fold symmetry instead of a complicated pseudo-lattice in which some sites have 7 neighbors. In this hexagonal grid, the exciton can move in 6 directions; each movement is described with a distinct rate, see Figure B.2.

The next simplification is actually just a convention: a rectangular matrix will be used to model the probability to find an excited state in the hexagonal lattice. The dynamics is made similar by ensuring the interaction between 2 diagonal neightbors, see Figure B.3.

(a) k_{up1} and k_{down1}

(b) k_{up2} and k_{down2}

(c) k_{Left} and k_{Right}
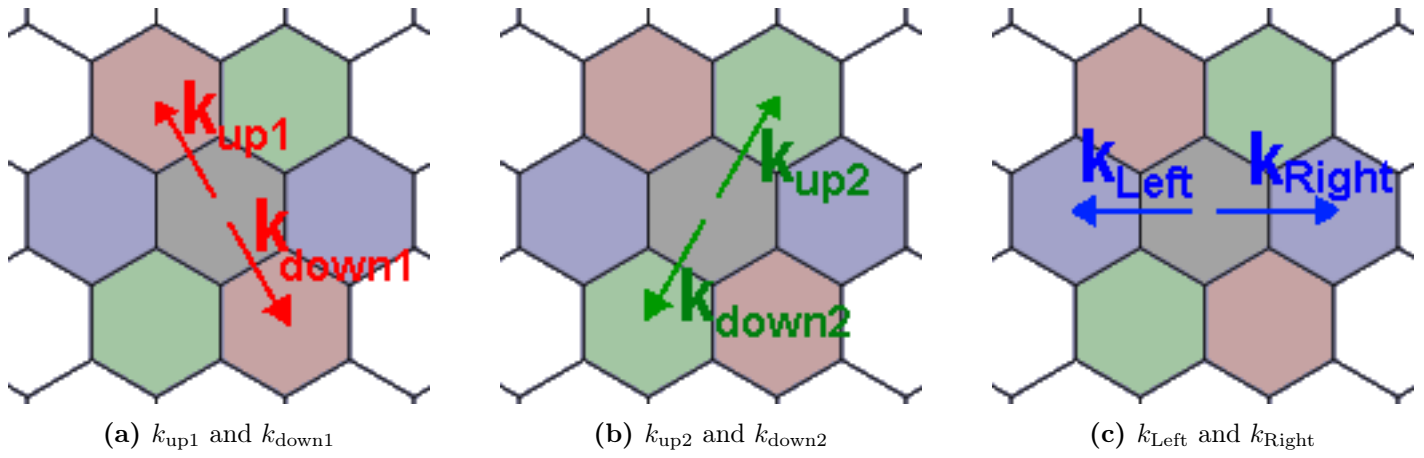
Figure B.2: Movements in the hexagonal lattice

(a) k_{up1}

(b) k_{up2}

(c) k_{Left}

(d) k_{down1}

(e) k_{down2}

(f) k_{Right} and k_{Right}
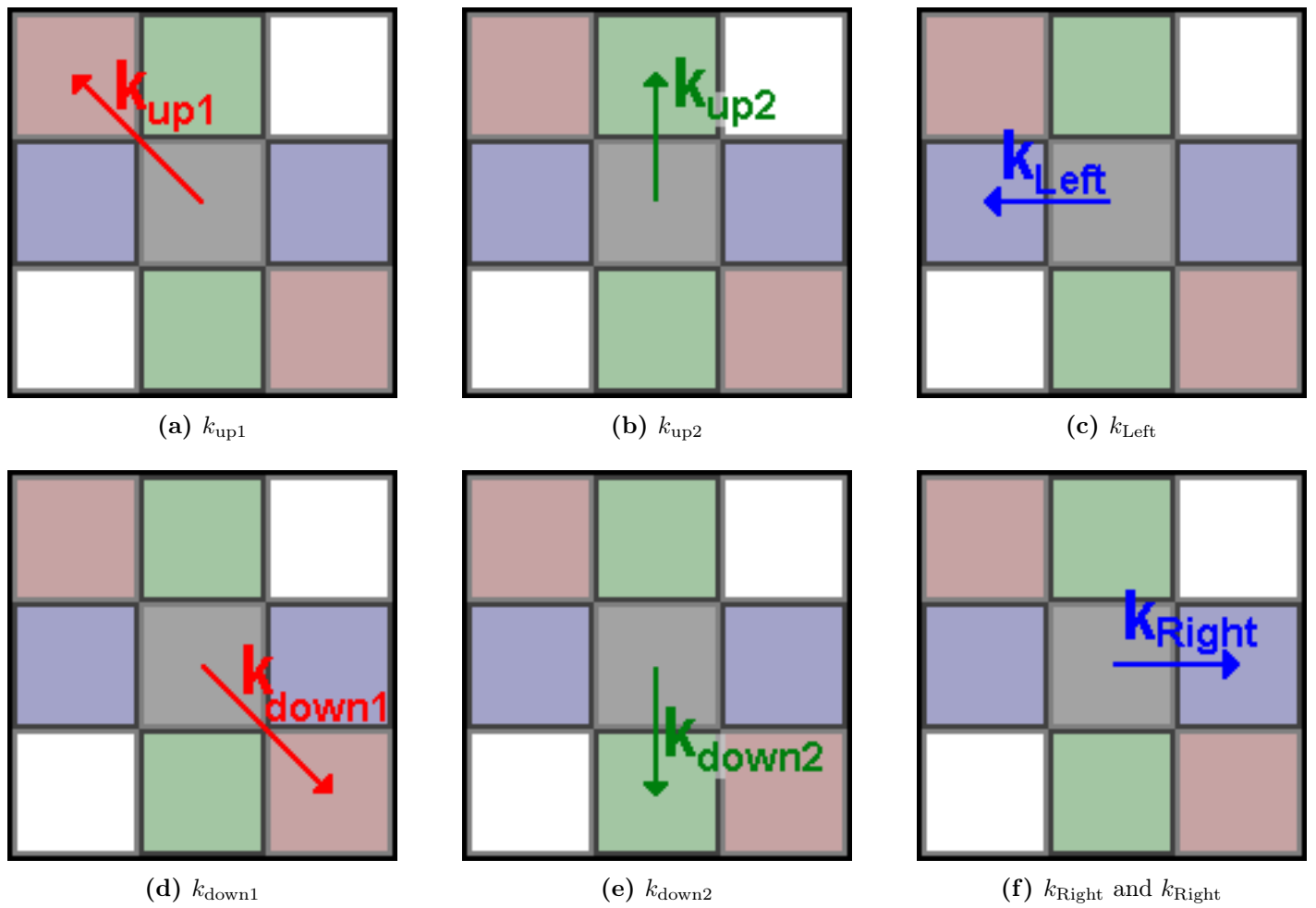
Figure B.3: Square matrix movements.

The first thing to do is to make an LH1/LH2 grid with n LH1 complexes. The script below places them in random positions.

```python
def makeLH1LH2grid(nx, ny, nLH1, max_try=100, sigmarescale=1):
    '''This function makes the LH grid.  2 means LH2, 1 means LH1, 0 means no LH molecule.
    It also makes the kinetic (k) grids'''
    LHgrid = np.zeros([(nx+2),(ny+2)])
    #set edge-sites to 0:
    LHgrid[ 0:, 0] = LHgrid[ 0:,-1] = 0
    LHgrid[ 0, 0:]  = LHgrid[-1, 0:]  = 0
    #Make the code fail-safe:  see safety-measure #1:  Eq.  B.1.2
    try_count = 0
    for i in range(0, nLH1):
        placed = False
        while placed == False and  try_count < max_try:
            acceptable = True
            x_try = round(1 + random.random() * nx)
            y_try = round(1 + random.random() * ny)
            if LHgrid[x_try,y_try] == 1 or LHgrid[x_try,y_try] == 0:
                acceptable = False
                try_count += 1
            if acceptable = True:
                LHgrid[x_try,y_try] = 1
                placed = True
                break
    ...   # code goes on to make k-grids...  Eq.  B.1.3.
    return LHgrid, kmatL, kmatR, kmatupp, kmatdwn, kma2upp, kma2dwn
```
(Eq. B.1.1)

The `while placed == False` loop ensures that the final `LHgrid` contains exactly `nLH1` units of LH1's. Without this loop, it could occur that the same randomly generated location is location is assigned to be LH1 multiple times.

The code is double fail-safe. Without safety measures, the code would get stuck in this loop forever if `nLH1 >= nx * ny`. One way to block it from looping forever that the `while try_count < max_try` statement is no longer satisfied. The other safety measure is to explicitly check that `nLH1 < nx * ny`.

```
        if nLH1 >= nx * ny:

            print("The number of LH1 molecules (",nLH1,")

            exceeds the number of grid points (",nx*ny,").

            This is unacceptable!")

            return
```
(Eq. B.1.2)

The next thing is to set rates between each of the grid points. In order to make this a bit realistic, the rates are pulled from a normal distribution, with a mean and width calculated from the numbers encountered in Figure A.1 on page 69[7].

```
kLH2LH2min  = 1/0.0083

kLH2LH2meh  = 1/0.0063

kLH2LH2max  = 1/0.0043

kLH2LH2mean = np.mean([kLH2LH2meh,kLH2LH2min,kLH2LH2max])

kLH2LH2stdef = np.std([kLH2LH2meh,kLH2LH2min,kLH2LH2max]) * sigmarescale

print("kdif(LH2LH2) = ", kLH2LH2mean, " +- ", kLH2LH2stdef)
```
(Eq. B.1.3a)

which prints

$$\text{kdif(LH2LH2) = 170.59 +- 46.517}$$
(Eq. B.1.3b)

in unit's of ns^{-1}. Note that `sigmarescale = 1` by default, but can be set to 0 if we are doing test-simulations in order to see of our code is working at all.

We can now pull numbers from the gaussian distribution with $\mu = 170.59$ ns^{-1} and $\sigma = 46.517$ ns^{-1} using `np.random.normal(...)`, see below. This is exactly what we do to generate 6 k-grids (up, down, left, right, and the two diagonals upleft downright, recall Figure B.3), e.g. like this:

```
#rates vertical:

kmatupp = np.random.normal(loc=kLH2LH2mean, scale=kLH2LH2stdef, size=(nx+2,ny+2))

#correct edges:

kmatupp[ 0:, 0] = 0

kmatupp[ 0:,-1] = 0

kmatupp[ 0, 0:]  = 0

kmatupp[-1, 0:]  = 0

#LH2 <=> LH2 is symmetric:

kmatdwn = np.copy(kmatupp)

kmatupp[1:-1,1:-1] = kmatdwn[1:-1,2:  ]
```
(Eq. B.1.3c)

As it is very important that the wall remains free of excited state, and because I thought that we might at some point include vaccuum bubbles (so a wall-unit (0) in the middle of the simulation box), I actually over-engineered the code with some extra lines to ensure that the diffusion both from the wall, as well as towards the wall is zero, see Eq. B.1.3d.

```
....# continuation of makeLH1LH2grid
for i in range(0, nx+2)
    for j in range(0, ny+2)
        if LHgrid[i,j] == 0:  # If this is vacuum or the wall
            kmatdwn[i,j] = 0
            kmatupp[i,j] = 0
            try:
                kmatdwn[i,j+1] = 0
            except Exception:
                pass
            try:
                kmatupp[i,j-1] = 0
            except Exception:
                pass
```

(Eq. B.1.3d)

The above subroutines (Eq. B.1.3c and Eq. B.1.3d) are also done for horizontal movement (`kmatL` and `kmatR`) and diagonal movement (`kma2upp` and `kma2dwn`).

The next step is to see if there are any sites other than LH2 in this grid. There are! We have LH1, and we also set the diffusion toward the wall (`if LHgrid[x,y] == 0`) to 0.

The rates between LH1 and LH2 are again pulled from a distribution:

```
kLH1LH2min = 1/0.0073
kLH1LH2max = 1/0.0066
kLH1LH2mean = np.mean([kLH1LH2min,kLH1LH2max])
kLH1LH2stdef = np.std([kLH1LH2min,kLH1LH2max]) * sigmarescale
print("kdif(LH1LH2) = ", kLH1LH2mean, " +- ", kLH1LH2stdef, " ns-1")
```

(Eq. B.1.3e)

which prints

$$\text{kdif(LH1 to LH2)} = 144.25 +\!- 10.27 \qquad \text{(Eq. B.1.3f)}$$

in unit's of ns^{-1}. The assymetry is simply set by multiplying the number with `LH1LH2_ratio = 4.686` (calculated at T = 40°C), so that

$$\text{kdif(LH2 to LH1)} = 675.96 +\!- 48.14 \text{ ns}^{-1}. \qquad \text{(Eq. B.1.3g)}$$

I implement a function which loops over all the LH1-entries, and corrects the rates accordingly.

```
....# continuation of makeLH1LH2grid
for i in range(1, nx+1)
    for j in range(1, ny+1)
        if LHgrid[i,j] == 1:
            if LHgrid[i,j+1] == 2:  # LH1 <=> LH2
                test_LH1_to_LH2_rate = np.random.normal(loc=kdifLH1LH2mean,
                                                   scale=kdifLH1LH2stdef)
                kmatupp[i,j ] = test_LH1_to_LH2_rate
                kmatdwn[i,j+1] = test_LH1_to_LH2_rate * LH1LH2_ratio


            if LHgrid[i,j-1] == 2:  # LH1 <=> LH2
                test_LH1_to_LH2_rate = np.random.normal(loc=kdifLH1LH2mean,
                                                   scale=kdifLH1LH2stdef)
                kmatdwn[i,j ] = test_LH1_to_LH2_rate
                kmatupp[i,j-1] = test_LH1_to_LH2_rate * LH1LH2_ratio
```
$\hfill$ (Eq. B.1.3h)

Again, similar routines for horizontal movement (`kmatL` and `kmatR`) and diagonal movement (`kma2upp` and `kma2dwn`) is done in Eq. B.1.3h, but note that they sense different locations relative to the reference molecule (e.g. `LHgrid[i±1,j]` and `LHgrid[i±1,j±1]`).

Code-wise, this is all that comes into play to initialize the rate-matrices. We can now end our `def makeLH1LH2grid()`: with

```
return LHgrid, kmatL, kmatR, kmatupp, kmatdwn, kma2upp, kma2dwn
```
$\hfill$ (Eq. B.1.4)

Note that later versions of `makeLH1LH2grid()` are adapted to also generate the k-grids for specific/predefined LH1/LH2 configurations, by feeding this function of list with LH1 positions. This modification will not be elaborated here, but can be seen/used in the publicly available code.

B.2 Taking a time-step

Now that we have our k-grids, it's time to define a time-step.

```python
def time_step():
    '''Update the excited state concentrations according to nearest neighbor diffusion'''
    in1 = kmatL[2:  ,1:-1] * singleexcitedstate[2:  ,1:-1]
    in2 = kmatR[0:-2,1:-1] * singleexcitedstate[0:-2,1:-1]
    in3 = kmatdwn[1:-1,2:  ] * singleexcitedstate[1:-1,2:  ]
    in4 = kmatupp[1:-1,0:-2] * singleexcitedstate[1:-1,0:-2]
    in5 = kma2upp[0:-2,0:-2] * singleexcitedstate[0:-2,0:-2]
    in6 = kma2dwn[2:  ,2:  ] * singleexcitedstate[2:  ,2:  ]
    out = (kmatL[1:-1,1:-1] + kmatR[1:-1,1:-1] + kmatdwn[1:-1,1:-1] +
           kmatupp[1:-1,1:-1] + kma2dwn[1:-1,1:-1] + kma2upp[1:-1,1:-1])
             * singleexcitedstate[1:-1,1:-1]
    singleexcitedstate[1:-1,1:-1] = singleexcitedstate[1:-1,1:-1] +
                dt * (in1 + in2 + in3 + in4 + in5 + in6 - out)
    # Code goes on with photon counting, see Eq.  B.3.5
    return
```
(Eq. B.2.1)

Upto now, our simulations are accurate for a single exciton, and has a faster diffusion towards LH1 units than towards LH2 units. Figure B.4 shows a test-simulation.

(a) 1 single excited state, frame 0 (t = 0.000 ns)

(b) 1 single excited state, frame 10 (t = 0.010 ns)
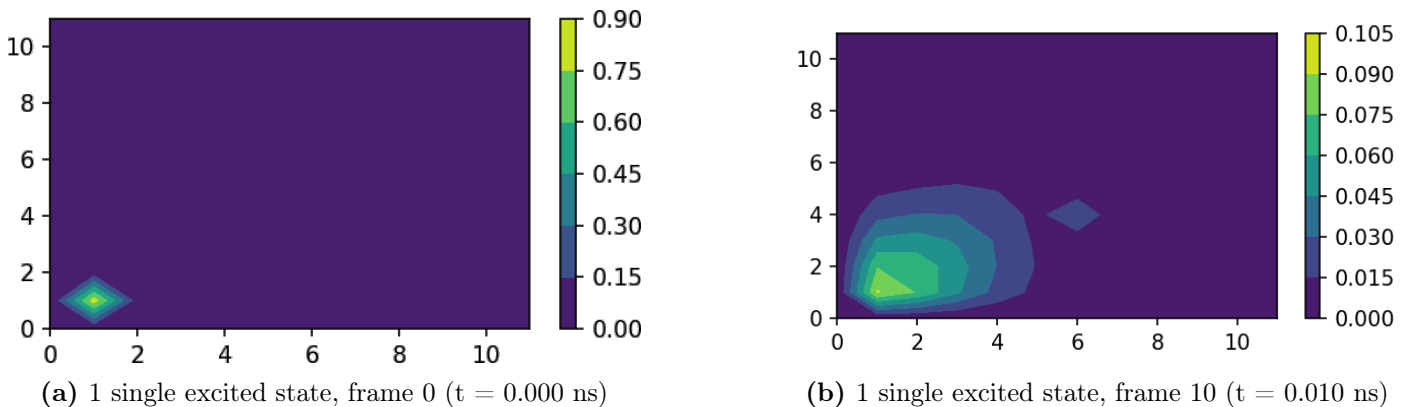
Figure B.4: Example of a single excited state which moves over the Light Harvesting network. On the left you see the initial state. On the right you see the state after 10 000 timesteps (dt = 1 fs). In pannel (b) we can see that the excited state starts accumulating on one molecule in the (6,4) position in the grid; this is the random location where the algorithm decided to put the LH1 unit.

B.3 Fluorescence & photon counting

Section B.1 generates almost all k-grids which we will need in the future. There is one k-grid which I programmed in a slightly different way: the k-grids for fluorescence.

Since I will be dragging around many matrices through many different modules, I try to keep the information in the matrices as compact as possible. However, sometimes we don't want compact information. Below, we have a function which splits the LH-matrix in two matrices: one for LH1 and one for LH2.

$$
\begin{aligned}
&\texttt{def sep\_LH\_grid(LHgrid):} \\
&\quad \texttt{nx = len(LHgrid)} \\
&\quad \texttt{ny = len(LHgrid.T)} \\
&\quad \texttt{LH1grid = np.zeros([(nx),(ny)])} \\
&\quad \texttt{LH2grid = np.zeros([(nx),(ny)])} \\
&\quad \texttt{for i in range(1, nx-1)} \\
&\quad\quad \texttt{for j in range(1, ny-1)} \\
&\quad\quad\quad \texttt{if LHgrid[i,j] == 1:} \\
&\quad\quad\quad\quad \texttt{LH1grid[i,j] = 1} \\
&\quad\quad\quad \texttt{elif LHgrid[i,j] == 2:} \\
&\quad\quad\quad\quad \texttt{LH2grid[i,j] = 1} \\
&\quad \texttt{return LH1grid, LH2grid}
\end{aligned}
\tag{Eq. B.3.1}
$$

Next, we need the rates at which fluorescence takes place. All numbers are from Ref. [19].

$$
\begin{aligned}
&\texttt{kLH1toG = 1/0.680 \# Ref. [19]} \\
&\texttt{kLH2toG = 1/0.986 \# Ref. [19]} \\
&\texttt{kLH1toGR = 1/8.4   \# Ref. [19]} \\
&\texttt{kLH2toGR = 1/10. \# Ref. [19]}
\end{aligned}
\tag{Eq. B.3.2}
$$

Now, we can generate the following k-grids:

$$
\begin{aligned}
&\texttt{k\_fluorescence\_grid = LH1grid * kLH1toG + LH2grid * kLH2toG} \\
&\texttt{k\_\_Radiative\_\_\_grid = LH1grid * kLH1toGR + LH2grid * kLH2toGR}
\end{aligned}
\tag{Eq. B.3.3}
$$

These are the two grids we will be using to calculate the fluorescence and photon counting in the future. Speaking of photon counting; let's initialize the photon counting grids:

$$
\begin{aligned}
&\texttt{LH1\_photon\_counter = np.zeros([(nx),(ny)])} \\
&\texttt{LH2\_photon\_counter = np.zeros([(nx),(ny)])}
\end{aligned}
\tag{Eq. B.3.4}
$$

And our time-step can be expanded to include fluorescence + photon counting as follows:

```python
def time_step():
    # ...  see Eq.  B.2.1 on page 79
    fluorescence = dt * singleexcitedstate[1:-1,1:-1] * k_fluorescence_grid
    photons = dt * singleexcitedstate[1:-1,1:-1] * k__Radiative___grid
    LH1_photon_counter[1:-1,1:-1] += photons * LH1grid
    LH2_photon_counter[1:-1,1:-1] += photons * LH2grid
    singleexcitedstate[1:-1,1:-1] -= fluorescence
    fullgroundstate[1:-1,1:-1] += fluorescence
    return
```

$$(\text{Eq. B.3.5})$$

Photon counting becomes slightly more difficult when we have to consider two excited states in the Light Harvesting network, and my best guess would be that it should look something like this:

```python
def time_step():
    # modified version of Eq.  B.2.1 on page 79 to include dynamics for multiexcitedstates
    fluorescence1 = dt * multiexcitedstate1[1:-1,1:-1] * k_fluorescence_grid
    fluorescence2 = dt * multiexcitedstate2[1:-1,1:-1] * k_fluorescence_grid
    fluorescence3 = dt * singleexcitedstate[1:-1,1:-1] * k_fluorescence_grid
    photons1 = dt * multiexcitedstate1[1:-1,1:-1] * k__Radiative___grid
    photons2 = dt * multiexcitedstate2[1:-1,1:-1] * k__Radiative___grid
    photons3 = dt * singleexcitedstate[1:-1,1:-1] * k__Radiative___grid
    totalphotons = (photons1 + photons2 + photons3)
    LH1_photon_counter[1:-1,1:-1] += totalphotons * LH1grid
    LH2_photon_counter[1:-1,1:-1] += totalphotons * LH2grid
    addto1excitedstate = np.sum(fluorescence1) * multiexcitedstate2[1:-1,1:-1]
    addto2excitedstate = np.sum(fluorescence2) * multiexcitedstate1[1:-1,1:-1]
    multiexcitedstate1[1:-1,1:-1] -= (fluorescence1 + addto2excitedstate)
    multiexcitedstate2[1:-1,1:-1] -= (fluorescence2 + addto1excitedstate)
    singleexcitedstate[1:-1,1:-1] += addto1excitedstate + addto2excitedstate
    singleexcitedstate[1:-1,1:-1] -= fluorescence3
    fullgroundstate[1:-1,1:-1] += fluorescence3
    return
```

$$(\text{Eq. B.3.6})$$

However, the main problem then actually is: how do we describe a two photon system? This is exactly the question I will address in the next section.

B.4 Converting the matrices to vector

	A	B	C	D
A		AB	AC	AD
B			BC	BD
C				CD
D				

Table B.1: The number of double excited states can be calculated as the surface of a triangle: $\frac{1}{2}n^2$, except for that the diagonal elements are fully missing instead of half, so we need to subtract n red-triangles with area $\frac{1}{2}$, so the total number of double excited states is calculated as: $\frac{1}{2}n^2 - \frac{1}{2}n = \frac{1}{2}n * (n-1)$.

How do we describe two excited states?

The most easy approximation is that each of the two excited states behave just like the single excited state. And that is true for most part. The only exception you'll have to deal with is: what happens if the two excited states end up on the same molecule? Well, as we discussed in Section 2.2.3 on page 18, the second excited state is generated, which decays very rapidly towards the first excited state. In fact, for as far as we know, it's the only decay path. I thought to myself, do we actually need to describe the population present in the second excited states in of each of the Light Harvesting complexes? Then I thought, well, no. We can do without it. Then, when two excited states end up on the same unit, we immediately observe the single excited state. Of course this would be an approximation, but the approximation is assumed to be a fairly accurate one.

How would we do it?

We need to imagine one very long vector or array which contains all of the possible states where the system can be in. If it helps, imagine the example of a `LHgrid` containing $n = 4$ Light Harvesting complexes, A, B, C, D.

0. Element 0 is describing the full ground state (fgs).

1. Elements 1 to n are describing the single excited states (A, B, C, D...)

2. Elements $n+1$ to $\frac{1}{2}n * (n+1)+1$ are describing the double excited states (AB, AC, AD, BC, BD, CD...). The boundaries are set this way so that there exactly $\frac{1}{2}n * (n-1)$ double exciton elements, just as much as we need according to the calculation in the caption of Table B.1

3. Elements $n * (n+1)/2 + 2$ and $n * (n+1)/2 + 3$ are reserved for the photon counters for LH1 and LH2 respectively.

Now that we roughly know which elements goes where, we can start looping over the different grid elements to put all elements in the place where they belong in the vector. In order to know which element I stored where, I keep a dictionary.

```python
def convert_grid_to_vector(LHgrid, multiexcitedstate1, multiexcitedstate2, singleexcitedstate
            fullgroundstate, LH1_photon_counter, LH2_photon_counter, tag = ""):
    nx = len(LHgrid) -2
    ny = len(LHgrid.T) -2
    number_of_elements_in_grid = nx * ny
    number_of_elements_in_vector = round((number_of_elements_in_grid) *
                (number_of_elements_in_grid + 1) / 2 + 3) # incl. photon counter


    new_population_vector = np.zeros(number_of_elements_in_vector)
    vec_index_dict = {}
    vec_index_dict_inv = {}
    vec_index_new = 0
    vec_index_dict[vec_index_new] = "fgs"
    vec_index_dict_inv["fgs"] = vec_index_new
    # Code updates new_population_vector with singleexcitedstate elements, see Eq. B.4.2.
    # Code updates new_population_vector with multiexcitedstates elements, see Eq. B.4.3.
    # Code updates new_population_vector with LH1 and LH2 photon-counters, see Eq. B.4.4.
    return new_population_vector, singleexcitedstate
```
(Eq. B.4.1)

For the single excited states, note that this is the excellent place to calculate annihilation, as we are looping over the single excited states anyways now.

```python
    for i in range(1,nx+1):  # single excited states
        for j in range(1,ny+1):
            vec_index_new += 1
            vec_index_dict[vec_index_new] = "[" + str(i) + "," + str(j) + "]"
            vec_index_dict_inv["[" + str(i) + "," + str(j) + "]"] = vec_index_new
            annihilatexy = min(multiexcitedstate1[i,j], multiexcitedstate2[i,j])
            singleexcitedstate[i,j] += annihilatexy
            multiexcitedstate1[i,j] -= annihilatexy
            multiexcitedstate2[i,j] -= annihilatexy
            new_population_vector[vec_index_new] = singleexcitedstate[i,j]
```
(Eq. B.4.2)

Next, we update the double excitons, have the risk of being double counted (e.g. AB = BA be-

cause we don't care which of the two excited state is where). Note that also keep an inverse dictionary, to which I also add the other combination. The second loop will only add an element to the `new_population_vector` if that element is not present in the dictionary yet.

```
for i in range(1,nx+1):  # multi excited states
    for j in range(1,ny+1):
        for k in range(1,nx+1):
            for m in range(1,ny+1):
                if [i,j] != [k,m] and "[" + str(i) + "," + str(j) + "],[" + str(k)
                                        + "," + str(m) + "]" not in vec_index_dict_inv:
                    vec_index_new += 1
                    vec_index_dict[vec_index_new] = "[" + str(i) + "," + str(j) +
                                            "],[" + str(k) + "," + str(m) + "]"
                    vec_index_dict_inv["[" + str(i) + "," + str(j) + "],[" +
                                        + str(k) + "," + str(m) + "]"] = vec_index_new
                    vec_index_dict_inv["[" + str(k) + "," + str(m) + "],[" +
                                        + str(i) + "," + str(j) + "]"] = vec_index_new
                    new_population_vector[vec_index_new] = min(multiexcitedstate1[i,j],
                                                    multiexcitedstate2[k,m])
```

(Eq. B.4.3)

Last but not least, the final two elements in the population vector are

```
        vec_index_new += 1
        vec_index_dict[vec_index_new] = "[LH1_photon_counter]"
        vec_index_dict_inv["[LH1_photon_counter]"] = vec_index_new
        new_population_vector[ vec_index_new ] = LH1_photon_counter
        vec_index_new += 1
        vec_index_dict[vec_index_new] = "[LH2_photon_counter]"
        vec_index_dict_inv["[LH2_photon_counter]"] = vec_index_new
        new_population_vector[ vec_index_new ] = LH2_photon_counter
```

(Eq. B.4.4)

And if everything is good now, we should have converted a state which was initially described by three matrices and two photon counters and a ground state counter, to one vector containing all this information!

Unfortunately, however, if we go on to the next step, to combine all these states to huge K-matrix, we encounter a normalization problem: for some reason, after one fluorescence time-step with multiple

excited states (Eq. B.3.6), the state is no longer normalized, meaning that the total amount of state in one array is no longer equal to 1. This is very inconvenient, and I've wasted a lot of time to investigate if I could program the time-step better, but for so far I haven't solved the issue yet. I did find a work-around tho: simply normalize the rows which are not normalized.

```python
if np.sum(new_population_vector[0:-2]) != 0:
    if np.sum(new_population_vector[0:-2]) != 1:
        print(tag + "np.sum(new_population_vector[0:-2]) = ",
                    np.sum(new_population_vector[0:-2]), " != 1, let's normalize this.")
        new_population_vector = new_population_vector / np.sum(new_population_vector[0:-2])
```

$$\text{(Eq. B.4.5)}$$

I use the `print` and `tag` for debugging, and for so far I still have not managed to perfectionalize this, but maybe if someone else stares at the code for a few days, they will figure it out. At least you now know why this is taking so long. You could comment out the printing step if you want to accelerate the code.

B.5 Converting the vectors to one big $\vec{\mathbf{K}}$-matrix

Now that we have a way to convert a state to a vector, we can make big transformation matrix $\vec{\mathbf{K}}$ so that:

$$\vec{P}(t + \mathrm{d}t) = \vec{\mathbf{K}} \cdot \vec{P}(t). \tag{Eq. B.5.1}$$

We can actually do this for many timesteps at the same time, by raising the transformation matrix $\vec{\mathbf{K}}$ to some power:

$$\vec{P}(t) = \left(\vec{\mathbf{K}}\right)^{t/\mathrm{d}t} \cdot \vec{P}(0). \tag{Eq. B.5.2}$$

Now, note that if we calculate $\left(\vec{\mathbf{K}}\right)^{t/\mathrm{d}t}$ one time, we can see how any system has evolved from its initial state $\vec{P}(0)$ to a final state $\vec{P}(t)$. This is called a Master-equation, and has been introduced in Sections 2.2-2.2.5. For a recap, see Figure B.5.

(a) The $\vec{\mathbf{K}}$ matrix for 1 timestep (dt = 0.1 ps).

(b) $\left(\vec{\mathbf{K}}\right)^{100000}$ matrix for 10 ns.
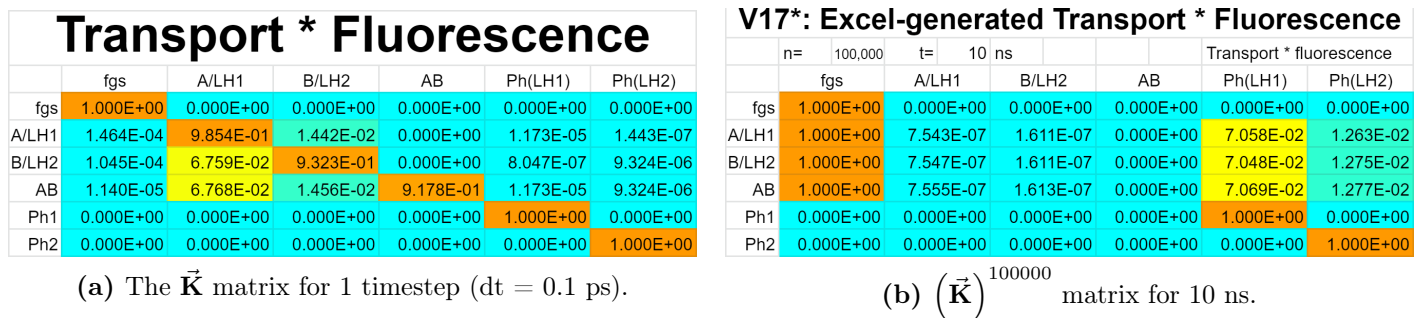
Figure B.5: The Master equations for a dimer. Note that the tag labeling each row indicates it's starting configuration, and it ends up in many other states. The output states are labeled in the top row of each column. Reprint of Figures 2.10 and 2.11.

Let's start simple. We modify the definition of a timestep (Eq. B.2.1 on page 79) to include the movement of the population density of each of the separate excited states: `singleexcitedstate`, `multiexcitedstate1`, `multiexcitedstate2`. We basically copy all the lines and just interchange the tag for each block of code.

Then we cycle through all the loops of Section B.4 again, in exactly the same order, keeping track of the `vec_index_new`, which now corresponds to the row-number of our $\vec{\mathbf{K}}$ matrix. But now, we set the matrices (`singleexcitedstate`, `multiexcitedstate1`, `multiexcitedstate2`) up to match the corresponding state, and we take a time-step. The formed situation is converted to a vector using the `convert_grid_to_vector(LHgrid, multiexcitedstate1, multiexcitedstate2, singleexcitedstate, fullgroundstate, LH1_photon_counter, LH2_photon_counter)` command.

From here onwards, I tested and wrote many variations on the code. One could probably also think of more efficient algorithms for setting up the k-matrix, but since I assumed time stepping would take the core of the CPU time, I didn't focus on optimizing the part in which the equations are set up.

B.6 Testing different versions of the code

Recall the discission on whether to do the fluorescence or the exciton transfer step first. When I did simulations on the dimer (Figure 2.11 on page 26, reprinted here for convenience), it turned out that there was barely any difference between taking the exciton fluorescence or the exciton transfer step first.

V17*: Excel-generated Transport * Fluorescence

	n=	100,000	t=	10 ns		Transport * fluorescence	
	fgs	A/LH1	B/LH2	AB	Ph(LH1)	Ph(LH2)
fgs	1.000E+00	0.000E+00	0.000E+00	0.000E+00	0.000E+00	0.000E+00
A/LH1	1.000E+00	7.543E-07	1.611E-07	0.000E+00	7.058E-02	1.263E-02
B/LH2	1.000E+00	7.547E-07	1.611E-07	0.000E+00	7.048E-02	1.275E-02
AB	1.000E+00	7.555E-07	1.613E-07	0.000E+00	7.069E-02	1.277E-02
Ph1	0.000E+00	0.000E+00	0.000E+00	0.000E+00	1.000E+00	0.000E+00
Ph2	0.000E+00	0.000E+00	0.000E+00	0.000E+00	0.000E+00	1.000E+00

(a) Transport × Fluorescence.

V18: Script generated Fluorescence * Transport

	n=	100,000	t=	10 ns;	wall-time= 0	Fluorescence * Transport	
	fgs	A/LH1	B/LH2	AB	Ph(LH1)	Ph(LH2)
fgs	1.000E+00	0.000E+00	0.000E+00	0.000E+00	0.000E+00	0.000E+00
A/LH1	1.000E+00	7.543E-07	1.611E-07	0.000E+00	7.058E-02	1.263E-02
B/LH2	1.000E+00	7.547E-07	1.611E-07	0.000E+00	7.047E-02	1.276E-02
AB	1.000E+00	7.557E-07	1.613E-07	0.000E+00	7.071E-02	1.278E-02
Ph1	0.000E+00	0.000E+00	0.000E+00	0.000E+00	1.000E+00	0.000E+00
Ph2	0.000E+00	0.000E+00	0.000E+00	0.000E+00	0.000E+00	1.000E+00

(b) Fluorescence × Transport.

Figure B.6: When simulating the dimer, there is very little difference in the final result, whether we do the fluorescence- or exciton transfer-timestep first. Reprint of Figure 2.11 on page 26.

In versions 18 & 19 of the code, we first do a time-step in fluorescence and then do a time-step in exciton transfer, and then apply the conversion from 3 matrices to 1 vector (see section B.4), which in practise gives the exact same matrix as doing $\mathbf{K}_F \times \mathbf{K}_{tr}$.

In version 20 of the code, I first do a time-step in exciton transfer, and then convert 3 matrices to a vector, then back to 3 matrices (exciton annihilation is done in the conversion step), and then do a fluorescence-time-step. In practise, this gives the same matrix as doing $\mathbf{K}_{tr} \times \mathbf{K}_F$. As the exciton transfer is fast (compared to fluorescence), it makes most sense to perform that step first.

B.7 Version 18/19 vs Version 20/21

As I described in section 4.2, I did simulations on different kinds of Light Harvesting chains, depicted in Figure 4.2 on page 44. Something which I didn't discuss in the main results, is that I actually did it this simulation multiple times with different versions of the code, because I noticed that my assumption that which can be downloaded here:

Version 19: `https://www.dropbox.com/s/5ii7vnaso6snuz8/Kinetics%20simulation%20on%20grid%20step%2019%20cleanup.py?dl=0`

Version 21: `https://www.dropbox.com/s/t6fig25j3f0qbon/Kinetics%20simulation%20on%20grid%20step%2021%20include%20LH1-LH1.py?dl=0`

In version 19, I first take a fluorescence time-step before I take a dynamics time-step, while in version 20 I take a dynamics timestep first, then do a (recall comparison in Figure 2.11 on page 26).

Now I must admit that I initially thought that the difference was going to be insignificant, but it turns out that there is a difference. The reason why I present the results from the bit less accurate code

anyways, is because the graphs are conveniently not overlapping constantly, which is the case for the 21th version.
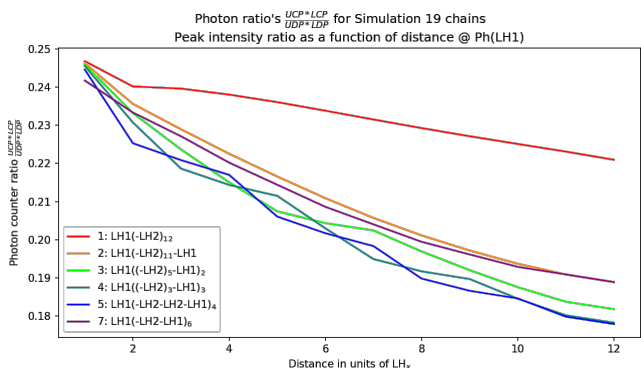
(a) This graph was made with version 19 of the code, in which the k-grid is generated via Fluorescence × Transport.
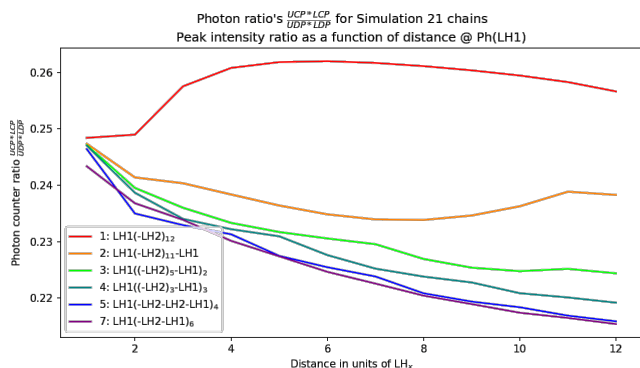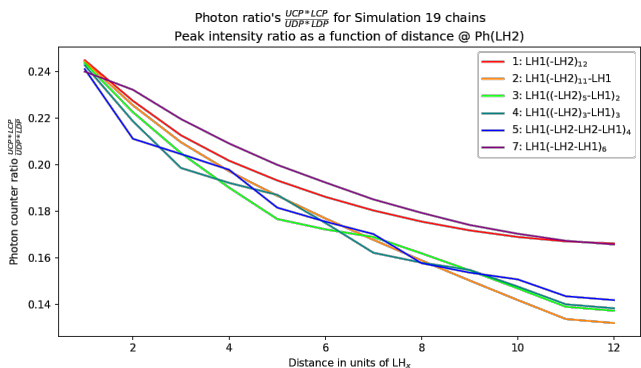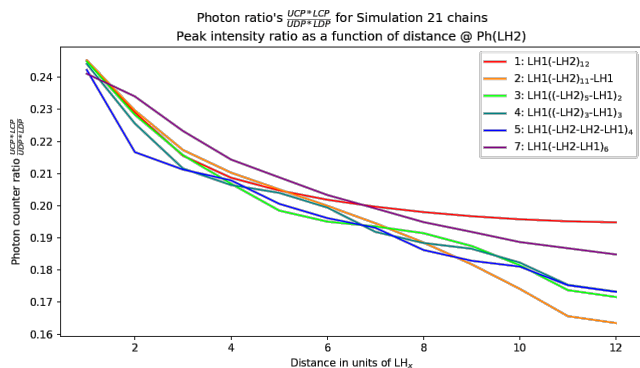
(b) This graph was made with version 21 of the code, in which the k-grid is generated via Transport × Fluorescence.

Figure B.7: Cross-peak to Diagonal-peak ratio according to photon counters calibrated to LH1.

(a) This graph was made with version 19 of the code, in which the k-grid is generated via Fluorescence × Transport.

(b) This graph was made with version 21 of the code, in which the k-grid is generated via Transport × Fluorescence.

Figure B.8: Cross-peak to Diagonal-peak ratio according to photon counters calibrated to LH2.

The kinks are an indication that this Light Harvesting complex is neighboring a LH1 complex on the right. Personally I feel like these kinks are slightly better visible in version 19 than in version 20 of the code, but then I also have in the back of my mind that version 20 is a more accurate simulation. But in the end I think that the conclusion is that we can simulate whatever we like, but there will be very little contrast for experiments, because the overlap between the different simulations is huge.

Version 21 includes the $LH_1 \rightleftharpoons LH_1$ exciton dynamics as an option[9].

Version 24 includes the option to gradually add vacancies[10].

---

[9]   Download: `https://www.dropbox.com/s/1k1ffgh4cpohtua/Kinetics_simulation_v.21_incl_LH1-LH1.py?dl=0`

[10]   Download: `https://www.dropbox.com/s/il9u71znubwzxhw/Kinetics_simulation_v.24_incl_vacancies.py?`

B.8   Timing

For each simulation, the k-matrix is raised to the 100 000'th power, in order to obtain the situation (mainly the photon counters) after 10 nanosecond. I did some tests to see if the code would actually run faster if I were to take fewer timesteps.

Figure B.9a concludes that there is no sensitivity for more CPU time at higher power's after roughly $n = 1000$. Probably this has to do with the fact that the `matrix_power()` function is optimized to deal with higher powers.

(a) As a function of k-power (k^n)

(b) As a function of number of elements in the grid.
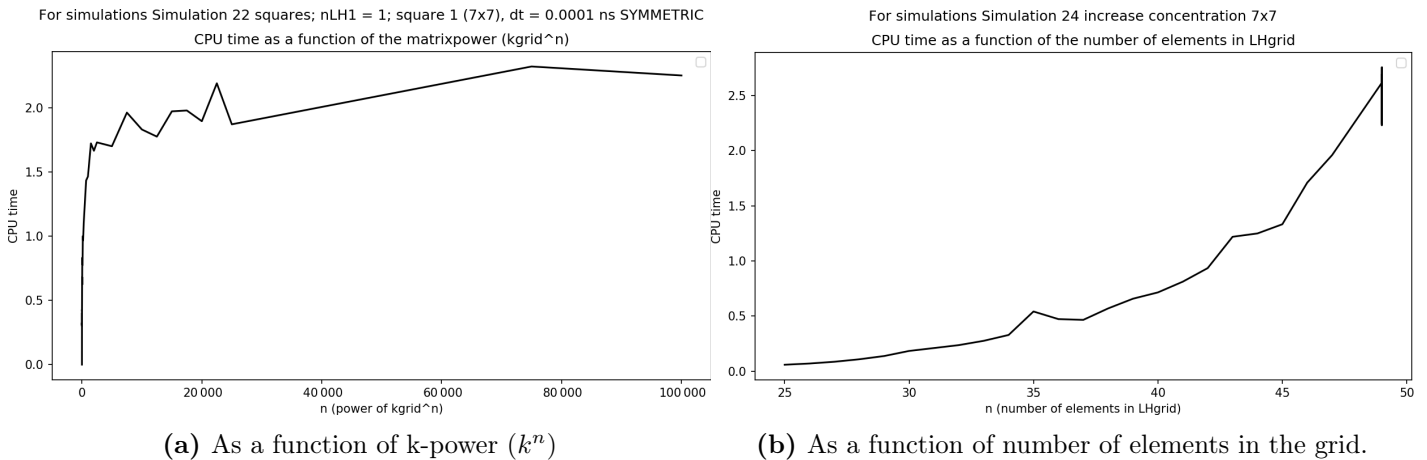
Figure B.9: Determination on what has a higher sensitivity towards more CPU time: more elements in the `LHgrid`, or raising the k-grid higher power.

But how is the CPU sensitivity for having more elements in the light harvesting grid (which I called `LHgrid` in the Python code)? This is something which I tracked in the very last simulations, I timed each simulation, also when we had a vacancy introduced. Note that the spike at x is an artifact. It is simply the overlay of many data points at $n = 49$, since this was a similar experiment as performed in section 4.5 on page 52 (introducing vacancies).

Note that a full simulation is actually a lot more than just raising the `k_grid` to the n-th power: constructing the `k_grid` also consumes a lot of time. I put a timer around a few simulations, the results are plotted in Figure B.10.

---

dl=0

Including the k_grid_generation

CPU time as a function of the number of elements in LHgrid

(a) Till max 64 entries

Including the k_grid_generation

CPU time as a function of the number of elements in LHgrid
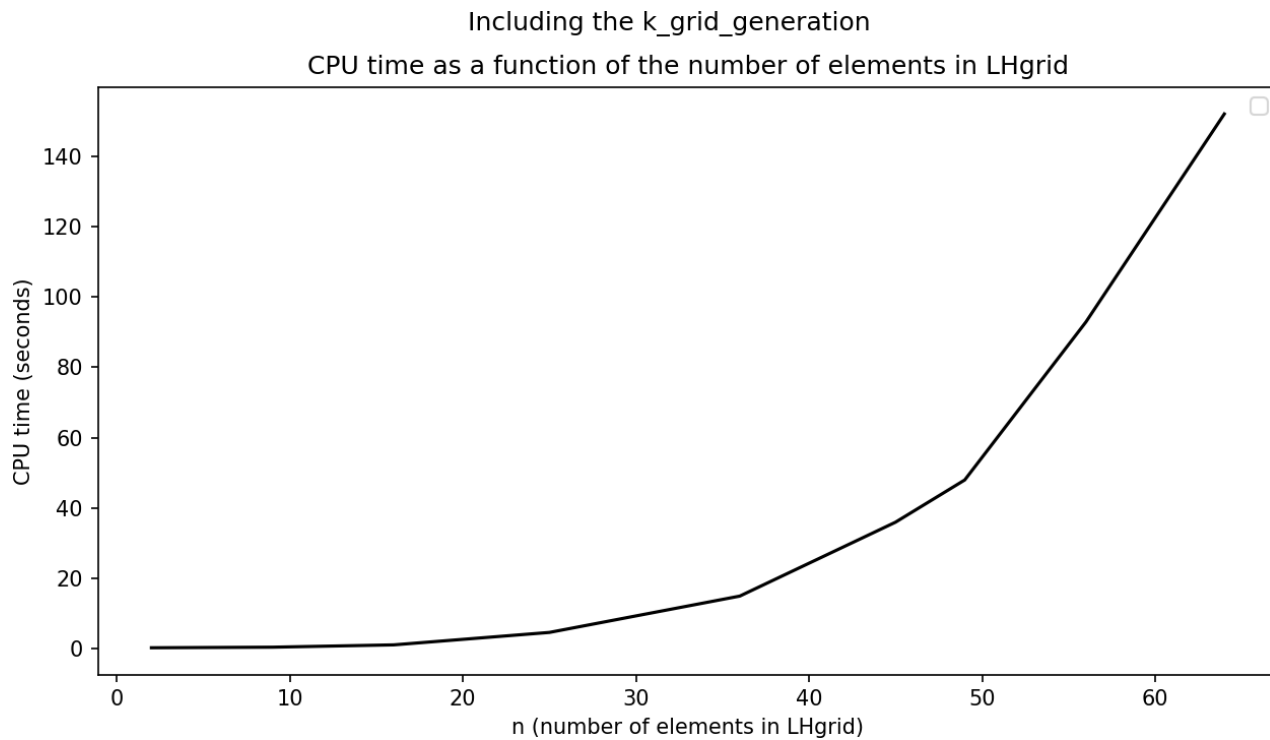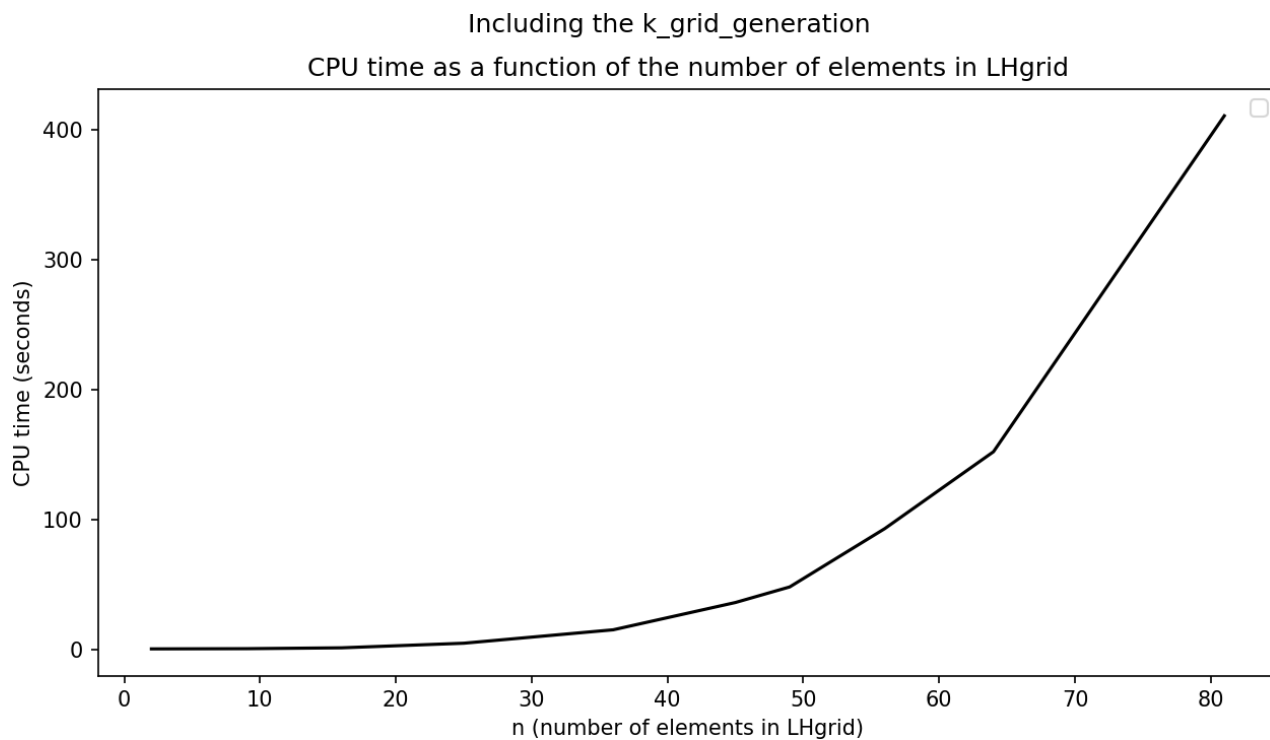
(b) Till max 81 entries

Figure B.10: Investigating full CPU time as a function of the number of elements in the LH grid.

Bibliography

[1] Miyamoto K. Chapter 1 - Biological energy production. `http://www.fao.org/3/w7241e/w7241e05.htm#1.2.1`, accessed: 2021-07-08.

[2] J. Thomas Beatty, Jörg Overmann, Michael T. Lince, Ann K. Manske, Andrew S. Lang, Robert E. Blankenship, Cindy L. Van Dover, Tracey A. Martinson, and F. Gerald Plumley. An obligately photosynthetic bacterial anaerobe from a deep-sea hydrothermal vent. *Proceedings of the National Academy of Sciences*, 102(26):9306–9310, 2005. ISSN 0027-8424. doi:10.1073/pnas.0503674102. URL `https://www.pnas.org/content/102/26/9306`.

[3] Lisa M. Günther, Alexander Löhner, Carolin Reiher, Tenzin Kunsel, Thomas L. C. Jansen, Marcus Tank, Donald A. Bryant, Jasper Knoester, and Jürgen Köhler. Structural variations in chlorosomes from wild-type and a bchqr mutant of chlorobaculum tepidum revealed by single-molecule spectroscopy. *The Journal of Physical Chemistry B*, 122(26):6712–6723, 2018. doi:10.1021/acs.jpcb.8b02875. PMID: 29863357.

[4] Johannes F. Imhoff. Transfer of rhodopseudomonas acidophila to the new genus rhodoblastus as rhodoblastus acidophilus gen. nov., comb. nov. *International Journal of Systematic and Evolutionary Microbiology*, 51(5):1863–1866, 2001. ISSN 1466-5026. doi:10.1099/00207713-51-5-1863.

[5] Norbert Pfennig. Rhodopseudomonas acidophila, sp. n., a new species of the budding purple nonsulfur bacteria. *Journal of Bacteriology*, 99(2):597–602, 1969. ISSN 0021-9193. URL `https://jb.asm.org/content/99/2/597`.

[6] Kõu Timpmann, Manoop Chenchiliyan, Erko Jalviste, John A. Timney, C. Neil Hunter, and Arvi Freiberg. Efficiency of light harvesting in a photosynthetic bacterium adapted to different levels of light. *Biochimica et Biophysica Acta (BBA) - Bioenergetics*, 1837(10):1835–1846, 2014. ISSN 0005-2728. doi:https://doi.org/10.1016/j.bbabio.2014.06.007. URL `https://www.sciencedirect.com/science/article/pii/S0005272814005222`.

[7] Danielle E. Chandler, Johan Strümpfer, Melih Sener, Simon Scheuring, and Klaus Schulten. Light harvesting by lamellar chromatophores in rhodospirillum photometricum. *Biophysical Journal*, 106 (11):2503 – 2510, 2014. ISSN 0006-3495. doi:10.1016/j.bpj.2014.04.030.

[8] Frauke Baymann, Myriam Brugna, Ulrich Mühlenhoff, and Wolfgang Nitschke. Daddy, where did (ps)i come from? *Biochimica et Biophysica Acta (BBA) - Bioenergetics*, 1507(1):291–310, 2001. ISSN 0005-2728. doi:https://doi.org/10.1016/S0005-2728(01)00209-2. URL `https://www.sciencedirect.com/science/article/pii/S0005272801002092`.

[9] Vivek Tiwari, Yassel Acosta Matutes, Alastair T. Gardiner, Thomas L. C. Jansen, Richard J. Cogdell, and Jennifer P. Ogilvie. Spatially-resolved fluorescence-detected two-dimensional electronic spectroscopy probes varying excitonic structure in photosynthetic bacteria. *Nature Communications*, 9(1), October 2018. doi:10.1038/s41467-018-06619-x.

[10] Tenzin Kunsel, Vivek Tiwari, Yassel Acosta Matutes, Alastair T. Gardiner, Richard J. Cogdell, Jennifer P. Ogilvie, and Thomas L. C. Jansen. Simulating fluorescence-detected two-dimensional electronic spectroscopy of multichromophoric systems. *The Journal of Physical Chemistry B*, 123 (2):394–406, 2019. doi:10.1021/acs.jpcb.8b10176.

[11] Tihana Mirkovic, Evgeny E. Ostroumov, Jessica M. Anna, Rienk van Grondelle, Govindjee, and Gregory D. Scholes. Light absorption and energy transfer in the antenna complexes of photosynthetic organisms. *Chemical Reviews*, 117(2):249–293, 2017. doi:10.1021/acs.chemrev.6b00002. PMID: 27428615.

[12] Graham R Fleming and Rienk van Grondelle. Femtosecond spectroscopy of photosynthetic light-harvesting systems. *Current Opinion in Structural Biology*, 7(5):738–748, 1997. ISSN 0959-440X. doi:https://doi.org/10.1016/S0959-440X(97)80086-3.

[13] Robert W. Boyd. *Nonlinear Optics, Third Edition*. Academic Press, Inc., USA, 3rd edition, 2008. ISBN 0123694701.

[14] Peter Hamm and Martin Zanni. *Concepts and Methods of 2D Infrared Spectroscopy*. Cambridge University Press, 2011. doi:10.1017/CBO9780511675935.

[15] Andrew F. Fidler, Ved P. Singh, Phillip D. Long, Peter D. Dahlberg, and Gregory S. Engel. Time scales of coherent dynamics in the light-harvesting complex 2 (LH2) of rhodobacter sphaeroides. *The Journal of Physical Chemistry Letters*, 4(9):1404–1409, 2013. doi:10.1021/jz400438m. PMID: 23878622.

[16] Guido Van Rossum and Fred L. Drake. *Python 3 Reference Manual*. CreateSpace, Scotts Valley, CA, 2009. ISBN 1441412697. doi:10.5555/1593511.

[17] Charles R. Harris, K. Jarrod Millman, Stéfan J. van der Walt, Ralf Gommers, Pauli Virtanen, David Cournapeau, Eric Wieser, Julian Taylor, Sebastian Berg, Nathaniel J. Smith, Robert Kern, Matti Picus, Stephan Hoyer, Marten H. van Kerkwijk, Matthew Brett, Allan Haldane, Jaime Fernández del Río, Mark Wiebe, Pearu Peterson, Pierre Gérard-Marchant, Kevin Sheppard, Tyler Reddy, Warren Weckesser, Hameer Abbasi, Christoph Gohlke, and Travis E. Oliphant. Array programming with NumPy. *Nature*, 585(7825):357–362, September 2020. doi:10.1038/s41586-020-2649-2. URL https://doi.org/10.1038/s41586-020-2649-2.

[18] Wolfram Research, Inc. Mathematica, Version 12.2, 2020. URL `https://www.wolfram.com/mathematica`. Champaign, IL.

[19] René Monshouwer, Malin Abrahamsson, Frank van Mourik, and Rienk van Grondelle. Superradiance and exciton delocalization in bacterial photosynthetic light-harvesting systems. *The Journal of Physical Chemistry B*, 101(37):7241–7248, 1997. doi:10.1021/jp963377t.

[20] Paul Adrien Maurice Dirac and Niels Henrik David Bohr. The quantum theory of the emission and absorption of radiation. *Proceedings of the Royal Society of London. Series A, Containing Papers of a Mathematical and Physical Character*, 114(767):243–265, 1927. doi:10.1098/rspa.1927.0039.

[21] Larry Lüer, Vladimíra Moulisová, Sarah Henry, Dario Polli, Tatas H. P. Brotosudarmo, Sajjad Hoseinkhani, Daniele Brida, Guglielmo Lanzani, Giulio Cerullo, and Richard J. Cogdell. Tracking energy transfer between light harvesting complex 2 and 1 in photosynthetic membranes grown under high and low illumination. *Proceedings of the National Academy of Sciences*, 109(5):1473–1478, 2012. ISSN 0027-8424. doi:10.1073/pnas.1113080109.

[22] A.P. Shreve, J.K. Trautman, Harry A. Frank, T.G. Owens, and A.C. Albrecht. Femtosecond energy-transfer processes in the B800–850 light-harvesting complex of rhodobacter sphaeroides 2.4.1. *Biochimica et Biophysica Acta (BBA) - Bioenergetics*, 1058(2):280 – 288, 1991. ISSN 0005-2728. doi:10.1016/S0005-2728(05)80248-8.

[23] J. T. M. Kennis, A. M. Streltsov, S. I. E. Vulto, T. J. Aartsma, T. Nozawa, and J. Amesz. Femtosecond dynamics in isolated LH2 complexes of various species of purple bacteria. *Journal of Physical Chemistry B*, 101(39):7827–7834, 1997. URL `https://www.scopus.com/record/display.uri?eid=2-s2.0-0031233135&origin=inward&txGid=d2f23c1b0d13cc9061bc079bc79a4aa9`.

[24] Y. Ma, R. J. Cogdell, and T. Gillbro. Energy transfer and exciton annihilation in the B800-850 antenna complex of the photosynthetic purple bacterium rhodopseudomonas acidophila (strain 10050). a femtosecond transient absorption study. *Journal of Physical Chemistry B*, 101(6):1087–1095, 1997. URL `https://www.scopus.com/record/display.uri?eid=2-s2.0-0031555706&origin=inward&txGid=2aaa993349bc59493a4f5f24d58651bc`.

[25] G. Trinkunas, J. L. Herek, T. Polívka, V. Sundström, and T. Pullerits. Exciton delocalization probed by excitation annihilation in the light-harvesting antenna LH2. *Physical Review Letters*, 86 (18):4167–4170, April 2001. doi:10.1103/physrevlett.86.4167.

[26] Jennifer L. Herek, N.J. Fraser, T. Pullerits, P. Martinsson, T. Polívka, H. Scheer, R.J. Cogdell, and V. Sundström. B800→B850 energy transfer mechanism in bacterial LH2 complexes investigated by B800 pigment exchange. *Biophysical Journal*, 78(5):2590 – 2596, 2000. ISSN 0006-3495. doi:10.1016/S0006-3495(00)76803-2.

[27] Thomas La Cour Jansen. Ultrafast dynamics and multi-dimensional spectroscopy (course reader), 2020. URL `http://www.acmm.nl/molsim/han/2009/ LaCourJansen-multidim-spectrosc-Han11jan2010.pdf`. These lecture notes were prepared for the Ultrafast Dynamics course. Most recent version dates 2020. A publicly available version dates 2010, see link.

[28] H. Blom and H. Brismar. Sted microscopy: increased resolution for medical research? *Journal of Internal Medicine*, 276(6):560–578, 2014. doi:https://doi.org/10.1111/joim.12278.

[29] Hugo Gaspar, Flávio Figueira, Luiz Pereira, Adélio Mendes, Júlio C. Viana, and Gabriel Bernardo. Recent developments in the optimization of the bulk heterojunction morphology of polymer: Fullerene solar cells. *Materials*, 11(12), 2018. ISSN 1996-1944. doi:10.3390/ma11122560. URL `https://www.mdpi.com/1996-1944/11/12/2560`.